IN THIS ISSUE

IMAGE: OBSERVATORY WITH STAR TRAILS ON MOUNTAINS FOR CLEAR SKY

London Journals Press

www.journalspress.com

LONDON JOURNAL OF ENGINEERING RESEARCH

Print ISSN: 2631-8474
Online ISSN: 2631-8482
DOI: 10.17472/LJER

Volume 22 | Issue 7 | Compilation 1.0

COMPILED IN UNITED KINGDOM

ENGLISH

London Journal of Engineering Research

Volume 22 | Issue 7 | Compilation 1.0

PUBLISHER

London Journals Press
1210th, Waterside Dr, Opposite Arlington Building, Theale, Reading
Phone:+444 0118 965 4033 Pin: RG7-4TY United Kingdom

SUBSCRIPTION

Frequency: Quarterly

Print subscription
$280USD for 1 year
$500USD for 2 year
(color copies including taxes and international shipping with TSA approved)

Find more details at https://journalspress.com/journals/subscription

ENVIRONMENT

London Journals Press is intended about protecting the environment. This journal is printed using led free environmental friendly ink and acid-free papers that are 100% recyclable.

London Journals Press Headquaters

1210th, Waterside Dr,
Opposite Arlington
Building, Theale, Reading
Phone:+444 0118 965 4033
Pin: RG7-4TY
United Kingdom

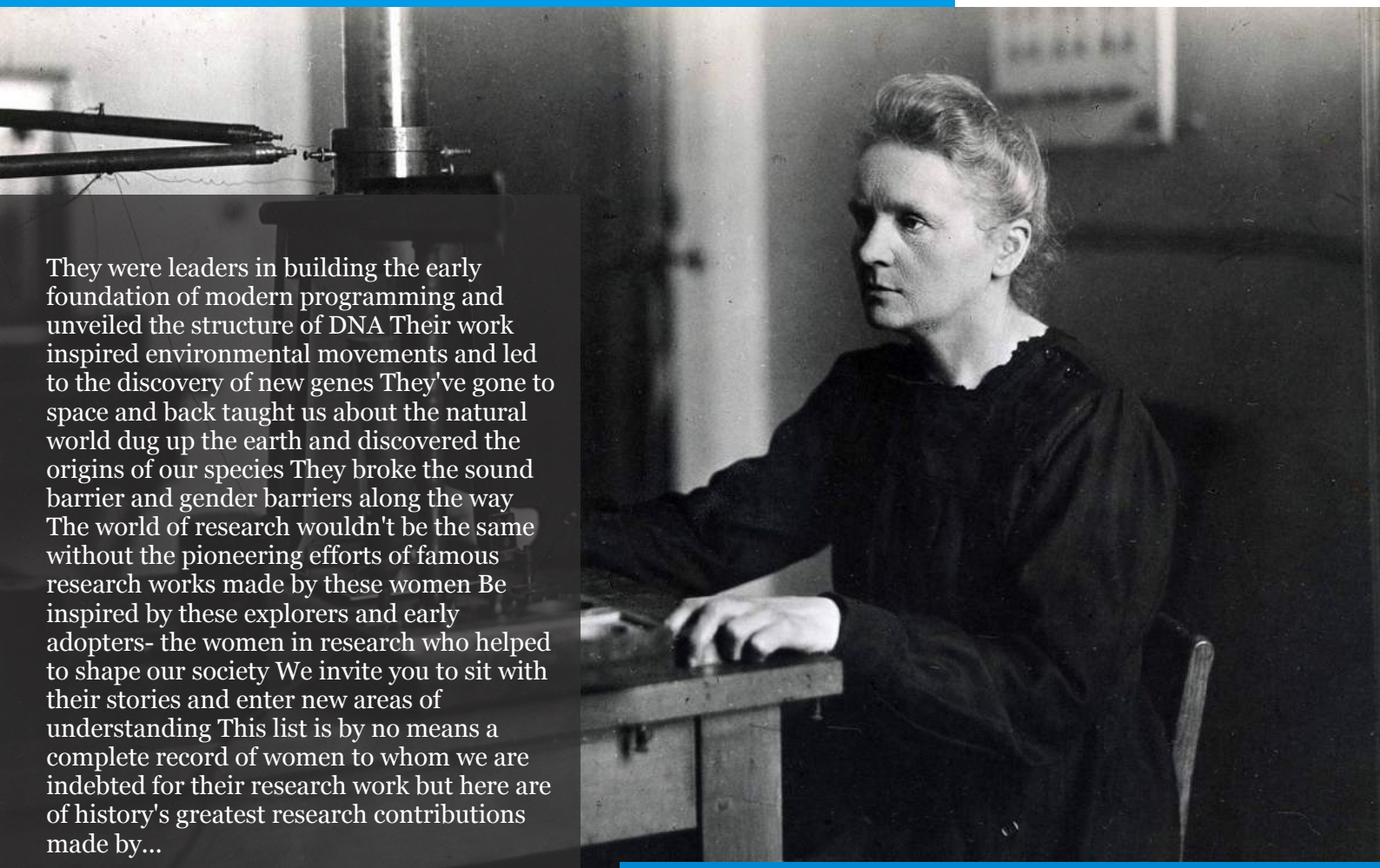

They were leaders in building the early foundation of modern programming and unveiled the structure of DNA Their work inspired environmental movements and led to the discovery of new genes They've gone to space and back taught us about the natural world dug up the earth and discovered the origins of our species They broke the sound barrier and gender barriers along the way The world of research wouldn't be the same without the pioneering efforts of famous research works made by these women Be inspired by these explorers and early adopters- the women in research who helped to shape our society We invite you to sit with their stories and enter new areas of understanding This list is by no means a complete record of women to whom we are indebted for their research work but here are of history's greatest research contributions made by...

Read complete here:
https://goo.gl/1vQ3lS

Women In Research

Computing in the cloud!

Cloud Computing is computing as a Service and not just as a Product Under Cloud Computing...

Read complete here:
https://goo.gl/VvHC72

Writing great research...

Prepare yourself before you start Before you start writing your paper or you start reading other...

Read complete here:
https://goo.gl/np73jP

Journal Content
In this Issue

London Journals Press

Editorial Board

Curated board members

Monitoring Unsteady Thermal-Stress State of Large Power Steam Turbines based on Mathematical Modeling – Semi-Centennial

Dr. Alexander S. Leyzerovich

ANNOTATION

Transients of large power steam turbines with the single capacity of 250-300 MW and more should be run based mainly on the unsteady thermal-stress state of the high-temperature rotors monitored with the use of mathematical modeling by means of computing techniques at disposal under power plant's real operational conditions. The problem was articulated and practical work started about half a century ago.

Keywords: large power steam turbines; high-temperature rotors; valve steam-chests; unsteady thermal-stress state monitoring; radial temperature differences; mathematical models; operator's errors at running transients.

Classification: DDC Code: 330.028 LCC Code: HB139

Language: English

London Journals Press

LJP Copyright ID: 392951
Print ISSN: 2631-8474
Online ISSN: 2631-8482

London Journal of Engineering Research

Volume 22 | Issue 7 | Compilation 1.0

Monitoring Unsteady Thermal-Stress State of Large Power Steam Turbines based on Mathematical Modeling – Semi-Centennial

Dr. Alexander S. Leyzerovich

ANNOTATION

Transients of large power steam turbines with the single capacity of 250-300 MW and more should be run based mainly on the unsteady thermal-stress state of the high-temperature rotors monitored with the use of mathematical modeling by means of computing techniques at disposal under power plant's real operational conditions. The problem was articulated and practical work started about half a century ago.

Reasonable is to apply the same approach (as to the rotors) to monitoring unsteady thermal-stress state of the HP valve steam-chests what is especially essential for supercritical- and ultra-supercritical-pressure turbines. Special field studies as well as long-term practice of operation have confirmed that introducing operational monitoring of non-stationary temperature and thermal-stress states of the turbine at the transients makes it possible to identify operator errors that usually remain unnoticed with the traditional approach, creates conditions for improving the quality of operation and extending the turbine service life. The quality of monitoring based on mathematical modeling to a large extent depends on reliability and representativeness of primary heating steam temperature measurements. It should be expected that in the nearest future under conditions of commissioning dominantly energy producers on renewable sources and the unresolved problem of accumulating the excess and covering the deficit of produced energy, a significant part of large fossil-fuel steam-turbine power units will be forced to operate in cyclic and standby modes what retains the actuality of the considered problem.

Keywords: large power steam turbines; high-temperature rotors; valve steam-chests; unsteady thermal-stress state monitoring; radial temperature differences; mathematical models; operator's errors at running transients.

Author: Consultant, Mountain View, CA, the USA.

In these years of the early 2020s we could celebrate a semi-centennial anniversary of a kind of revolution in our views on running, controlling and monitoring large steam turbines at their transients, even though even nowadays the sense and results of this revolution are hardly completely accepted, as well as comprehended, learnt, employed and deployed.

What Was New? With raising the rated output of power steam turbines, the radial dimensions of their rotors enlarge too and for turbines with the single capacity of over 250-300 MW the unsteady thermal stresses in the rotors of the high temperature high-pressure (HP) and intermediate pressure (IP) or integrated HP-IP cylinders become the main factor limiting the rate of turbine transients: start-ups, shut-downs, load changes within the governed range, and so on.

Hence, the transients should be scheduled and run based on unsteady thermal stresses arising in the high-temperature rotors. Repeated, cycling action of these stresses is fraught with low-cycle fatigue cracking, especially in the case of inadequate quality of operation. These principal propositions have been generally recognized and articulated, and this understanding fundamentally changed our approach to the steam turbine transients–their pre-operating scheduling and setting, operational control and surveillance, as well as post-operating analysis [1-9].

London Journal of Engineering Research

In order to run the transients or follow up their automatic or automated control, the operator should be provided with feedback, that is, should have a possibility of monitoring the indices of unsteady thermal-stress state of the rotors just like for steam turbines of less capacity the operators have monitored temperature differences across the thickness of the most massive high-temperature casing elements. Since the direct, immediate thermometry of the turbine rotors for operating purposes is too laborious and unreliable, it should be substituted for modeling.

For the HP and IP or HP-IP rotors, their maximum thermal stresses take place on the outside, heated surface nearby the steam admission zone and can be characterized by so called "effective" metal temperature difference: of the heated surface in the most stressed section and the average integral metal temperature in the same section: $\overline{\Delta t} = t_s - \bar{t}$.

Some History. In the mid-1960s up to the early 1970s, in the absence of any computational techniques with sufficient experience of usage at power plants, it was unreal to use mathematical models of rotors in the operating purposes, and for the time being these mathematical models were substituted for physical ones. So, some large steam turbine producers, primarily Brown Boveri (aka BBC, then ABB, ABB Alstom and, finally, Alstom Power, which in 2015 merge in GE), Siemens (aka Kraftwerk Union AG) and Škoda, provided high-temperature cylinders of their large power steam turbines with so-called "thermometric probes" installed within the cylinder's intercasing space [7-10]. Such a probe

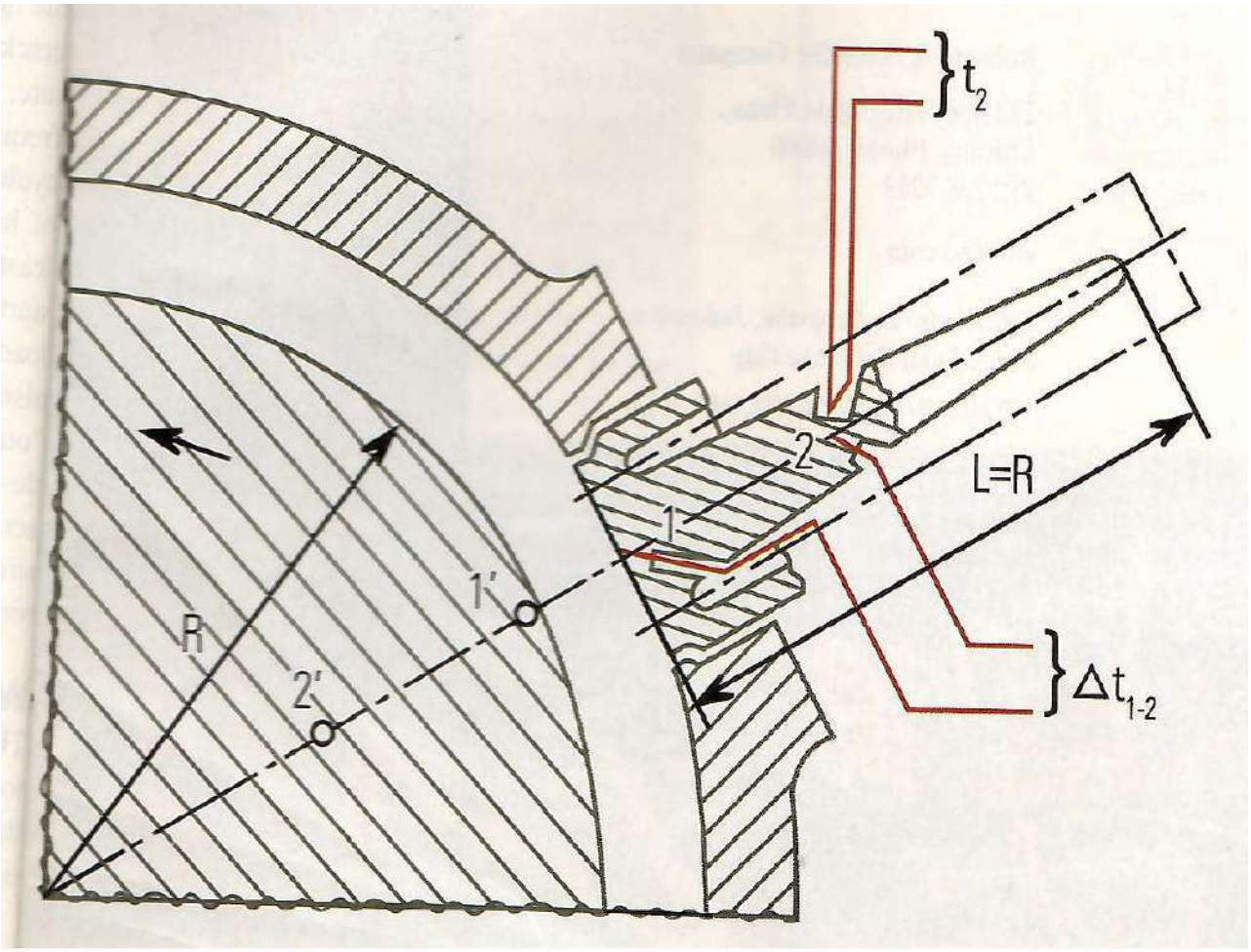

Fig. 1: Schematic of a thermometric probe used to model physically the rotor metal temperature state [8, 9]

as if imitates physically a sector of the rotor, and its butt-end is heated with the same steam flow that sweeps the rotor surface near the considered section. The use of differential iron-constantan thermocouples enables measuring directly the temperature difference between the probe's butt-end and mid-length that is believed to be close to the actual "effective" temperature difference in the rotor to be monitored.

This proxy method has several serious shortcomings. The main of them is that the true heat transfer conditions from steam to the rotor surface differ significantly from those for heated surfaces of stator pieces, including butt-end of the probe. As a result, the probe's butt-end surface temperature permanently lags behind variations of the actual surface temperature of the rotor, and the temperature difference measured in the probe occurs to be essentially less than the rotor's actual "effective" temperature difference to be monitored, more inertial and less sensitive to heating steam temperature excursions. Another immanent drawback is that heat fluxes from the probe's side surface can also produce essential methodical errors in modeling. What is more, it's not so easy to accommodate a probe in the narrow and crowded intercasing space of the turbine –

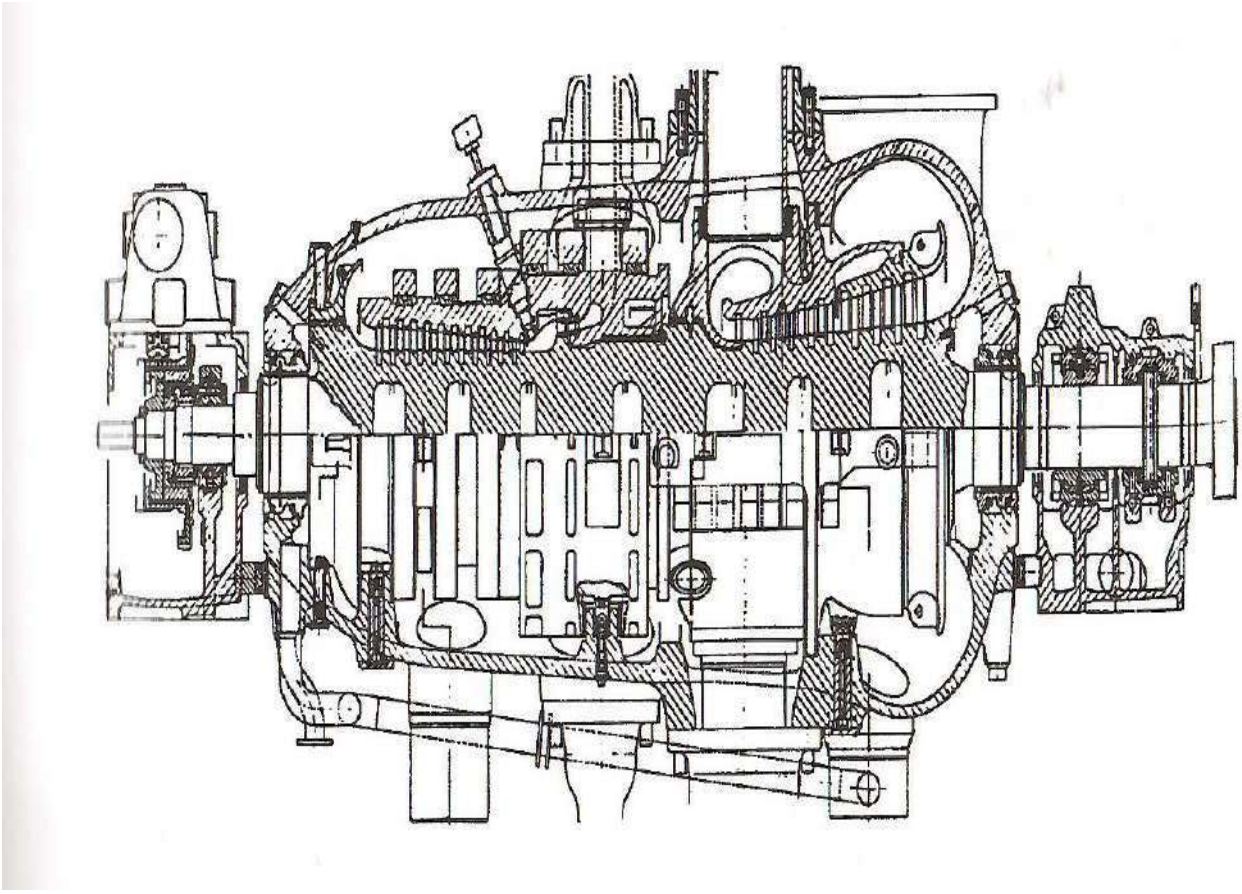

Fig. 2: Longitudinal section of the integrated HP-IP cylinder of 600-MW supercritical-pressure steam turbine of ABB (US power plant Cardinal) with a thermometric probe for the HP part of the rotor [10]

Adequate mathematical models materialized by means of analogous or digital computing techniques do not have these shortcomings. Even a quite simple, prototypical mathematical model shown in

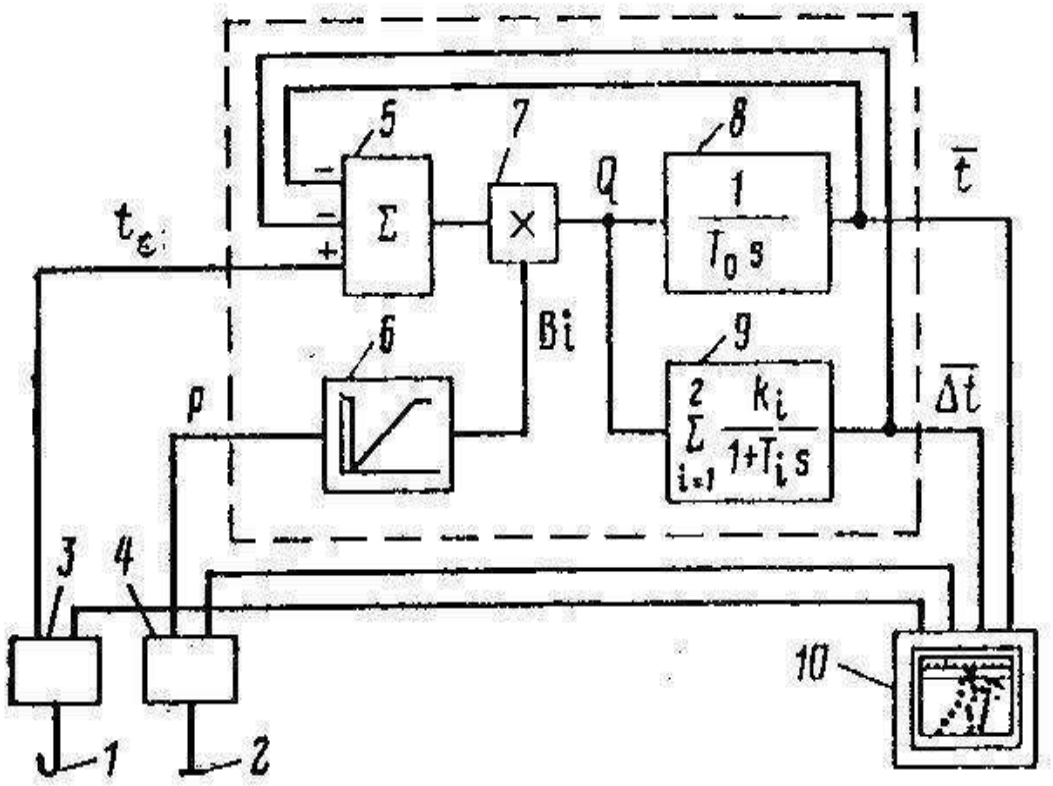

Fig. 3: Functional block-chart of a prototypical analogous model for monitoring the unsteady temperature and thermal-stress state of a turbine rotor [7, 8, 12, 13] 1 – heating steam temperature sensor, 2–steam pressure sensor, 3 and 4–unifying converters, 5–inlet adder, 6 – non-linear converter, 7 – multiplier, 8 – integrator, 9 – first order elements, 10 - multipoint recorder

provides the divergences between the actual (precisely calculated or gotten by means of experimental immediate thermometry) and monitored radial temperature differences making up not more than 10-13% what is quite acceptable for operational purposes [11-13]. Such a mathematical model did serve as a basis for analogous electronic devices for monitoring unsteady thermal-stress states of the HP and IP rotors as applied to widespread in the former USSR supercritical-pressure steam turbines with the output of 300 MW of two different types - produced by Leningrad Metallic Works (LMZ) and Kharkov Turbine-Generator Works (KhTGZ).

A pilot serial sample of such a device passed field tests in 1976-1977 at the HP cylinder of a 300-MW LMZ steam turbine with comparing its outputs with results of experimental immediate thermometry of the same rotor at the same transients fulfilled by the turbine manufacturer [13]. Some samples of such devices had been successfully employed and used at power plants for over 25 years [14].

The mathematical model shown in Fig. 3 is built using the method of approximate transfer functions [8, 11-13]. Values of the time constants T_0, T_1, T_2 and amplification factors k_1, k_2 of the model links are determined by the radial dimensions of the selected, most thermally stressed section of the rotor and the thermophysical properties of the rotor steel. The main problem of materializing this and similar models using analog technique has been the need to reproduce large time constants for rotors with a large shaft diameter (for example, for the forged double-flow IP rotor of 800-MW LMZ turbine T_0 = 9110 sec, T_1 = 1110 sec and T_2 = 310 sec [11-13]).

Because the heat flow from steam to the rotor surface and further along the rotor's radius is much more intense than the heat fluxes by thermal conductivity through the rotor body in the axial direction, the use of a one-dimensional model is believed to be quite justified. The model itself consists of the integrator and few first order elements connected in parallel and closed with the negative feedback. Their outputs are just the variables to be monitored: the average integral metal temperature $\bar{t}$ and "effective" temperature difference $\overline{\Delta t}$ for the considered section. These variables, together with the input ones, are brought to a multipoint recorder. The model's inputs are fed with the normalized (unified) measured signals from the sensors of the heating steam temperature t_{st} (at the HP control stage or in the IP steam admission chamber) and steam pressure p as an indicator of the steam flow amounts through the turbine cylinders. The output signal of the inlet adder corresponds to the temperature difference between heating steam and the heated rotor surface. Multiplied by the value of Biot number *Bi* (dimensionless heat transfer coefficient), it turns into the heat flow Q in the units of temperature. A non-linear converter materializes the dependence $Bi(p)$, which approximates results of calculating the heat transfer coefficients on the rotor surface at the considered section with the use of well-known criteria equations $Nu = f(Re, Pr)$ [7, 8]. The initial (pre-start) rotor metal temperature (before steam enters the cylinder) is accepted as following up the temperature measured by the thermocouple for the heating steam temperature t_{st}. So, if the measured value of steam pressure p within the cylinder is less than its set minimum value, the converter brings the signal equal to the maximum value of *Bi* to the multiplier.

Appearance of microprocessor-based freely programmable controllers (so called REMICONT™) made it possible to extend the gotten experience to other turbine types (in particular, supercritical-pressure 800 MW turbines of LMZ) and raise the accuracy of modeling due to some complications of the applied models [12-14]. In particular, the advanced model took into consideration the dependence of the metal thermal diffusivity on the metal temperature, as well as the influence of the turbine rotation speed on the heat transfer conditions on the rotating surfaces. The rotation speed signal was also employed for more precise identification of the instance when steam enters the cylinder, and before this instance the rotor temperature $\bar{t}$ was taken equal to the regularly measured metal temperature of the cylinder's casing. Possibility of varying freely the model's scheme made it also possible to reproduce different for diverse turbine types correlations between the measured steam temperature(s) at the IP entrance and heating steam temperature for the most stressed IP rotor section following results of special measurements in the process of field tests [8].

The widespread use of computer-based Data Acquisition Systems (DASs) at power plants made it possible to attract computers to solution of the set task – on-line monitoring the thermal-stress state of the steam turbine rotors. This task can also be considered with more general statements of the problem – as a part of a computerized system of complex diagnostic monitoring for the power plant unit as a whole or a local subsystem of diagnostic monitoring for the turbine, or a system of informative support for the operator at the turbine transients, and so on. Such systems can be arranged based on the "common" computer(s) of the unit's or the plant's DAS or with the use of an additional PC connected to the DAS' database or directly (via unified transformers) to the turbine measurements [13-16].

With transition to the use of digital computing techniques, it seems advisable to employ mathematical models based on the finite difference method (preferably in its simpler explicit form) rather than the aforesaid method of approximate transition functions [11, 12]. The former gives even more freedom for taking into consideration different factors influencing the model's accuracy. For monitoring the temperature and thermal-stress state of the HP and IP rotors of diverse steam turbine types as applied to the

aforesaid systems and subsystems, it has been believed reasonable to develop and use a united calculation algorithmic module named "CONTUR"–common for various large power steam turbines and for diverse types of computing means and complexes, as well as diverse program systems and computer languages [8, 12-16]. The algorithm is adapted to the specific turbine type by setting the "key" input constants, including the radial sizes of the HP and IP rotors, the dependences of the metal's thermal diffusivity on the metal temperature $a(\bar{t})$ and heat transfer conditions for the considered rotor sections on the rotation speed n and steam pressure p within the turbine Bi (n, p), as well as correlation characteristics for the heating steam temperatures as applied to the HP and IP rotors and steam temperatures available for measuring, the values of n and p indicating steam entering the turbine, the way of setting the rotors' metal temperatures at the stopped turbine, the addresses of the measured input and calculated output variables in the data base.

Monitoring thermal-stress state of the HP valve steam-chests with the use of mathematical models. In just the same way as for the HP and IP rotors, similar mathematical models can be applied to temperature monitoring some turbine stator elements if they turn out to be "critical" in some pieces of transients along with the high-temperature rotors. This mainly refers to the HP stop-valve steam-chests. Commonly, their thermal-stress state is characterized by the temperature difference across the wall thickness (sometimes with some correction for the metal temperature unevenness in the axial direction, that is along the wall height [7, 8]). It presupposes drilling the steam-chest wall especially for measuring the metal temperature directly on the heated surface or within its immediate vicinity, what is equally undesirable because lowers the steam-chest wall strength. The alternative is to calculate on-line the metal temperature distribution across the wall thickness with the use of a sufficiently accurate even though quite simple mathematical model, regularly measured steam temperatures before the HP stop-valves and metal temperatures on the external, thermally insulated surfaces of the valve steam-chests. The main problem is to set the heat transfer conditions from steam to the inner steam-chest surface depending on the steam flow through the valve. The required dimensionless equation Nu = f (Re, Pr) for sufficiently widespread design types of the HP valve steam-chests was gotten based on processing results of special field tests [7, 8, 13, 14]. It's also necessary to find an approximate empiric dependence between the steam flow amounts through the HP valves, steam pressure before the HP stop-valves and within the turbine, vacuum in the condenser, rotation speed and its acceleration while rolling up, etc.

Results of monitoring. As shown in Fig. 3, the input and output data of the models employed for monitoring the thermal-stress state of the turbine rotors, their change in time during the turbine transients may be brought on regular multipoint recorders. These data are to be used on-line by the operator for running the turbine transients, and the same diagrams are used by the power plant engineers for post-operative analysis and evaluation of the operation quality [8, 14, 17].

With the use of computerized DAS, operative information is presented in the most convenient for the operator graphic forms on the monitor(s) on the operator request, and the stored data are intended for post-operative analysis, including estimations of thermal fatigue of the rotor metal caused by the transients [12, 14-17].

The first experience of using analogous electronic and microprocessor-based mathematical models of the turbine rotors at the 300-MW power units revealed serious errors in the practice of operation. By that time, many of 300-MW supercritical units were operated under conditions of regular shut-downs for week-ends and nights with subsequent "warm" or "hot" start-ups and/or deep unloading within the limits of the governed range in the week-day evenings with subsequent raising the load up to the rated value in the morning. With regard to this circumstance and on agreement with the turbine manufacturers, the admissible ranges of varying the "effective" temperature differences in the rotors were set equal: as applied to the HP rotors for start-ups – from +25 °C to –20 °C and within

±20 °C for load changes within the governed range and as applied to the IP rotors correspondingly - from +40 °C to –25 °C and within ±25 °C [7, 8, 13].

Actual values of the monitored temperature differences in certain cases remarkably and repeatedly exceeded these limits, and it required hard work with the power plant's operational personnel, including post-operative analysis of monitoring results and correcting, if necessary, the power plant's operation manuals. Such work resulted in substantial reduction of a number and depth of violations for the set temperature difference resulted in essential violations of the set limits for the rotors. Introduction of such monitoring accompanied with special training the power plant's operational personnel makes it possible to avoid operative errors in running the transients without sacrifice of turbine flexibility or at least make these errors less frequent and influential -

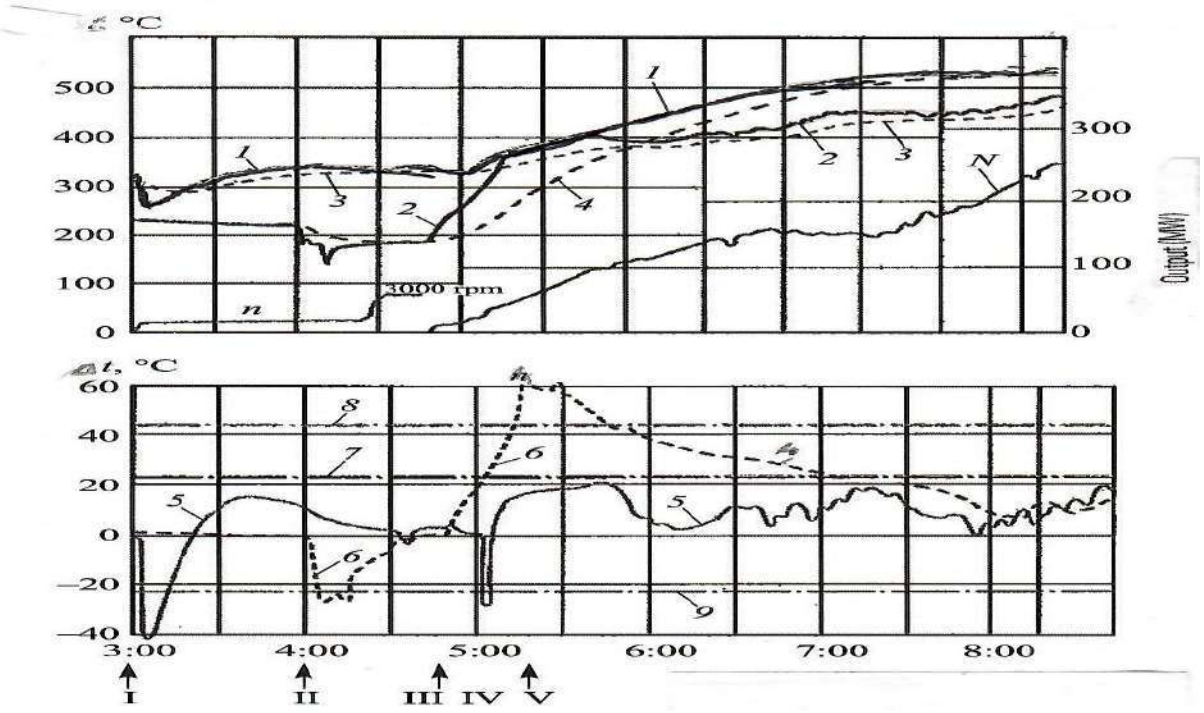

Fig. 4: Results of monitoring temperature and thermal-stress states of the HP and IP rotors of 300-MW supercritical-pressure steam turbine of LMZ for a regular "warm" start-up after a week-end outage [8. 9]

1 and 2 – measured steam temperatures at the HP control stage and in the IP the HP and IP rotors, respectively, in their monitored (most thermal-stressed) sections, 5 and 6 -effective radial temperature differences in the monitored sections of the HP and IP rotors, 7 and 8 –upper (positive) admissible values for effective temperature differences in the HP and IP rotors respectively, 9 –lower (negative) value for the both HP and IP rotors Operative actions: I – the HP valves open, steam enters the HP cylinder with the IP intercept valves closed (too early, before heating the main-steam-lines is finished), II - the IP intercept valves open and steam enters the IP cylinder (somewhat early, before heating the hot-reheat-steam-lines is finished), III –the turbogenerator is synchronized and switched on to the grid, IV – the reheater's steam bypass valve open (5 min too late after synchronization)

Several fragments of genuine regular diagrams with recorded results of temperature and thermal-stress monitoring for the HP and IP rotors of a 300-MW supercritical turbine of LMZ as a part of a coal-fired power unit in the course of a warm start-up after the week-end outage and daily load changes can be seen in

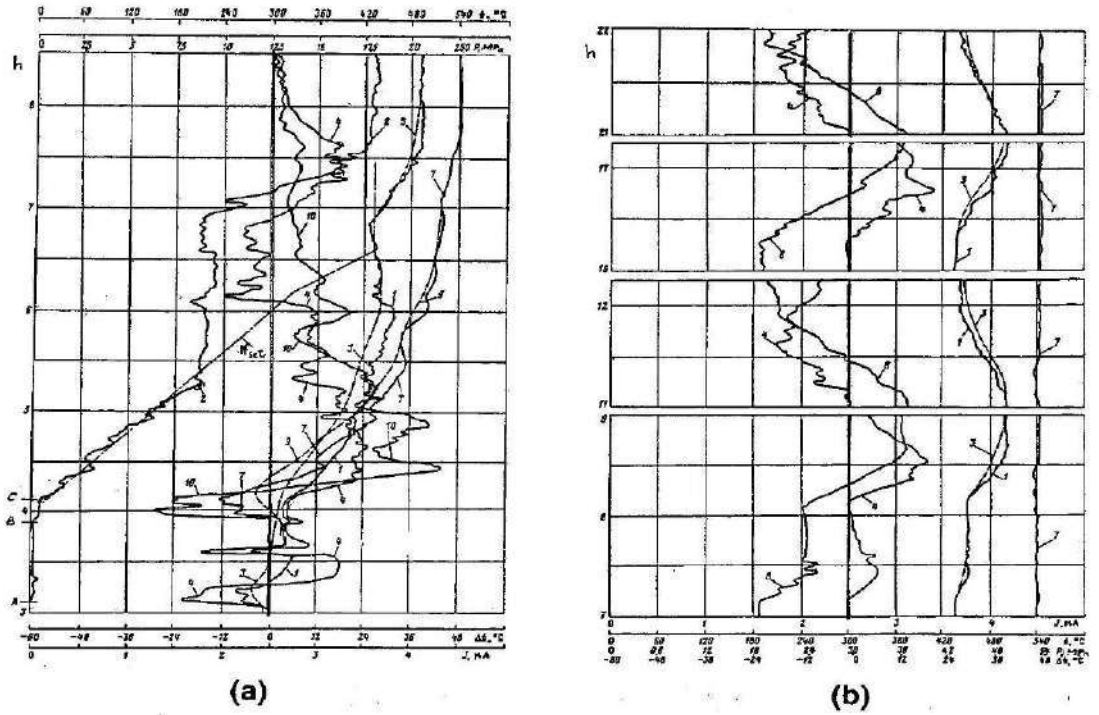

Fig. 5: Fragments of a regular diagram with recorded results of monitoring the HP and IP rotors of 300-MW supercritical-pressure steam turbine of LMZ at start-up after week-end outage (a) and daily changes of the load (b) [18]

Recorded variables: 1 and 2 – steam temperature and pressure at the HP control stage, 7 and 8 – steam temperature and pressure in the IP steam admission chamber, 3 and 9 – average integral metal temperatures of the HP and IP rotors in the most stressed sections, 4 and 10 – effective radial temperature differences in the most stressed sections of the HP and IP rotors

Notes on the diagram: N_{set} - instruction schedule of loading, A - giving steam into the HP cylinder for raising the rotation speed up to 900 rpm with closed IP intercept valves, B – end of heating up the reheat steam-lines and giving steam into the IP cylinder with raising the rotation speed up to 3000 rpm, C – connecting the generator to the grid with closing the turbine bypass, accepting the initial load, and opening the bypass valve of the boiler's steam reheater

[18]. Therewith, all the monitored indices of the turbine's temperature and thermal-stress states, including "effective" temperature differences in the HP and IP rotors, do not exceed their limits.

Recorded data of long-term monitoring the unsteady thermal-stress state of the supercritical 300-MW sister turbines at several power plants were used to calculate specific rotor metal lifetime expenditures caused by low-cycle (thermal) fatigue. These calculations were carried out together with Prof. A.D. Trukhny of the Moscow Power Engineering Institute (Technical University) and following his methodology [19, 20]. At some of the mentioned power plants, the transients were run practically without regard to thermal-stress monitoring of the rotors, whereas at others the transients were attentively controlled with the feedback of the monitored and recorded data. The results of aforesaid calculations (see Table) show that in the first case the values of specific low-cycle fatigue are up to two orders of magnitude greater than in the second case. It's also important to note that, without monitoring the rotors, the plant's operators and engineers usually were not able to recognize and prevent the operational errors that caused undesirable heating steam temperature excursions, inadmissible thermal stresses in the rotors, and

resultant increased lifetime expenditures. With on-line thermal-stress monitoring of rotors, the turbine transients are endured with greater load change rates, lower fuel losses and turbine lifetime expenditures.

Table 1: Variations of specific low-cycle fatigue values at the characteristic transients (in % lifetime expenditure per cycle) for the HP and IP rotors of a few 300-MW supercritical steam-pressure turbines of KhTGZ [19]

Cycles of transients and the way of running them	HP rotor	IP rotor
Shut-down for weekend (48-54 h) and subsequent warm start-up - without mandatory monitoring the rotors - with mandatory monitoring the rotors	0,065 ÷ 0,130 0,0025 ÷ 0,005	0,20 ÷ 0,81 0,06 ÷ 0,10
Shut-down for night (6-8 h) and subsequent hot start-up - without mandatory monitoring the rotors - with mandatory monitoring the rotors	0,1÷ 0,5 0,0025 ÷ 0,05	0,20 ÷ 0,35 0,05 ÷ 0,08
Load changes within the governed range - under sliding main steam pressure - under constant main steam pressure	0,002 0,01	0,0025 0,0025

Main obstacles for widespread use of monitoring the unsteady thermal-stress state of the turbine rotors based on their mathematical modeling. In consequence of more intense heat transfer conditions from heating steam to the heated rotating surfaces as compared to casing components being more inertial in its heating up process, requirements to the quality of running the turbine transients based on monitoring the thermal-stress state of the rotors are remarkably higher and conversion to running the transients in such a way at once brought to exposure of numerous operational errors that earlier remained unnoticed or at least were considered insignificant, required to change some habitual stereotypes in operation. It's quite natural that such a conversion was met with certain distrust, psychological resistance and required some special training for not only the operational personnel but also for the power plant's engineers and authorities. Where such training did not take place, introducing the new approaches to running the transients was ignored or bore rather formal character.

But the most serious, objective obstacle has been a problem with measuring the heating steam temperatures, especially for the HP rotors. Unfortunately, in the operation practice there repeatedly happened breakdowns of protective heads of these thermocouples with necessity to stop the turbine. That is why turbine producers often prefer to waive these measurements.

As to the heating steam for the IP rotor, it can be accepted equal to the measured steam temperature at the IP section inlet (within the steam admission sleeves) with some calculated static and dynamic corrections depending on the steam flow amount through the IP section (in particularly, such special researches were carried out on the IP cylinder of 800-MW supercritical-pressure steam turbine of LMZ [21]). Unfortunately, such an approach is not suitable for the HP sections, especially if the turbine is operated with nozzle-group control.

So, for computing devices called Turbine Stress Evaluator and Turbine Stress Controller of Siemens as constituents of its automatic monitoring and control system [17, 22, 23] the measured temperature on the heated surface of the probe installed into the cylinder casing is considered to be representative for the rotor heated surface, and the temperature difference characterizing the rotor's thermal-stress state is calculated based on this temperature. As it was noticed above, such a solution causes a significant error. As applied to another specialized computing device called "Tensomax" developed by ABB for retrofitting steam turbines without measuring the steam temperature in the HP steam admission chamber, the heating steam temperature and heat transfer conditions to the heated surface in the most stressed section to be monitored are calculated based on the available steam temperature and pressure measurements

inside a nearest interim chamber in the casing or at the casing outlet [17, 24, 25]. It's needless to say that such an approach is also fraught with remarkable errors in monitoring. It would be desirable to arrange more reliable measurement of the heating steam temperature at the HP cylinder's entrance. Without reliable and representative heating steam temperature measurements, it's a vain hope to achieve representative monitoring.

What's ahead? Nowadays, the modern power industry is characterized by a dominant growth in the installed capacity of electricity producers from renewable sources - solar and wind power plants with significantly lower values of their capacity utilization factors compared to nuclear and fossil-fuel power plants as a result of uncontrolled, predictable or completely stochastic daily and seasonal changes in electricity generation. Under these conditions, with insufficient development of compensating systems for accumulating surpluses and filling the deficit in electricity production, it is almost inevitable that many fossil-fuel and possibly some nuclear power plants, will shift to work in a cyclic and stand-by modes [26]. This will make the temperature and thermal-stress state monitoring of large steam turbines based on mathematical modeling especially urgent.

It could also be said that monitoring the thermal-stress state of large power steam turbines based on mathematical modeling can be considered the first step in digitalizing fossil-fuel power plants of the next generation and their operation. General Electric, being with its Predix cloud-based platform an initiator and a clear leader of this movement, takes aim at creating "a digital twin of the physical steam plant that is continuously monitored in real time…" [27].

Therewith, the author declares that "today's power plant operators are only reading approximately 2% of the available data we have from typically more than 10,000 sensors on control systems across the plant. By analyzing the other 98% of the data and really optimizing whole plant operations…, efficiency and flexibility can be significantly improved". To tell the truth, I'm not sure that these 10,000 measurements will be really necessary and even involved in solution of the set problems. Rather part of them may be useful for complex technical diagnostics and prognostics of the power units, planning their maintenance and overhauls based on their current state, scheduling their most efficient operating conditions, and so on. At least as applied to the power unit's flexibility this problem should be solved with the use of complex mathematical models and indices which cannot be built and perceived by human beings as power plant operators. And it is not so substantial which techniques is processing the measured data – of importance is if these measured data are reliable and representative as well as the used mathematical models.

General Electric with good reasons considers the aims of digitalization as applied to the next generation of coal-fired steam-turbine-based power units with ultra-supercritical steam conditions (a coal power technology called SteamH). As the prototype under consideration is the power unit already in operation - 912-MW RDK8 (Karlsruhe, Germany) for steam parameters of 275 bar, 600/620 °C (the boiler and turbine were produced by Alstom [28]), as well as a similar to it Manjung 4 in Malaysia. It may be definitely said that the transients of such units are predominately limited by thermal stresses in the HP rotor, as well as in the steam admission zone of the double-flow IP rotor at start-ups and in the HP stop-valve steam-chests at pre-start heating up and rolling up the turbine.

The thermal-stress states of all these turbine components should be monitored based on their mathematical models with the use of maybe cloud-based platform.

REFERENCES

1. Pahl G., Reitze W., Salm M. "Observance of Admissible Thermal Stresses in Steam Turbines" (in German), BBC-Nachrichten, 1964 (vol. 46), No. 3, pp. 139-147.
2. Berry W.R. and Jonson I. "Prevention of Cyclic Thermal Stress Cracking in Steam

Turbine Rotors", Transactions of the ASME, ser. A, 1964, No. 3, pp. 361-368.
3. Timo D.P. and Sarney G.W. "The Operation of Large Steam Turbines to Limit Cyclic Thermal Cracking", Paper ASME 67-WA/PWR-4, 1967.
4. Leyzerovich A. "Limitations for Start-ups of Large Steam Turbines Based on the Strength of Their Rotors" (in Russian), Teploenergetika, 1971 (vol. 18), № 10, pp. 88-91.
5. Spencer R.C. and Timo D.P. "Starting and Loading of Large Steam Turbines", Proceedings of the American Power Conference, Chicago, 1974 (vol. 36), pp. 511-521.
6. Hohn A. "Steam Turbines on Start-ups", Combustion, 1976 (vol. 47), No. 8, pp. 21-32.
7. Plotkin E.R, Leyzerovich A.Sh. StartUps of Steam Turbines in Power Plant Units (in Russian). Energiya, Moscow: 1980.
8. Leyzerovich A. Large Power Steam Turbines: Design & Operation. 2 vols. PennWell Books, Tulsa (OK): 1997 (as well Tech Book International, New Delhi: 2007).
9. Leyzerovich A. "Reduce stress with proper on-line rotor temperature monitoring", Power, 2007 (vol. 151), No. 5, pp. 48-52.
10. Mülhäuser H, Eckert F. "Steam Turbines in Power Stations for Peak and Medium Load", Combustion, vol. 48 (1977), No. 9, pp.11-23.
11. Leyzerovich A.Sh., Kozlov V.N., Mironov V.D. et al. "Thermal Monitoring of Steam Turbine Rotors with the Use of Analogous Models" (in Russian), Teploenergetika, 1977, No. 8, pp. 10-13.
12. Leyzerovich A.Sh. "Mathematical Modeling of Large Steam Turbine Rotor HeatingUp for Operational Monitoring", Bulletin of the USSR Academy of Sciences. Power Engineering and Transport, 1981, No. 2, pp. 121-131.
13. Leyzerovich A.Sh. Technological Foundations for Automation of Steam Power Turbine StartUps (in Russian). Energoatomizdat, Moscow: 1983.
14. Leyzerovich A.Sh., Plotkin E.R. "Developing Temperature and Thermal-Stress State Monitoring for Rotors of Large Steam Turbines" (in Russian), Elektricheskie Stantsii, 2016, No. 6, pp.51-59.
15. Leyzerovich A.Sh., Safonov L.P., Zhuravel A.M., et al. "Automated Diagnostic Systems and Subsystems for Fossil Power Plant Units: the Experience of Designing and Operational Mastering in the Former USSR", Proceedings of the American Power Conference. Chicago, 1993, Vol. 55. Part 1, pp. 881-885.
16. Leyzerovich A. "PC Based Operative Information Support at Transients and Their Postoperative Analysis in Reference to Steam Turbines", Proceedings of the American Power Conference. Chicago, 1994, Vol. 56, Part 1, pp. 36-40.
17. Leyzerovich A. Steam Turbines for Modern Fossil Fuel Power Plants. The Fairmont Press, Lilburn (GA): 2007.
18. Leyzerovich A.Sh., Tikhonova K.N., Kuzmin A.F., et al. "Experience of LongTerm Operational Monitoring the Temperature State of the HP and IP Rotors for LMZ Steam Turbines K-300-240" (in Russian), Elektricheskie Stantsii, 1988, No. 3, pp. 3035.
19. Leyzerovich A.Sh., Trukhny A.D., Grak V.G., et al. "LowCycle Thermal Fatigue of Steam Turbine Rotors at Transients" (in Russian), Elektricheskie Stantsii, 1989, No. 11, pp. 61-67.
20. Trukhny A.D., Leyzerovich A.Sh., Grak V.G., Shishko A.Yu. "Diagnostic Monitoring of Accumulation of LowCycle Thermal Fatigue Damage to the Rotor Metal of a Steam Turbine" (in Russian), Teploenergetika, 1989 (vol. 36), No. 12, pp. 40-45.
21. Avrutsky G.D., Leyzerovich A.Sh., Nakhimov V.I., Ostrovetsky R.M. Steam temperature variations within the IP steam path of the 800-MW turbine" (in Russian), Teploenergetika, 1981 (vol. 28), No. 1, pp. 20-23.
22. Sill U., Zörner W. Steam Turbine Generators Process Control and Diagnostics, Publicis MCD Verlag, Erlangen: 1996.
23. Termuehlen H. 100 Years of Power Plant Development. Focus on Steam and Gas Turbines as Prime Movers, ASME Press, New York: 2001.
24. Šindelař R., Toewe W. "Thermal Stress Monitoring of Steam Turbines" (in German), BWK, 1999, No. 10, pp.46-49.

25. Šindelař R., Toewe W. "TENSOMAX – a Retrofit Thermal Stress Monitoring System for Steam Turbines", VGB PowerTech, 2000 (vol. 80), No. 1, pp. 41-43.
26. Leyzerovich A.Sh. "Redistribution of Roles in Covering Energy Production and Consumption" (in Russian), Elektricheskie Stantsii. 2020, No. 1, pp. 36-40.
27. Keroulle M. SteamH raising the bar", Moderr Power Systems, 2018, No. 4, pp. 30, 31.
28. Stamatelopoulos G., Lorey H. "The RDK 8 Ultra-Supercritical boiler, a showcase for the next coal-fired plant generation" (in German) *VGB PowerTech*, 2016 (vol. 86), No. 3, pp 27-32.

Contact Angle and Wettability of Commercial Polymers after Plasma Treatment

Péricles Lopes Sant'Ana, José Roberto Bortoleto & Steven F. Durrant

State University of São Paulo

ABSTRACT

Polymers have a wide range of applications in different manufacturing areas, including 'food packaging'. This is mainly due to properties, such as excellent thermal stability, low density and low cost. In recent studies regarding the surface treatment of PVC. This material showed interesting properties such as, low roughness, high transparency in the visible range, and hydrophobic or hydrophilic surfaces. Possible alterations of the surface of PVC may be produced using plasma technology at low- temperature (in many cases the treatment can be achieved at room temperature, which avoids the thermal degradation of the material).

Keywords: wettability, plasma treatment, surface analysis, commercial polymers.

Classification: DDC Code: 547.7 LCC Code: QD381

Language: English

London Journals Press

LJP Copyright ID: 392952
Print ISSN: 2631-8474
Online ISSN: 2631-8482

London Journal of Engineering Research

Volume 22 | Issue 7 | Compilation 1.0

Contact Angle and Wettability of Commercial Polymers after Plasma Treatment

Péricles Lopes Sant'Ana[α], José Roberto Bortoleto[σ] & Steven F. Durrant[ρ]

ABSTRACT

Polymers have a wide range of applications in different manufacturing areas, including 'food packaging'. This is mainly due to properties, such as excellent thermal stability, low density and low cost. In recent studies regarding the surface treatment of PVC. This material showed interesting properties such as, low roughness, high transparency in the visible range, and hydrophobic or hydrophilic surfaces. Possible alterations of the surface of PVC may be produced using plasma technology at low-temperature (in many cases the treatment can be achieved at room temperature, which avoids the thermal degradation of the material).

Among the techniques applied for PVC, PET, LDPE, PP or other polyolefin surface modification, Plasma Immersion techniques were recently studied in three different electronic configurations: (i) sample grounded (anode), (ii) sample polarized by radiofrequency (cathode), (iii) sample polarized with high voltage negative pulses (PIII) using fluorine plasmas at low temperature. To our knowledge, there is no extant literature that compares those three different configurations of PECVD techniques, focusing on the gain in thermodynamic properties (wettability and surface roughness).

Θ values for the polymers investigated depend strongly on the treatment conditions such as: the pressure, treatment time, rf power, and the gases used. Stop and Range Ions in Matter software was used to simulate the thickness of the modified layers, especially for high energies treatments, for the three polymers (targets) investigated, and some parameters of Simulation were reported.

Keywords: wettability, plasma treatment, surface analysis, commercial polymers.

Author α: State University of São Paulo – UNESP Technological Plasmas Laboratory, Av. Três de Março 511, Alto da Boa Vista, Sorocaba, SP, Brazil. 18087-180. Orcid: 0000-0002-8590-6260.
σ: Orcid: 0000-0003-4129-7819.
ρ: Orcid: 0000-0002-4511-3768.

I. INTRODUCTION

1.1 Surface treatments of polymers using Plasma: Preliminary Considerations

Polymers have a wide range of applications in different manufacturing areas, such as food packaging, surgical implants and automobile production. This is attributable to properties such as excellent thermal stability, low density and low cost [1]. Hence, new techniques are being sought to optimize surface modification processes of polymers and reduce costs [2].

Some polymers are characterized by an inherently low to moderate surface energy (or surface tension), which accounts for why liquids form bead-like drops instead of wetting the surface, and why coatings tend to adhere only poorly, if at all. However, when the surface is functionalized by exposure to a plasma [3], its energy can be raised and the above-mentioned problems overcome. These principles find application in all industries that make extensive use of plastics, be it in packaging, health care, textiles, etc.

The use of plasma treatment can improve the surface properties of polymers. Such techniques form an environmentally friendly alternative to conventional surface modification methods [4].

Plasma surface treatment is of great interest because it allows the modification of surface characteristics to, for example, obtain adhesion to other layers, or improve wettability or permeability to gases, without affecting the bulk

properties of the polymer [5, 6]. Plasma-induced effects on the polymer surface are nowadays exploited in surface functionalization of packaging polymers, for promoting adhesion or enhanced printability [7].

Using plasma, one can increase the surface energy of polymeric substrates in an environmentally friendly process without the use of wet chemistry.

Plasma activates polymeric surfaces by producing free radicals in the polymeric chain and thus creating new functional and reactive molecular groups [8].

One purpose of fluorinating polymers is to increase hydrophobicity, thus producing an anti-sticking surface, also characterized by low friction, corrosion resistance, low flammability, low refractive index, low dielectric constant, and water/oil repellence properties. It has also been reported that direct fluorination by immersion is an effective method to improve the surface properties of virgin polymeric materials, including barrier properties, adhesion, printability, gas separation properties, chemical resistance, antibacterial properties (biocompatibility), etc. [9]. Moreover, fluorinated polymers can be useful in the preparation and manufacture of organic light emitting diodes (called OLEDs) which require a transparent and conductive electrode (TCO) both for the injection of charge carriers and to transmit the emitted light output. In this context, to fully exploit the flexibility of large electronic devices based on this technology (such as TV monitors, flexible light panels and even solar cells), it is essential that TCO be deposited on plastic substrates, which automatically prohibits the use of high temperature processing techniques. In this case, low-temperature treatment/deposition methods become essential for technological progress in this area of opto-electronics [10].

Thus, new technologies may be applied for those purposes [11]. Among them, plasma surface treatments cause the improvement of surface polymers, as reported by Pankaj [12], Gorjanc [13-14] and Lopez-Garcia [15-16]. Plasma-induced effects on the polymer surface are nowadays exploited in surface functionalization of packaging polymers, for promoting the printability for the treated polymer [17], and assuring anti-mist properties and antibacterial coatings as reported by Primc [18], Gorjanc [19], Popelka [20], Asadinezhad [21] and Sulovska [22], which are of interest for food packaging.

Properties modified by plasma treatment of polymeric materials include the wettability, the surface functionalization, and adhesion. This may be necessary for the food-packaging coating in foils with antibacterial layers [23]. Some processes such as painting and gluing may also be improved [24].

Other polymers had their surfaces changed using Atmospheric Pressure Plasma treatments (APPT) [25]. To functionalize the surface of blown low-density polyethylene (LDPE) and cast polypropylene (CPP) films, and ultimately to maximize the attachment of active molecules onto them, the optimum treatment parameters of capacitively-coupled radio-frequency (13.56 MHz) oxygen plasma have also been investigated [26].

1.2 The use of Different Plasma Techniques

We start this section citing some techniques for the surface treatment of polyolefins such as APPT, corona discharge, sol-gel, atomic layer deposition, and chemical vapor deposition. In particular, PECVD (Plasma Enhanced Chemical Vapor Deposition) allows the production of films that exhibit a wide range of properties through the control of the process parameters. Examples include the insulating / conductive layers (with controlled thickness) which are used in the manufacture of electronic devices, transparent films suitable for application as optical windows, anti-reflective layers, coatings of lenses or sports glasses. Biocompatible and hydrophobic films suitable for applications in food packaging or solar cells [27].

More intense changes are obtained when the sample is exposed to plasma subjected to polarized pulses of high negative voltage, thus attracting positive ions. The interaction of these energetic ions with the atoms of the solid can cause excitation, ionization, bond breaking,

emission of species and atomic displacements, thus producing compositional changes and structural rearrangements. This process is known as Plasma Immersion Ion Implantation (PIII) [28], and was created to overcome certain limitations of conventional implantation with ion beams.

Compared with conventional methods, plasma treatment has many advantages, such as lower consumption of reagents and energy, producing no waste water, being non-hazardous, dry, fast and environmentally friendly. Moreover, bulk properties are unaffected [29-31]. In addition, it is possible to produce functionalized surfaces using low pressure plasmas. The top 10 to 50 Å of a polymer surface may be altered, without affecting the bulk properties [32]. The study of the induced changes is important for new and advanced technological fields, such as optoelectronics, microelectronics, filters, electrochemical sensors, medicine, etc. [33]. In this sense, glow discharge plasma-based treatments are of particular interest because they allow surface hydrophilization without producing bulk modifications. However, the instability of the modified surfaces limits their use in many applications [34, 35].

Investigations have shown that ions are the most efficient species in the plasma for modifying polymer surfaces. Since the penetration depth of low energy ions in a solid is extremely small, ions seem to be very important for modification of the first few nanometers of the polymer during plasma treatment. Using plasma, one can increase the surface energy of polymeric substrates in an environmentally friendly process without the use of wet chemistry. Plasma activates polymeric surfaces by producing free radicals in the polymeric chain and thus creating new functional groups [36]. There are many techniques that can be used to modify or alter the surface properties of materials by the addition of coatings and functional groups [37, 38].

The partial hydrophobic nature of polyolefins, i.e., PET results in poor uptake and adhesion of dyes, particles and microcapsules [39], which reinforce the importance of treatment to improve the wettability of polyolefins, or even to create hydrophobic surfaces.

In this chapter we discuss the effects of low pressure plasmas on the wetting of commercial polymers. Depending on the plasma composition, process temperature and technique applied, it is possible to obtain hydrophobic or hydrophilic surfaces. As noted before, the treated material finds many applications.

II. CONTACT ANGLE MEASUREMENTS

When a drop of a liquid comes into contact with the surface of a solid, it may spread, indicating that the solid is receptive to that liquid, or it may form a quasi-spherical droplet, a result of the low affinity between the solid and the liquid. This property is called wettability.

Qualitatively, one can determine the receptivity of a surface to a given liquid, depositing a drop on it and analyzing whether or not the drop has spread. However, quantitative results can be obtained by measurements of the contact angle [3, 40]. The contact angle, Θ, is defined by the intersection of the line tangent to the drop with that which defines the surface of the sample.

When a water drop spreads on the surface, indicating that there is affinity between the drop and the surface of the substrate, θ is less than 90º. However, when θ > than 90°, it can be said that the surface is hydrophobic. An intermediate situation may occur characterizing the surface as partially hydrophilic or partially hydrophobic. Fig. 2 shows the drop of a liquid proof interacting on two different surfaces, which imply two distinct degrees of wettability, depending on θ [41-44].

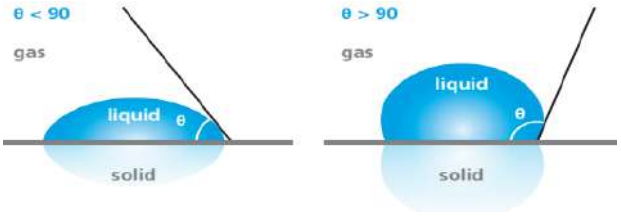

Fig. 1: Illustration of the contact angle of a surface with: high wettability for Θ < 90° (hydrophilic surfaces); low wettability for Θ > 90° (hydrophobic surfaces). *Courtesy Dr. Pericles L. SantAna – Technological Plasmas Laboratory, Sao Paulo State University, Sorocaba SP, Brazil, 2021.*

One common method for measuring surface free energy, SFE is by measuring the contact angles of several sessile droplets of standard liquids resting on the solid surface of interest. The static contact angle is an indication of the balance of surface tensions between the liquid and solid (γ_{sl}), liquid and gas (γ_{lv}), and solid and gas (γ_{sv}), as described by Equation 1, known as Young's equation: [45]

$$\gamma_{lv}\cos\theta + \gamma_{sl} = \gamma_{sv} \quad (1)$$

Where:

γ_{sv} is the surface tension at the solid-vapor interface; γ_{sl} is the surface tension at the solid-liquid interface; γ_{lv} is the surface tension at the liquid-vapor interface; and θ is the angle formed between the drop and the surface.

Hence, Fig. 3(a) shows a single drop of a liquid-proof on surface due to its surface free energy, while 3(b) shows the image of a agglutinated drop over a hydrophobic surface using water as liquid proof, captured by the camera of a Goniometer.

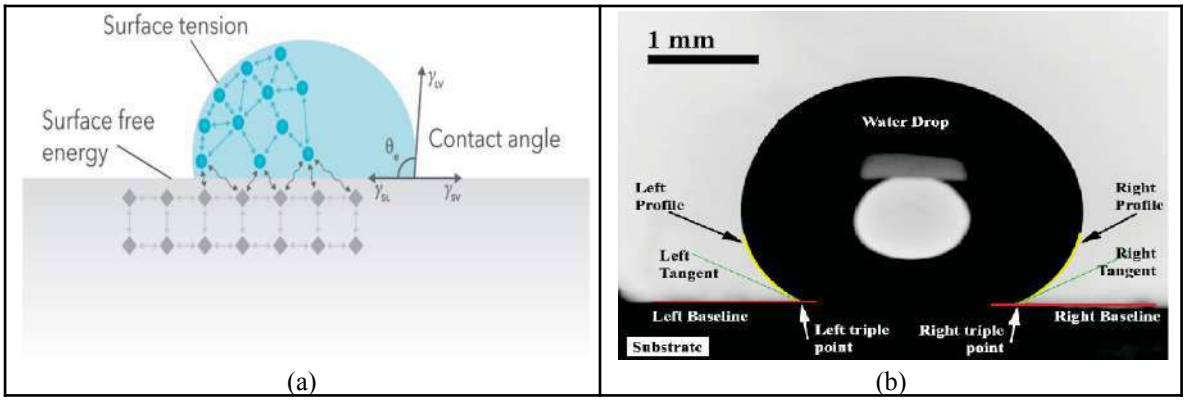

Fig. 2: (a) Schematic of a sessile drop and the balance of surface tensions at the three-phase contact line; [45] (b) A sessile drop agglutinated over a hydrophobic surface captured by a microscope CCD camera [46]. Reproduced with permission of Taylor & Francis Group; and IEEE Xplore.

The system will experience *cohesive* forces from adjacent molecules, causing the molecules to tend to stay in the bulk. As we move toward the surface of the liquid where it is in contact with another phase, the molecules will experience cohesive forces toward the bulk but also some weaker *adhesive* forces toward the adjacent phase. The result is a net attraction into the bulk that tends to reduce the number of molecules at the surface and increase the intermolecular space between surface molecules. The increased separation requires energy, just like when stretching a spring, and this excess energy gives rise to *surface tension* and SFE [45], which is defined as the energy necessary to form a unit area of new surface or the energy necessary to move a molecule from the bulk to the surface. The excess energy (or surface free energy) may be minimized by minimizing surface area. This tendency is called *surface tension* if the surfaces are liquid and a vapor.

Accurate measurement of contact angles can define the surface material properties. Drop shape analysis was developed to accurately determine the contact angle and surface tension of a solid surface. The technique involves capturing a reflected image of the drop profile, acquiring coordinate points along the contour and finding the mathematical best-fit accordingly.

Most conventional equipment utilizes this method through manual acquisition and analysis of data. This is an arduous, time-consuming task which can introduce inaccuracies. Nevertheless, partially automated equipment can be prohibitively expensive [46]. In the literature it is possible to observe interesting measurements of contact angle in diverse materials, including polymers [47].

Commonly, a small drop of distilled, deionised water is put on the surface with a microsyringe. The height (h) and radius (r) values for the spherical segment may be determined by a special microscope and the contact angle (θ) is calculated by applying Eq. 2 [48]

$$\text{Contact angle } (\theta) = \arcsin [2rh/ r^2+h^2] \text{ [deg.°]} \quad (2)$$

In 1869, Dupré observed that the surface contact angle could be connected to the thermodynamic adhesion work. He defined work of adhesion (W_a) as directly related θ via Eq. 3. [48]

$$W_a = \gamma_{sl}(1+\cos\theta) \text{ [J/m}^2\text{]} \quad (3)$$

The θ measurements of a given surface may be performed using static and dynamic methods. The contact angle of a liquid sample on a polymer is known as the static contact angle (SCA). Moreover, other wettability measurement can be performed using the sliding angle (SA) or contact angle hysteresis (CA hysteresis). The SA can indicate low adhesion of a sessile drop to the solid surface [49-51]. CA hysteresis is induced by surface particularities, such as, surface roughness, or deformation [52].

For hydrophobic surfaces, the solid-vapor surface energy γ_{SV} is less than the solid-liquid surface energy γ_{SL}. Hence, analyzing the equation (2), the surface energy becomes lower owing to trapped air immediately below the sessile drop in a surface with about 30 μm of surface roughness. In hydrophilic surfaces, γ_{sl} is lower than the γ_{sv}. Thus, the solid-liquid interface follows the roughness of the solid, which constitutes the Wenzel state [53].

To make these surfaces prone to printing and coating processes, different strategies have been developed including using a blending ethylene/propylene rubber to form thermoplastic polyolefin (TPO) [54], and exploiting physical-chemical phenomena based on plasma, corona, laser, and flame treatments. Although all of them have been suggested as suitable approaches for enhancing polymer adhesion strength, which is the most effective and feasible one is still the subject of debate. However, it is generally agreed that flame treatment, together with corona discharge, is the most widely used for the surface activation of polyolefin substrates [55].

Electrical discharges maintained in a gas have been used in plasma treatments [56]. Advantages include the possibility of modifying the topmost surface layers, and the possibility to modify the surfaces of different materials. Among the various plasma treatments, the low-pressure glow discharges permits better control of the processing parameters, which results in high reproducibility, which is essential for large scale production. In another study [57], LPP produces the increase of adhesive properties by cleaning, sputtering, etching, and can promotes new functionalities by the interaction of active species in the plasma regime. Hence, CA analysis may be performed to understand the wetting properties and the adhesive bond strengths [58].

III. RESULTS AND DISCUSSION

Table 1 shows the water contact angles of pristine substrates. Three drops were measured and the mean of 30 values is given.

Table 1: Calculated Contact Angle Values for the Pristine Polymer Substrates Obtained From Sessile Drop Measurements at Room Temperature.

Pristine substrates (without treatment)	Mean values ± standard deviation (°)	
Polyvinyl chloride PVC	70 ± 4	[3, 40]
Polyethylene Taraphthalate PET	66 ± 5	[3, 40]
Low Density Polyethylene LDPE	74 ± 1	[3, 40]
Poliamide 6	62 ± 3	
Silicone	108 ± 1	
Polypropilene	104 ± 2	
Natural rubber	28 ± 6	
Polytetrafluoroethyene (PTFE)	112 ± 5	[59]
Polymethylmethacrylate (PMMA)	53 ± 1	[60]

Fig. 3 Shows Values of the Contact Angle of PVC (6.665 Pa of SF6 and N2 Under Different Plasma Immersion Techniques for 300 S, at Different Rf Applied Power).

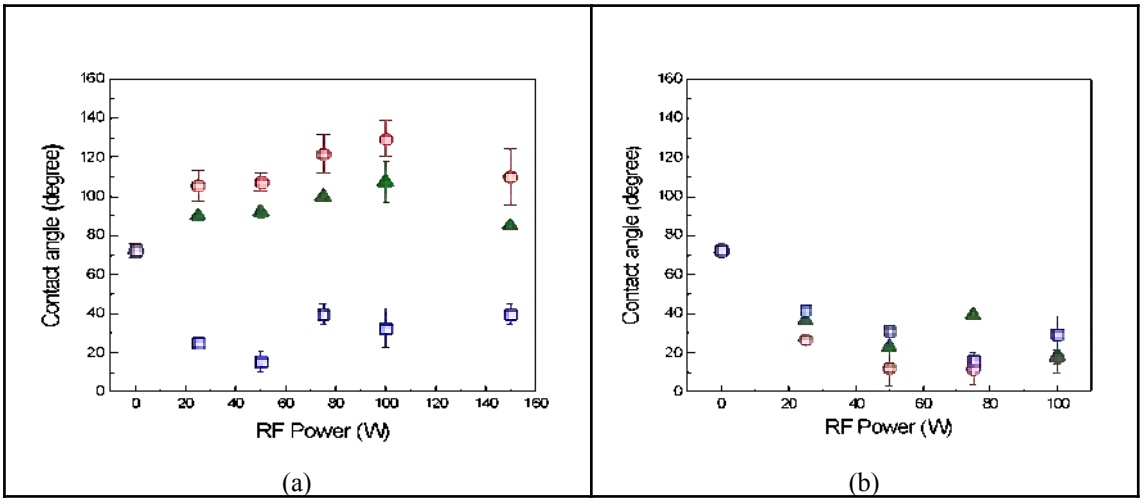

Fig. 3: Contact angle as a function of applied rf power. White PVC treated by: (a) SF_6 plasma and (b) N_2 plasma. The symbols on the graphs are associated with the following plasma techniques: ○ (PI cathode), Δ (PI anode), and □ (PIII), with error bars of one standard deviation. Temperature during the treatments was 358 K. Pressure was 6.65Pa of gases for 300 s at different rf powers. The parameters of PIII were -2400 V, 300 Hz and 30 μs

The PVC and PET surfaces were fluorinated, producing C-F bonds. Although C-F bonds are highly polar, when these species are present on the surface of PVC and PET, they increase its hydrophobicity. After fluorine insertion into the polymer backbone, the surface becomes hydrophobic, owing to the process of fluorination, which results in a substantial change of the chemical composition of PVC and PET. Owing to a relatively high C–F bond energy inside the fluorinated layer, most of O, Cl or H-atoms are easily replaced by F-atoms and double bonds are saturated with fluorine to form C–F bonds on PVC.

The availability of fluoride ions in plasma immersion can be a determining factor in the reorganization of molecular and free radical groups, which influences the Θ values. Owing to

their high ionization energy (17.4 eV) few F^+ ions are produced. Even if we increase the pressure of fluorine inside the reactor, a saturation condition may be reached, and the available of reactive fluorine becomes reduced and scant, as seen in Fig. 4, in which, shows the graph of contact angle as function of pressure of SF_6 inside the reactor to obtain hydrophobic surfaces, on commercial polymers.

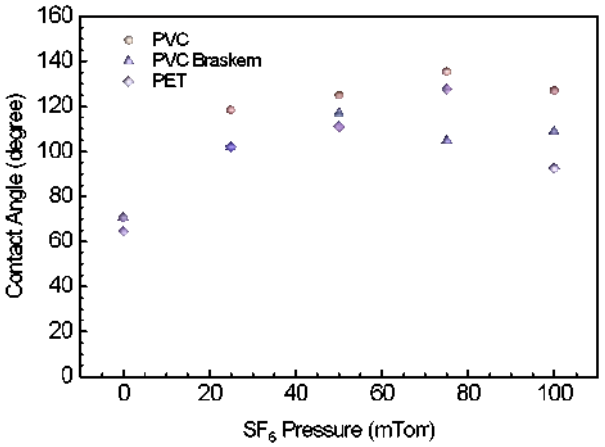

Fig. 4: Contact angle as function of SF_6 pressure: Samples of commercial white PVC, PVC from Company Braskem (yellow PVC) and PET from 2 L Coke™ bottles were treated by PI cathode at 100 W for 900 s and a temperature ~358 K. *Reproduced with permission of Brazilian Vacuum Society*.

For the polymers investigated in this series, the contact angle values increased with increasing pressure of SF_6 in the reactor, making the surface of the substrates hydrophobic. Hence, here, we have a clear case of fluorination of polymer surfaces. The increase of θ, however, was small for pressures above 25 MTorr (~3.33 Pa), that is, after 25 MTorr the contact angle values tend to stabilize. The highest value of Θ, 140°, was observed for commercial PVC treated with different SF_6 pressures. This value is 20° higher than the value of Θ found in a study made under similar thermodynamic conditions [27].

In fact, even increasing the amount of gas, it is understood that, there is not enough ionized gas to chemically modify the surface, because with the increase in pressure, there is a decrease in the mean free path, thus decreasing the cross section and, consequently, the average kinetic energy of the molecules that make up the plasma [27]. Soon the availability of fluorine ions is reduced, thus decreasing the degree of fluorination of the polymers.

For the nitrogen treatment, the combination of polar functional groups on the surface usually led to the hydrophobicity of the material. When polar groups such as C-O, C=O, C-OH and (C=O)-O, are present on the surface and the liquid used is also polar, such as deionized water, electrostatic attraction prevails. In this case, the attraction between the surface oxygen and the hydrogen in water is greater than the repulsion between the oxygen atoms (surface / liquid). So the higher the proportion of oxygen on the surface, the more hydrophilic it will be. In addition, the atoms and O-groups, together, cause greater etching of polymers, mainly on the amorphous regions.

Treatments using PI and PIII at double the pressure (~13.33 Pa) of SF_6 or N_2 at rf of 25 to 100 W for 300s, at room temperature (~298 K) have been made. High values of θ were found for fluorinated surfaces and low values of θ were found for nitrogenated surfaces. The key is: for SF_6 plasma, the hydrophobic behavior of polymeric surfaces is much more stable upon ageing. Table 2 shows the results obtained at a low electrode sample-holder temperature.

Table 2: Contact angle as a function of the cycle time for PET and LDPE samples treated with (13.33 Pa) of N_2 for 300 s, 25 W of rf power for different Ion Implantation cycle times. Pulses of -1000 V at 300 Hz were applied

Cycle time (μs)	PET Coke™ bottle contact angle (°)	LDPE contact angle (°)
0 (untreated)	70 ± 1	76 ± 1
1	50 ± 1	31 ± 1
30	45 ± 1	25 ± 1
100	30 ± 2	15 ± 2
500	18 ± 1	10 ± 1

Recent studies of the improvement in wettability showed that molecular groups containing O on the PET surface were found in greater concentrations after the plasma treatment. The changes in wettability observed after plasma treatment of polymer surfaces after storage of the modified material are explained by mobility of the macromolecules on the top surface. Accepted models of the surface energy decrease and recovery of hydrophobicity with time in these plasma-treated polymers involve the rotation of high energy surface functional groups back into the polymer bulk. Surface energy is thereby reduced and hydrophobicity increased. Such rotations seem unlikely to give the highly carbonized structure associated with high fluence modification. Independently of the efficacy of the treatment, the reduction of Θ, is a transient effect, as observed in treatments of silicone surfaces.

Moreover, to better understand the wetting mechanism of membrane pores during their prolonged contact with adsorbents, polypropylene (PP) hollow fibers were immersed in three different absorbents for up to 90 days.

Monoethanolamine, methyldiethanolamine, and deionized water were applied as absorbent solutions and the contact angle was measure as function of immersion time treatment.

Characterizations of the membrane samples confirm that the absorbent molecules diffuse into polypropylene (PP) polyolefin during the exposure process, resulting in swelling. The absorption-swelling wetting mechanism is proposed to explain observations made during the wetting process. The strong reduction in contact angles indicates that the membranes surface hydrophobicity decreases remarkably during immersion because of membrane–absorbent interactions.

The contact angle of immersed fibers continuously decreased with increases in immersion time. For example, the contact angle decreased from 121.6° to 90.8° when the PP fibers were immersed in 30% MDEA for 60 days.

A 30.8° reduction in the contact angle indicated that membrane surface hydrophobicity significantly decreased upon immersion. Further increasing the immersion time to over 60 days resulted in a slowing down of the decrease in the contact angle, until an almost stable regime was reached. In addition, the contact angles of all studied membranes were over 90°, so each membrane was still hydrophobic [61].

The results can be explained since absorbent molecules diffuse into the PP polymer during immersion in the amine solution. As the absorbent is hydrophilic, surface energy and hydrophobicity decrease when the absorbent molecules penetrate into the membrane. When immersion time is prolonged, the absorbent concentration in the PP polymer increases and thus the concentration difference between the PP polymer and the amine solution decreases. In accordance with Fick's theory of molecular diffusion, the decrease in the concentration difference may result in a decrease in the driving force for diffusion and therefore slow the shrinking of the contact angle. This decreasing tendency of the contact angle is in agreement with the experimental results that the initial CO_2 absorption flux decreases when the steady-state regime is reached [62].

The use of oxygen plasma for wettability treatment on fibril tip surfaces in polymer elastomeric polyurethane (PU) and polydimethylsiloxane (PDMS) fibrillar adhesives improved their wettability and adhesion capacity. Surface modifications of fibril tips involved UV/ozone and oxygen plasma treatments to make the fibril tips more hydrophilic. The adhesion capacity of treated fibrillar arrays is sensitive to the relative humidity of the environment [63].

Even at a low power (20 W), the plasma was rich in radical species that react with methylene (C–O) and ester groups (O–C=O) present in the polyolefin chains, producing a slight etching of the material and new hydrophilic species as carbonyl groups are introduced. At a high power (200 W), a more efficient incorporation of hydrophilic species into the PET surface was observed. Contact angle measurements confirmed the enhancement of the surface wettability as a function of plasma power [64].

Although PLLA and polyhydroxybutyrate with 8 % polyhydroxyvalerate (PHBV) can be found in biomedical applications, both are hydrophobic, making their interaction with cells difficult. Thus, the surface modification of these polymers is important for all applications involving their contact with physiological components [65,66]. The influence of the oxygen and nitrogen plasmas on the hydrophilicity of the PLLA and PHBV has been studied. Oxygen plasma treatments on both PLLA and PHBV samples, typically caused a reduction in the CA and an increase in the SE. This increase in the SE reflects an increase in surface hydrophilicity.

High-density polyethylene (HDPE) was modified by air and oxygen plasmas (operating pressure from 0.1 to 1 Torr, power ranging between 5 W and 10 W). The CA measurement, ATR FTIR, and XPS analysis revealed the hydrophilic character of the HDPE surfaces. A hydrophilic surface was created mainly due to the generation of the carboxylic, carbonyl, and peroxide groups at the surface [67].

The changes in wettability of 2-hydroxy-ethyl-methacrylate (HEMA) and 2-ethyloxyethyl-methacrylate (EOEMA) induced by Ar plasma treatment were measured using goniometry. The experiment was performed on a Balzers SCD 050 device, and the processing parameters were as follows: the time of modification was 0–400 s, and the discharge power was 1.7 W [68]. Based on the analyses, the creation of the "new" groups containing oxygen on HEMA and EOEMA chains leads to changes in wettability. The CAs were immediately evaluated (in 6 min) and 386 h after the plasma irradiation.

It was found that the plasma modification leads to the rapid decrease in CA in the first few minutes after modification, the decrease being greater for longer modification times. Comparable dependence was observed for both polymers. Then, 386 h after plasma modification, the CA increased compared with the CA measured immediately after the plasma treatment.

The experiment in ref. [69] proved that the concentration of oxygen groups created by Ar plasma irradiation does not change with treatment time. This result [69] and the finding from goniometry analyses [68] can be explained by the reorganization of surface layers and rotation of degraded macromolecules and newly created structures to the "free volume of polymer" [68, 70].

Dependences of the CA on the aging time for plasma-modified Polyethylene (PE) and plasma-modified PE and subsequently grafted with PEG showed a pronounced decrease in CA after PEG grafting owing to the binding of oxygen-rich compounds onto the activated polymer surface. Based on the biological experiments performed in vitro with the VSMCs, it was found that the cell's adhesion, proliferation, and viability depend on the PEG concentration on the surfaces of polymeric samples, and on the lengths of its polymeric chains [71].

The grafting of glycine on the PE surface leads to the increase in oxygen concentration on the modified surface and a decrease in WCA [72]. In particular, PEG brushes can be used to repress protein adsorption, which is responsible for several unwanted effects, such as fouling of

contact lenses, clotting on blood-containing devices, and triggering of inflammation around artificial organs [73].

Spherically shaped gold nanoparticles (AuNPs) with an average diameter of 12 nm were bound on the plasma pretreated polymer surface, which is the polyolefin, HDPE. The AuNPs were "grafted" from the citrate colloid solution. Surface wettability was measured by goniometry, i.e., the static (sessile) water drop CA method. The samples exhibited an increase in wettability after modification by plasma discharge and AuNPs. This increase was more pronounced for samples pretreated in plasma for less time [75].

Moreover, cysteamine was grafted on several polymer foils of different polarity (PLLA, PS, lowdensity polyethylenes (LDPE), HDPE, PET, PTFE, polyvinylfluoride (PVF) and polyvinylidenefluoride (PVDF)) previously activated in plasma discharge [76]. Wettability was determined by measurement of WCA on all samples, pristine, plasma treated for different times, plasma treated, and subsequently cysteamine grafted. It was found that plasma treatment leads to a dramatic decrease in CA, indicating an increase in surface wettability of all polymers. For some polymers, this CA decrease strongly depended on the plasma exposure time (e.g., PTFE), but for others, the plasma exposure time is not of such importance (e.g., HDPE and LDPE) [76]. The most dramatic dependence of CA is observed for PTFE. The cysteamine grafting caused a dramatic increase in CA (i.e., decrease in surface wettability) on all polymers, and the increase was the highest for PTFE.

As a consequence of surface treatment polyolefin containing reactive groups, i.e., molecular oxygen groups may be absorbed owing to the reactions between a polymeric surfaces and nano-particles. On the other hand, nanoparticles from inert polymers are trapped along the polymeric chains [77]. The insertion of oxygen groups on the surface of inert polymers may promote nanoparticles adhesion in the material [78]. The insertion of hydroxyl groups on the surface of hydrophilic membranes also performed good adherent properties for the polymeric samples [79].

The increasing of wettability in PP membranes generates good deposition of titanium dioxide nanoparticles on the surface of the PP [80] θ decreased from 135° to 90° after O_2 plasma, and decreased again from 90° to 40° as UV treatment time evaluated until 120 min. The mechanism responsible for promoting greater wettability to surfaces of TiO_2 is associated with the electron-hole pair formation, and these reactions may cause the increase of absorption of H_2O and O_2 molecules into TiO_2 surfaces.

In other studies, a high degree of fluorination was obtained, on both polymers when treated by PI or PIII with SF_6 plasma; and analogously, a high degree of polar groups containing O was obtained on both polymers when treated by PI and PIII with N_2 plasma. A priori, the high energy of electrons and ions in the plasma can compromise the insertion of fluorine on a micro or nanometric scale. In fact, the predominance of sputtering mechanisms on the surface is compatible with the formation of sigma or double covalent bonds. It is noteworthy that the sputtering mechanism is necessary to the process, as there will only be a recombination of C with F or O, on the surface, if there are active sites (pendant C bonds on the surface). The vacuum level may not be sufficient to totally avoid the presence of contaminants, or groups containing oxygen [71].

J.P. Youngblood et al. controlled surface roughness of PP, using PTFE solid target, concomitant with noble gas plasmas [80]. The sputtering of PTFE, released greater number of fluorine atoms which etch PP, resulting in nanowrinkles. Di Mundo et al. have controlled the CF_4/O_2 gas flow rate ratio to generate super-hydrophobic surface in PS solid samples [81,82]. In this case, 17% content of oxygen in the feed was sufficient to generate a water repellent surface.

It is suggested that: (i) smooth surfaces cannot exhibit θ higher than 120° (ii) water repellent surfaces are associated with θ higher than 150° and (iii) an effect of hysteresis in θ may occur

after plasma treatments; (iv) In this regime, a suitable surface texturing may promote self cleaning surfaces, [83]; (v) on a textured surface a saturated value of the stable θ may be reached.

The control of the surface roughness for diverse polyolefins, depends on the parameters employed in Inductive Coupled Plasma Treatments [85].

For instance, wettability is important in food packaging, water-repellant and self-cleaning surfaces, inks and superhydrophobic coatings, injection of medical polymers, and particle attraction in deoxyribonucleic acid (DNA) purification [86, 87].

According to the obtained results, the major factor influencing the treatment process for all tested materials was gas composition. The overall gas flow rate did not play a crucial role in surface treatment. Plasma burning in ambient air enabled the formation of highly reactive oxidative compounds, such as singlet oxygen, hydroxyl radicals, and ozone [88].

IV. STOP AND RANGE IONS IN MATTER (SRIM SIMULATION)

SRIM simulation was run, considering the perpendicular incidence of: [fluorine (F+) mass = 18.998 a.m.u, and nitrogen (N+) mass = 14.003 a.m.u] ions on the polymeric targets with energies of 1 keV and 2.4 keV (for comparison). Density values provided by the software were: *rigid* PVC density ρ = 1.68 g/cm³; PET (*mylar*) density ρ = 1.397 g/cm³; LDPE (*marlex*) density ρ = 0.93 ± 0.3 g/cm³. As input dada was selected, *Ion Distribution with recoils and Quick Calculation of Damage* mode, which provides a statistical estimated based on the Kinchen-Pease formalism, which suggest that the number of point defects generated by an implanted ion is derived analytically from the energy that is transferred from an ion to an atom of the target material. It is assumed that the number of point defects generated by a primary recoil is proportional to the energy transferred from the ion to the primary recoil (for incident E < 25 keV).

Despite the targets possess similar atomic density (~10^{22} to 10^{23} at/cm³), the results shows that, the proportion of elements (%) are different in mass and number of atoms for the targets. In PVC, chloride is present in less quantity (number of atoms), however, it represents higher proportion in mass, because it is a.m.u (~35.4) is higher than carbon (~12.0) and hydrogen (~1.0). Analogously, hydrogen is present in the PET matrix in higher quantity (number of atoms) than oxygen, however it represent lower proportion in mass, because it is a.m.u (atomic mass unit) is much lower than oxygen (~15.9) a.m.u.

Table 3 shows the information about the compound correlation, atomic density and proportion of atomic masses and number of atoms, for the three polymeric targets [3].

Table 3: Information About the Compound Correlation, Atomic Density and Proportion of Atomic Masses and Number of Atoms, for the Three Polymeric Targets.

Target	Rigid PVC 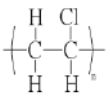	PET *mylar* 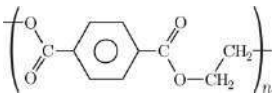	LDPE *marlex* 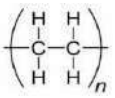
Atomic density	ρa = 9.71 × 10^{22} at/cm³	ρa = 9.63 × 10^{22} at/cm³	ρ = 1.2 × 10^{23} at/cm³
Compound correlation	σ = 0.9475607	σ = 0.9343234	σ = 1.0054160
Mass proportion (%)	H = 4.84 C = 38.43 Cl = 56.73	H = 4.2 C = 62.5 O = 33.3	H = 14.37 C = 85.63
Number of atoms (%)	H = 50.0 C = 33.33 Cl = 16.67	H = 36.36 C = 45.45 O = 18.18	H = 66.67 C = 33.33

Fig. 5 shows the graphs of the simulation on the three targets investigated.

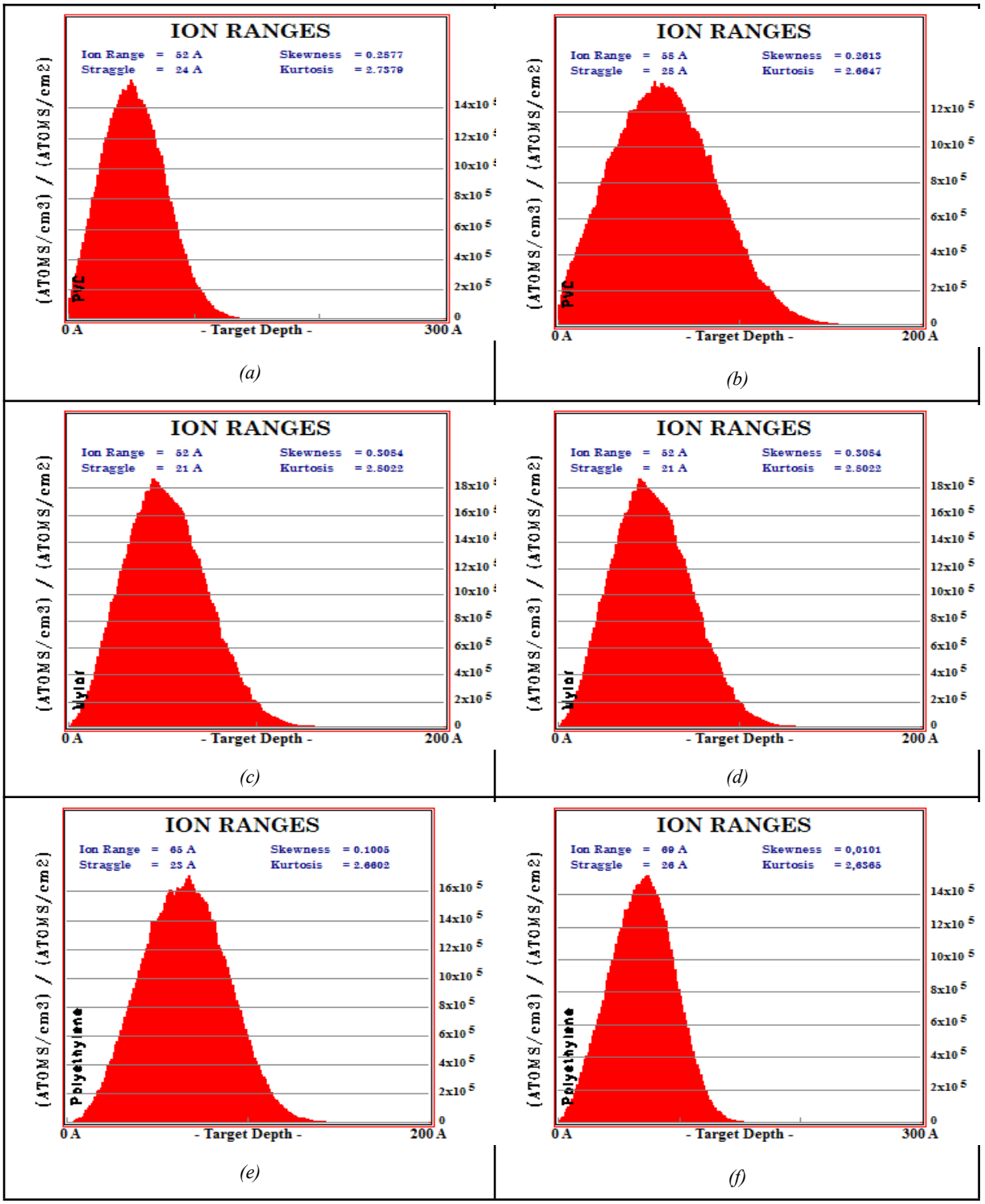

Fig. 5: (a) Depth (Angstroms) of incident ions (F+) for the PVC, using incident energy of 1 keV; (b) Depth (Angstroms) of incident ions (N +) for the PVC, using incident energy of 1 keV. The histogram shows the range of values average and maximum; (c) Depth (Angstroms) of incident ions (F +) for the PET, using incident energy of 1 keV; (b) Depth (Angstroms) of incident ions (N +) for the PET, using incident energy of 1 keV. The histogram shows the range of values average and maximum; (e) Depth (Angstroms) of incident (F +) ions, using incident energy of 1 keV (f) Depth (Angstroms) of incident ions (N +), using incident energy of 1 keV, both for the LDPE. The histogram represents the range of values average and maximum.

The distribution of the ions generates a matrix in profile of implanted ions. It is assumed that N+ ions can reach slightly deeper regions than F+ when stimulated with the same energy for implantation. Increasing the energy from 1 to 2.4 keV, the ions can reach deeper distances in the targets. In addition, targets containing C, H, N, O, F will need a compound correlation, σ. This parameter is a correction to accounts for the effects of bonding changes and target band-gap [3].

Table 4 shows the results about energy loss (eV/angstrom-ion) for F+ and N+ions and recoils.

Table 4: Ion Loss Energy (-dE/dx) of Incident Fluorine Ions (F +), and Nitrogen (N +), Using the Incident Energy of 1 keV. Three Parameters of Loss Energy Are Presented for the Three Polymer Targets Investigated: (I) Ionization, (Ii) Vacancy, (Iii) Phonons

Ion incident (99.999)		-dE/dx (energy loss) [eV/ angstrom-ion]	PVC	PET	LDPE
F+ (1 keV)	Ions	Ionization	7.75	8.75	9.68
		Vacancy	2.28	1.94	2.6
		Phonons	12.35	11.94	13.5
	Recoils	Ionization	14.85	15.61	17.4
		Vacancy	1.37	1.21	1.2
		Phonons	61.37	60.55	55.6
N+ (1 keV)	Ions	Ionization	11.78	13.9	14.6
		Vacancy	2.25	1.88	2.52
		Phonons	12.14	11.48	12.48
	Recoils	Ionization	14.00	14.76	16.88
		Vacancy	1.38	1.21	1.32
		phonons	58.45	57.48	52.95

As result of ion bombardment, the SRIM software recognizes the energy loss –dE/dx, in (%), which summaries the loss energy from the ion to the target electrons, and being possible to estimate the ionization, vacancy and phonons contribution (%) for either ions or recoil atoms (eV/angstrom) [3].

The author would like to thank, Ziegler et al by the opportunity to explore the SRIM simulation.

V. CONCLUSIONS

The type of functionalization can be varied by a selection of the plasma gas (Ar, SF_6, N_2 , O_2 , CO_2, and NH_3) and processing parameters (power, time, pressure, temperature and gas flow rate). Plasma treatment with oxygen or nitrogen provides polar functional groups on the surface, which alters the surface energy of polymers including polyolefins [89] and enhances the attachment of consequently applied chemical substances or particles. It is known that oxygen plasma can react with a wide range of polymers to produce a variety of oxygen functional groups.

While SF_6 plasma provides C-F bonds, and hydrophobic surfaces, oxygen plasma provides different functional groups on the polymer surface such: C–O, C=O, and O–C=O groups [90]. Numerous authors also reported excellent results of wettability for several types of polymers including polyethylene terephthalate [91-93], polyethersulphone [94-95], polyphenylene sulphide [96], polystyrene [97-98], polyvinylchloride [100-101], polymethyl methacrylate [102], cellulose [103-105] etc, and the treated polymers found a wide spectrum of applications in science and industry.

The limitations of cold plasma treatment were presented. The modification of polymer surfaces with cold plasma processing may not be maintained over time. Because of the minimisation of the free surface enthalpy, dynamic processes are observed on all functionalized surfaces which reduce the initial modification effect [106]. The loss of beneficial attributes derived from cold plasma processing of polymers over time is often called “ageing”.

For example, a loss in hydrophilicity is observed for treated polymeric films when stored. This is referred to as hydrophobic recovery. Such effects are attributed primarily to inward-diffusion, agglomeration or sublimation of "Low Weight Organic Molecules", the reorientation of polymer chains, whereby covalently bonded polar groups become "buried" beneath the outer surface; and migration of additives from the bulk towards the surface [106].

Ageing effects are significant when the power input to the plasma and process times are both low. For the aforementioned example, this signifies insignificant changes in the surface roughness, i.e. less etching [106]. Conversely, where intermediate to high plasma powers and times are used, a further post-processing decrease in contact angle occurs [106]. Cooling of the sample holder may minimize the effects of ageing, thereby producing more stable wetting properties.

In the literature, it is possible to observe a wide spectrum of surface functionalizations to introduce specific species to the treated surface, aiming, for example, to transform the surface characteristics from hydrophilic to hydrophobic using fluorine plasma, or the reverse using nitrogen plasmas [107-108].

List of Abbreviations

The list of abbreviations is not applicable in this work.

Declarations

Availability of Data and Material

The datasets used and analyzed during the current study available from the corresponding author on reasonable request

Competing interests

There are no conflicts of interest.

Funding

The research reported here was funded in part by the "Coordenaçao de Aperfeiçoamento de Pessoal de Nivel Superior (CAPES)" – Finance Code 001. We thank FAPESP (2017/15853-0) for financial support. In addition we would like to thank to CNPq and FAPESP, Brazilian agencies.

Author's Contribution

All authors, J.R.R.B, N.C.C, E. C. R and S.F.D. have contributed with formal conception, analysis and reviewing. P.L.S. analyzed the results and wrote the first draft. All co-authors are in agreement to this submission.

ACKNOWLEDGMENTS

The author, P.L.S. would like to thank to Plasma Research Group, from State University of Sao Paulo, UNESP and all support from the teachers and students of the Technological Plasmas Laboratory, UNESP.

REFERENCES

1. Shaw, D.; Gyuk, P.; West, A.; Momoh, M.; & Wagenaars, E. (2015). Surface Modification of Polymer Films Using an Atmospheric-Pressure Plasma Jet. In Proc 22nd ISPC,York; 3 p. (In Press).http://eprints.whiterose.ac.uk/95050/
2. Tomislava Vukuši´c 1, Alenka Vesel, Matej Holc, Mario Šˇcetar, Anet Režek Jambrak, Miran Mozetiˇc. (2018). Modification of Physico-Chemical Properties of Acryl-Coated Polypropylene Foils for Food Packaging by Reactive Particles from Oxygen Plasma. Materials. 11 (3), 372. https://doi.org/10.3390/ma11030372.
3. Sant'Ana P. L. (2019). Polimeros tratados a plasma para dispositivos e embalagens, Novas edições acadêmicas, v.1., p.118.ISBN- 10: 6139734703.
4. Ruey-Shin Juang, Wei-Ting Hou, Yin-Che Huang, Yu-Chian Tseng, Chun Huang. (2016). Surface hydrophilic modifications on polypropylene membranes by remote methane/oxygen mixture plasma discharges. Journal of the Taiwan Institute of Chemical Engineers. 65, p. 420-426. https://doi.org/10.1016/j.jtice.2016.04.032.
5. Ozdemir, M.; Yurteri, C. U.; Sadikoglu, H. (1999). Physical polymer surface modification methods and applications in food packaging polymers. Critical Review in Food Science and

Nutrition, Boca Raton, v. 39, p. 457–477. https://doi.org/10.1080/10408699991279240.
6. Lai, J. et al. (2006). Study on hydrophilicity of polymer surfaces improved by plasma treatment. Applied Surface Science, Amsterdam, 252, p. 3375–3379. Ht tps://doi.org/10.1016/j.apsusc.2005.05.038.
7. Gorjanc, M.; Mozetic, M. (2014). Modification of Fibrous Polymers by Gaseous Plasma: Principles, Techniques and Applications. Lambert Academic Publishing: Saarbrücken, Germany. ISBN: 978-3-659- 61460-6.
8. Huang, Chun; Tsai, Ching‐Yuan; Juang, Ruey‐Shin. (2012). Surface Modification and Characterization of an H_2/O_2 Plasma‐Treated Polypropylene Membrane. Journal of Applied Polymer Science, 124.S1. https:// doi.org/10.1002/app.34049.
9. A. P. Kharitonov, G. V. Simbirtseva, A. Tressaud, E. Durand, C. Labrugère, M. Dubois. (2014). Comparison of the surface modifications of polymers induced by direct fluorination and rf-plasma using fluorinated gases. Journal of Fluorine Chemistry, 165, p. 49-60. https://doi.org/10.1016/j.jfluchem.2014.05.002.
10. Vandana Singh, B. Saswat and Satyendra Kumar. (2005). Low temperature deposition of Indium tin oxide (ITO) films on plastic substrates, Mater. Res. Soc. Symp. Proc. 869. https://doi.org/10.1557/PROC-869-D2.9.
11. Tomislava Vukuši´c, Alenka Vesel, Matej Holc, Mario Šˇcetar, Anet Režek Jambrak, Miran Mozetiˇc. (2018). Modification of Physico-Chemical Properties of Acryl-Coated Polypropylene Foils for Food Packaging by Reactive Particles from Oxygen Plasma. Materials; 11 (3), 372. DOI: 10.3390/ma11030372.
12. Pankaj, S.K.; Bueno-Ferrer, C.; Misra, N.N.; Milosavljevi´c, V.; O'Donnell, C.P.; Bourke, P.; Keener, K.M.; Cullen, P.J. (2014). Applications of cold plasma technology in food packaging. Trends Food Sci. Technol; 35 (1), p. 5–17. https://doi.org/10.1016/j.tifs.2013.10.009.
13. Gorjanc, M.; Savic, A.; Topalic-Trivunovic, L.; Mozetic, M.; Zaplotnik, R.; Vesel, A.; Grujic, D. (2016). Dyeing of plasma treated cotton and bamboo rayon with fallopia japonica extract. Cellulose; 23 (3), p. 2221–2228. https://doi.org/10. 1007/s10570-016-0951-9.
14. Gorjanc, M.; Jazbec, K.; Sala, M.; Zaplotnik, R.; Vesel, A.; Mozetic, M. (2014). Creating cellulose fibres with excellent uv protective properties using moist cf4 plasma and zno nanoparticles. Cellulose; 21 (4), p. 3007–3021. https://doi.org/10.1007/s10570-014-0284-5.
15. Lopez-Garcia, J.; Primc, G.; Junkar, I.; Lehocky, M.; Mozetic, M. (2015). On the hydrophilicity and water resistance effect of styrene-acrylonitrile copolymer treated by CF_4 and O_2 plasmas. Plasma Process. Polym; 12 (10), p. 1075–1084. https://doi.org/10.1002/ppap.201400216.
16. Lopez-Garcia, J.; Lehocky, M.; Humpolicek, P.; Novak, I. (2014). On the correlation of surface charge and energy in non-thermal plasma-treated polyethylene. Surf. Interface Anal; 46 (9), p. 625–629.https://doi.org/10.1002/sia.5627.
17. Gorjanc, M.; Mozetic, M. (2014). Modification of Fibrous Polymers by Gaseous Plasma: Principles, Techniques and Applications. Lambert Academic Publishing: Saarbrücken, Germany. ISBN: 978-3-659- 61460-6.
18. Primc, G.; Tomsic, B.; Vesel, A.; Mozetic, M.; Razic, S.E.; Gorjanc, M. (2016). Biodegradability of oxygen-plasma treated cellulose textile functionalized with zno nanoparticles as antibacterial treatment. J. Phys. D Appl. Phys.; 49 (32), 324002. https://doi.org/10.1088/0022-3727/49/32/324002.
19. Gorjanc, M.; Sala, M. (2016). Durable antibacterial and uv protective properties of cellulose fabric functionalized with Ag/TiO_2 nanocomposite during dyeing with reactive dyes. Cellulose; 23 (3), p. 2199–2209. https://doi.org/10.1007/s10570-016-0945-7.
20. Popelka, A.; Novak, I.; Lehocky, M.; Bilek, F.; Kleinova, A.; Mozetic, M.; Spirkova, M.; Chodak, I. (2015). Antibacterial treatment of LDPE with halogen derivatives via cold

Chodak, I. (2015). Antibacterial treatment of LDPE with halogen derivatives via cold plasma. Express Polym. Lett.; 9 (5), p. 402–411,. https://doi.org/10.3144/expresspolymlett.2015.39.
21. Asadinezhad, A.; Novak, I.; Lehocky, M.; Sedlarik, V.; Vesel, A.; Junkar, I.; Saha, P.; Chodak, I. (2010). A physicochemical approach to render antibacterial surfaces on plasma-treated medical-grade pvc: Irgasan coating. Plasma Process. Polym.; 7 (6), p. 504–514. https://doi.org/10.1002/ppap.200900132.
22. Sulovska, K.; Lehocky, M. (2014). Characterization of plasma treated surfaces for food safety by terahertz spectroscopy. Proc. SPIE; 9252, 925209. https://doi.org/10.1117/12.2067162.
23. Tkavc, T.; Petrini˘c, I.; Luxbacher, T.; Vesel, A.; Risti´c, T.; Zemlji˘c, L.F. (2014). Influence of O2 and CO2 plasma treatment on the deposition of chitosan onto polyethylene terephthalate (pet) surfaces. Int. J. Adhes.; 48, p. 168–176. https://doi.org/10.1016/j.ijadhadh.2013.09.008.
24. Gancarz I, Bryjak M, Kujawski J, Wolska J, Kujawa J. (2015). Plasma deposited fluorinated films on porous membranes. Materials Chemistry and Physics; 151, p. 233-242. https://doi.org/10.1016/j.matchemphys.2014.11.059.
25. Encinas N, Díaz-Benito B, Abenojar J, Martínez M.A. (2010). Extreme durability of wettability changes on polyolefin surfaces by atmospheric pressure plasma torch. Surface and Coatings Technology (205) 2, p. 396-402. https://doi.org/10.1016/j.surfcoat. 2010.06.069.
26. Lee K.T., Goddard J.M., Hotchkiss J.H., Lee K.T. (2008). Plasma modification of Polyolefin surfaces. Packaging Technology and Sciences (22) 3, p.139-150.https://doi.org/10.1002/pts.829.
27. Sant'Ana P.L.; Bortoleto, J.R.R.; Cruz N.C.; Rangel E.C.; Durrant S.F. (2017). Study of wettability and optical transparency of pet polymer modified by plasma immersion techniques Revista Brasileira de Vácuo, 16 (2), p. 68-74. http://dx.doi.org/10.17563/ rbav.v36i2.1050.
28. Rangel E. C., Bento W. C. A., Kayama M. E., Schreiner W. H. e Cruz N. C. (2003). Surface and Interface Analysis 35, p. 179. https://doi.org/10.1002/sia.1518.
29. Nakaya M, Uedono A., Hotta A. (2015). Recent Progress in Gas Barrier Thin Film Coatings on PET Bottles in Food and Beverage Applications. Coatings. 5, p. 987-1001. https://dx.doi.org/10.3390/coat-ings5 040987.
30. Resnik M., Zaplotnik R., Mozetic M., Vesel A. (2018). Comparison of SF_6 and CF_4 Plasma Treatment for Surface Hydrophobization of PET Polymer. Materials. 11, p.311. https://dx.doi.org/10.3390/ma110 20311.
31. Kim Y, Lee Y, Han S, and Kim K. J. (2006). Improvement of hydrophobic properties of polymer surfaces by plasma source ion implantation. Surf. Coat. Technol. 200 (16/17), p. 4763-4769. https://doi.org/10.1016/j.surfcoat.2005.04.035.
32. Aflori M., Drobotă M., Ţîmpu D., Bărboiu V. (2007). Effect of Surface Modification by Ammonia Plasma on Vascular Graft: PET Film and PET Scaffold, in: 28th Int. Conf. Phenom. Ion. Gases Prague; Vol. 13, p. 727.
33. Shekhawat N., Aggarwal S., Sharma A., and Nair K. G. M. (2016). N^+ Implantation-Induced Surface Hardening of Poly (Allyl Diglycol Carbonate). Polymer. J. Macromol. Sci., Part B: Phys.; 55, p. 652–661. https://doi.org/10.1080/00222348. 2016.1187046.
34. Banik I.,. Kim K. S, Yun Y. I., Kim D. H., Ryu C. M. and Park C. E. (2002). Inhibition of aging in plasma-treated high-density polyethylene, J. Adhes. Sci. Technol.; 16 (9), p. 1155-1169. https://doi.org/10.1163/156856102320256828.
35. Larsson A. and Derand, H. (2002). Stability of Polycarbonate and Polystyrene Surfaces after Hydrophilization with High Intensity Oxygen RF Plasma, J. Colloid Interface Sci.; 246, p. 214-221. https://doi.org/10.1006/jcis.2001.8032.
36. Huang, C., Tsai, C.Y., Juang, R.S. (2012). Surface Modification and Characterization of an H_2/O_2 Plasma-Treated Polypropylene

Membrane. Journal of Applied Polymer Science; 124.S1. https://doi.org/10.1002/app.34049.
37. Rabies A, Shanduka's S. (2013). Processing and evaluation of bioactive coatings on polymeric implants. Journal of Biomedical Materials Research - Part A.; 101 A: p. 2621-2629. https://doi.org/10.1002/jbm.a.34557.
38. Hahn B-D, Park D-S, Choi J-J, Ryu J, Yoon W-H, Choi J- H, et al. (2013). Osteo conductive hydroxyapatite coated PEEK for spinal fusion surgery. Applied Surface Science; 283; p. 6- 11. https://doi.org/10.1016/j.apsusc.2013.05.073.
39. Al-Etaibi A., Alnassar H., El-Apasery M. , (2016). Dyeing of polyester with disperse dyes: Part 2. Synthesis and dyeing characteristics of some azo disperse dyes for polyester fabrics. Molecules. (21), 855.. https://doi.org/10.3390/molecules21070855.
40. Sant'Ana P. L. (2018). Polymers Treated by Plasma for Optical Devices and Food Packaging, Scholar's Press, Sorocaba-SP, Brazil. V.1. p.128. ISBN-13: 978-613-8-50737-6.
41. Sant'Ana P. L.; Bortoleto J. R. R.; Rangel E. C.; Cruz N. C. ; Durrant S.F.; Botti L. C. M.; dos Anjos C. A. R.; Teixeira; V. Azevedo S.;. Simoes C.I.S; Soares N.F.F.; Medeiros E.A.A.; Carneiro J. (2018). Surface Properties and Morphology of PET Treated by Plasma Immersion Ion Implantation for Food Packaging. Nanomedicine & Nanotechnology Open Access; v. 3, p. 1-13. ISSN: 2574-187X.
42. Prestes, S. M. D. & Mancini S. D. et al. (2015). Plasma Treatment to improve the surface properties of recycled post- consumer PVC. Plasma Processing and Polymers; 12 (5), p. 456-465. https://doi.org/10.1002/ppap.201400086.
43. Rangel E. C., Bento W. C. A., Kayama M. E., Schreiner W. H. e Cruz N. C. (2003). Enhancement of polymer hydrophobicity by SF_6 plasma treatment and argon plasma immersion ion implantation. Surface and Interface Analysis 35 (2), p. 179-183. https://doi.org/10.1002/sia.1518.
44. Mittal K. L.(2003). Contact Angle, Wettability and Adhesion, CRC Press. 3, 530. ISBN: 9789047403326.
45. Hiemenz P.C, Rajagopalan R. (1997). Principles of Surface and Colloids Chemistry. Taylor & Francis Group, Boca Raton, FL.
46. Senarathna R.M.D.M., Wanniarachchi W.K.I.L., Jayawardhana V, Rathnaweera D.R. (2018). Development of a Low-cost Automated Micro Dispense Digital Goniometric Device with Drop Shape Analysis. Computer Science. Moratuwa Engineering Research Conference (MERCon).
47. Yuan Y., Lee T.R. (2013). Contact Angle and Wetting Properties. In: Bracco G., Holst B. (eds) Surface Science Techniques. Springer Series in Surface Sciences; vol 51. Springer, Berlin, Heidelberg. https://doi.org/10.1007/978-3-642-34243-1_1. Print ISBN: 978-3-642-34242-4.
48. Baldan, A. (2012). Adhesion phenomena in bonded joints, International Journal of Adhesion and Adhesives, 38, pp. 95–116. https://doi.org/10.1016/j.ijadhadh.2012.04.007
49. Hsieh, C.T.; Wu, F.L.; Chen, W.Y. (2009). Super water- and oil-repellencies from silica-based nanocoatings. Surf. Coat. Technol., 203, (22), p.3377–3384. https://doi.org/10.1016/j.surfcoat.2009.04.025.
50. Liu, M.J.; Zheng, Y.M.; Zhai, J.; Jiang, L. (2010). Bioinspired Super-antiwetting Interfaces with Special Liquid-Solid Adhesion. Acc. Chem. Res., 43, p. 368–377. https://doi.org/10.1021/ar900205g.
51. Liu, M.J.; Wang, S.T.; Wei, Z.X.; Song, Y.L.; Jiang, L. (2009). Bioinspired Design of a Superoleophobic and Low Adhesive Water/Solid Interface. Adv. Mater., 21, p.665–669. https://doi.org/10.1002/adma.200801782.
52. Extrand, C.W. (2002). Water contact angles and hysteresis of polyamide surfaces. J. Colloid Interface Sci., 248 (1), p. 136–142. https://doi.org/10.1006/jcis.2001.8172.
53. Bico, J.; Thiele, U.; Quéré, D. (2002). Wetting of textured surfaces. Colloids Surf. A Physicochem. Eng. Asp. 206 (1-3), p. 41–46.

https://doi.org/10.1016/S0927-7757(02)00061-4.
54. Kumar CR, George KE, Thomas S. (1996). Morphology and mechanical properties of thermoplastic elastomers from nylon-nitrile rubber blends. Journal of Applied Polymer Science; 61:2383-2396. https://doi.org/10.1002/(SICI)1097-4628.
55. Farris S, Pozzoli S, Biagioni P, Duó L, Mancinelli S, Piergiovanni L. (2010). The fundamentals of flame treatment for the surface activation of polyolefin polymers e A review. Polymer (51) 16, p. 3591-3605. https://doi.org/10.1016/j.polymer.2010.05.036.
56. Hetemi, D.; Pinson, J. (2017). Surface functionalisation of polymers. Chem. Soc. Rev., 46, 5701–5713. https://doi.org/10.1039/C7CS00150A.
57. Encinas, N.; Dillingham, R.G.; Oakley, B.R.; Abenojar, J.; Martínez, M.A.; Pantoja, M. (2012). Atmospheric pressure plasma hydrophilic modification of a silicone surface. J. Adhes., 88, 321–336. https://doi.org/10.1080/00218464.2012.659994.
58. Mandolfino C, Lertora E, Gambaro C, Pizzorni M. (2019). Functionalization of Neutral Polypropylene by Using Low Pressure Plasma Treatment: Effects on Surface Characteristics and Adhesion Properties. Polymers; 11(2):202. https://doi. org/10.3390/polym11020202.
59. Lee L-H. (1974). Effect of surface energetics on polymer friction and wear. In Advances in Polymer Friction and Wear. Lee L-H, Ed. Boston: Springer US, p. 31–68. https://doi.org/10.1007/978-1-4613-9942-1_3.
60. Tirrell M. (1996). Measurement of Interfacial Energy at Solid Polymer Surfaces. Langmuir 12 (19): p. 4548–4551. https://doi.org/10.1021/la950894e.
61. Lva Y., Yua X, Tua S-T, Yan J, E. Dahlquist. (2010). Wetting of polypropylene hollow fiber membrane contactors. Journal of Membrane Science 362, p.444–452. https:// doi.org/10.1016/j.memsci.2010.06.067.
62. M. Mavroudi, S.P. Kaldis, G.P. Sakellaropoulos (2006). A study of mass transfer resistance in membrane gas–liquid contacting process, J. Membr. Sci. 272, (1-2), p.103–115. https://doi.org/10.1016/j.memsci.2005.07.025.
63. Peyvandi A., Abideen S. U., Huang Y., Lee I., Soroushian P., Lu J. (2014). Surface treatment of polymer microfibrillar structures for improved surface wettability and adhesion. Applied Surface Science; 289, p.586–591. https://doi.org/10.1016/j.apsusc.2013.11.048.
64. Vassallo E., Cremona A., Ghezzi F., Ricci A. (2010). Characterization by optical emission spectroscopy of an oxygen plasma used for improving PET wettability. Vacuum, 84 (7), p. 902–906. https://doi.org/10.1016/j.Vacuum.2009.12.008.
65. Hu S. G., Jou C. H., Yang M. C. (2004). Biocompatibility and antibacterial activity of chitosan and collagen immobilized poly (3-hydroxybutyric acid-co-3-hydroxyvaleri-cacid). Carbohydrate Polymers, 58, p. 173–179. https://doi.org/10.1016/j.carbpol.2004.06.039.
66. Zhijiang C., Guoxiang Ch., Zhiyuan T. (2004). Surface modification of poly(3-hydroxybutyrate) (PHB) by photografting and its properties evaluation. Journal of Polymer Research, 11, p. 99–104. https://doi.org/10.1023/B:JPOL.0000031065.88526.92.
67. Lehocký M., Drnovská H., Lapčíková H., Barros-Timmons A. M., Trindade T., Zembala M., Lapčí L. Jr. (2003). Plasma surface modification of polyethylene. Colloids and Surfaces A: Physicochemical and Engineering Aspects, 222 (1-3), p. 125-131. https://doi.org/10.1016/S0927-7757(03)00242-5.
68. Kolářová K., Kasálková N., Dvořánková B., Michálek J., Švorčík V. (2008). Surface modification of hydrogels and cell adhesion. Materials Science Forum, 567–568, p.265–268. https://doi.org/10.4028/www.scientific.net/MSF.567-568.265.
69. Švorčík V., Kotál V., Bláhová O., Špírková M., Sajdl P., Hnatowicz V. (2006). Modification of surface properties of polyethylene by Ar plasma discharge. Nuclear Instruments and Methods in Physics Research Section B: Beam Interactions with Materials and Atoms, 224

(2), p. 365–372. https://doi.org/10.1016/j.nimb.2005.10.003.
70. Kim K. S., Ryu Ch. M., Park Ch. S., Sur G. S., Park Ch. E. (2003). Investigation of crystallinity effects on the surface of oxygen plasma treated low density polyethylene using X-ray photoelectron spectroscopy. Polymer, 44 (20), 6287–6295. https://doi.org/10.1016/S0032-3861(03)00674-8.
71. Kasálková N., Makajová Z., Pařízek M., Slepička P., Kolářová K., Bačáková L., Hnatowicz V., Švorčík V. (2010). Cell adhesion and proliferation on plasma-treated and poly(ethylene glycol)-grafted polyethylene. Journal of Adhesion Science and Technology, 24 p. 743–754. https://doi.org/10.1163/016942409X12579497420762.
72. Pařízek M., Kasálková N., Bačáková L., Slepička P., Lisá V., Blažková M., Švorčík V. (2009). Improved adhesion, growth and maturation of vascular smooth muscle cells on poly- ethylene grafted with bioactive molecules and carbon particles. International Journal of Molecular Sciences; 10, p. 4352–4374. https://doi.org/10.3390/ijms10104352.
73. Brouette N., Sferrazza M. (2013). PEG polymer brushes via the Langmuir–Schaefer techni- que: The transfer ratio. Journal of Colloid and Interface Science 394, p.643–645. https://doi.org/10.1016/j.Jcis. 2012.12.019.
74. Slepičková Kasálková N., Slepička P., Kolská Z., Sajdl P., Bačáková L., Rimpelová S., Švorčík V. (2012). Cell adhesion and proliferation on polyethylene grafted with Au nanoparticles. Nuclear Instruments and Methods in Physics Research B; 272, p.391–395. https://doi.org/10.1016/j.nimb.2011.01.108.
75. Švorčík V., Kasálková N., Slepička P., Záruba K., Král V., Bačáková L., Pařízek M., Lisá V., Ruml T., Gbelcová H., Rimpelová S., Macková A. (2009). Cytocompatibility of Ar^+ plasma treated and Au nanoparticle-grafted PE. Nuclear Instruments and Methods in Physics Research B, 267, p. 1904–1910. https://doi.org/10.1016/j.nimb.2009.03.099.
76. Kolská Z., Řezníčková A., Nagyová M., Slepičková Kasálková N., Sajdl P., Slepička P., Švorčík V. (2014). Plasma activated polymers grafted with cysteamine improving surfa- ces cytocompatibility. Polymer Degradation and Stability, 101, p.1-9. https://doi.org/10.1016/j.polymdegradstab.2014.01.024.
77. Xu, Q.; Yang, J.; Dai, J.; Yang, Y.; Chen, X.; Wang, Y. (2013). Hydrophilization of porous polypropylene membranes by atomic layer deposition of TiO_2 for simultaneously improved permeability and selectivity. J. Membr. Sci. 448, p. 215–222. https://doi.org/10.1016/j.memsci.2013.08.018.
78. Szabová, R.; Cern ˇ áková, L.; Wolfová, M.; Cern ˇ ák, M. (2009). Coating of TiO_2 nanoparticles on the plasma activated polypropylene fibers. Acta Chim. Slovaca, 2, p. 70–76. https://ojs.fchpt.stuba.sk/ojs/index.php/ACS/article/view/69.
79. Chen, H.; Kong, L.; Wang, Y. (2015). Enhancing the hydrophilicity and water permeability of polypropylene membranes by nitric acid activation and metal oxide deposition. J. Membr. Sci., 487, p. 109–116. https://doi.org/10.1016/j.memsci.2015.03.044.
80. Youngblood, J.P.; McCarthy, T.J. (1999). Ultrahydrophobic polymer surfaces prepared by simultaneous ablation of polypropylene and sputtering of poly(tetrafluoroethylene) using radio frequency plasma. Am. Chem. Soc. Polym. Prepr. Div. Polym. Chem., 40, p. 563–564, https://doi.org/10.1021/ma9903456.
81. Bhushan, B. (2009). Biomimetics: Lessons from Nature. An overview. Philos Trans. R Soc. A Math. Phys. Eng. Sci., 367, p. 1445–1486. https://doi.org/10.1098/rsta.2009.0011.
82. Quéré, D. (2002). Reports on Progress in Physics. Phys. Stat. Mech. Appl. 313, p. 32–46. https://iopscience.iop.org/article/10.1088/0034-4885/68/11/R01/meta.
83. Di Mundo, R.; Palumbo, F.; D'Agostino. (2008). R. Nanotexturing of polystyrene surface in fluorocarbon plasmas: From sticky to slippery superhydrophobicity. Langmuir, 24, p. 5044–5051. https://doi.org/10.1021/la800059a.

84. Di Mundo, R.; Palumbo, F.; D'Agostino. (2010). R. Influence of chemistry on wetting dynamics of nanotextured hydrophobic surfaces. Langmuir, 26, 5196–5201. https://doi.org/10.1021/la903654n.
85. Palumbo F, Lo Porto C, Favia P. (2019). Plasma Nano-Texturing of Polymers for Wettability Control: Why, What and How. Coatings. 9 (10), p. 5196–5201. https://doi.org/10.3390/coatings9100640.
86. Kong J., Yung K. L., Xu Y., Tian W. (2010). Wettability transition of plasma-treated polystyrene micro/nano pillars-aligned patterns. Express Polym. Lett. 4, 753. https://doi.org/10.3144/expresspolymlett.2010.91.
87. O. Kylián, O. Polonskyi, J. Kratochvíl, A. Artemenko, A. Choukourov, M. Drábik, P. Solař, D. Slavínská, and H. Biederman. (2012). Control of Wettability of Plasma Polymers by Application of Ti Nano-Clusters. Plasma Processes Polym. 9, 180. https://doi.org/10.1002/ppap.201100113.
88. Kwiatkowski M., Terebun P., Mazurek P., Pawłat J. (2018). Wettability of Polymeric Materials after Dielectric Barrier Discharge Atmospheric-pressure Plasma Jet Treatment. Sensors and Materials, 30, (5), p.1207–1212. https://doi.org/10.18494/SAM.2018.1890.
89. Šorli I., Petasch W., Kegel B., Schmit H., Liebel G. (1996). Plasma processes part I: plasma basics, plasma generation. Informacije MIDEM; 26, p. 35–45.
90. de Geyter N., Morent R., Leys C., Gengembre L., Payen E. (2007). Treatment of polymer films with a dielectric barrier discharge in air, helium and argon at medium pressure. Surface and Coatings Technology; 201 (16-17), p.7066–7075. https://doi.org/10.1016/j.Surfcoat.2007.01.008.
91. Vesel A., Junkar I., Cvelbar U., Kovač J., Mozetič M. (2008). Surface modification of polyester by oxygen and nitrogen-plasma treatment. Surface and Interface Analysis; 40, p. 1444–1453. https://doi.org/10. 1002/sia.2923.
92. Kim Y. J., Kang I. K., Huh M. W., Yoon S. C. (2000). Surface characterization and in vitro blood compatibility of poly(ethylene terephthalate) immobilized with insulin and/or heparin using plasma glow discharge. Biomaterials, 21, p. 121-130. https://doi. org/10.1016/S0142-9612(99)00137-4.
93. Vesel A., Junkar I., Cvelbar U., Kovac J., Mozetic M. (2008). Surface modification of polyester by oxygen and nitrogen-plasma treatment. Surf. Interface Anal., 40; 11, p. 1444–1453.https://doi.org/10.1002/sia.2923.
94. Vrlinic T., Vesel A., Cvelbar U., Krajnc M., Mozetic M. (2007). Rapid surface functionalization of poly(ethersulphone) foils using a highly reactive oxygen-plasma treatment. Surf. Interface Anal., 39; 6, p. 476–481. https://doi.org/10.1002/sia.2548.
95. Feng J., Wen G., Huang W., Kang E., Neoh K. G. (2005). Influence of oxygen plasma treatment on poly(ether sulphone) films. Polym. Degrad. Stabil., 91; 1, p. 12–20. https://doi.org/10.1016/j.polymdegradstab.2005.05.001.
96. Cvelbar U., Mozetic M., Junkar I., Vesel A., Kovac J., Drenik A., Vrlinic T., Hauptman N., Klanjsek - Gunde M., Markoli B., Krstulovic N., Milosevic S., Gaboriau F., Belmonte T. (2007). Oxygen plasma functionalization of poly(p-phenilene sulphide). Appl. Surf. Sci., 253; 21, p. 8669–8673. https://doi.org/10.1016/j.apsusc. 2007.04.074.
97. Vesel A. (2010). Modification of polystyrene with a highly reactive cold oxygen plasma. Surf. Coat. Technol., 205 ; 2, p. 490–497. https://doi.org/10.1016/j.Surfcoat.2010.07.016.
98. Wang M. J., Chang Y. I., Poncin - Epaillard F. (2005). Acid and basic functionalities of nitrogen and carbon dioxide plasma-treated polystyrene. Surf. Interface Anal., 37; p. 348. https://doi.org/10. 1002/sia.2029.
99. Sowe M, Novak I., Vesel A., Junkar I., Lehocky M., Saha P., Chodak I. (2009). Analysis and Characterization of Printed Plasma-Treated Polyvinyl Chloride. Int. J. Polym. Anal. Chem., 14; 7, p. 641–651. https://doi.org/10.1080/1023666090322549 4.
100. Asadinezhad A., Novak I., Lehocky M., Bilek F., Vesel A., Junkar I., Saha P., Popelka A. (2010). Polysaccharides Coatings on

Medical-Grade PVC: A Probe into Surface Characteristics and the Extent of Bacterial Adhesion. Molecules, 15; 2, 1007–1027. https://doi.org/10.3390/molecules15021007.
101. Asadinezhad A., Novak I., Lehocky M., Sedlarik V., Vesel A., Junkar I., Saha P., Chodak I.. A (2010). Physicochemical Approach to Render Antibacterial Surfaces on Plasma-Treated Medical-Grade PVC: Irgasan Coating. Plasma Processes Polym.; 7; 6, p. 504–514. https://doi.org/10.1002/ppap.200900132.
102. Vesel A., Mozetic M.,. Hladnik A, Dolenc J., Zule J., Milosevic S., Krstulovic N., Klanjsek - Gunde M., Hauptman N. (2007). Modification of ink-jet paper by oxygen-plasma treatment**.** J. Phys. D: Appl. Phys., 40; 12, p. 3689–3696. https://iops cience. iop.org/article/10.1088/0022-3727/4 0/12/022/meta.
103. Gorjanc M., Bukosek V., Gorensek M., Vesel A. (2010). The Influence of Water Vapor Plasma Treatment on Specific Properties of Bleached and Mercerized Cotton Fabric**.** Tex. Res. J., 80; 6, p. 557–567. https://doi.org/10.1177/0040517509348330.
104. Jovancic P., Jocic D., Radetic M., Topalovic T., Petrovic Z. L. (2005). The Influence of Surface Modification on Related Functional Properties of Wool and Hemp. Curr. Res. Adv. Mater. Process; 494; p. 283–290. https://doi.org/10.4028/www. scientific.net/MSF.494.283.
105. Vesel A., Mozetic M., Strnad S., Stana–Kleinschek K., Hauptman N., Persin Z. (2010). Plasma modification of viscose textile. Vacuum, 84; 1, p. 79–82. https://doi.org/10.1016/j.vacuum.2009.04.028.
106. Pankaj et al. (2014). Applications of coldplasma technology infood packaging. Trends in Food Science & Technology; 35, p.5-17. https://doi.org/10.1016/j.tifs.2013.10.009.
107. Kuo Y.-L., Chang K.-H., Chiu C. (2017). Carbon-free SiOx ultrathin film using atmospheric pressure plasma jet for enhancing the corrosion resistance of magnesium alloys, Vacuum, vol. 146, p. 8-10. https://doi.org/10.1016/j.vacuum.2017.09.028.
108. Audronis M., Hinder S.J., Mack P., Bellido-Gonzalez V., Bussery D., Matthew A., Baker M.A. (2011). A comparison of reactive plasma pre-treatments on PET substrates by Cu and Ti pulsed-DC and HIPIMS discharges, Thin Solid Films; vol. 520 (5), p. 1564-1570. https://doi.org/10.1016/j.tsf.2011.09.011.

This page is intentionally left blank

Production of Tuwo from Sorghum-Cowpea and Millet-Cowpea Composite Flours: Assessment of Flour Quality Parameters and the Textural Properties and Acceptability of Tuwo

S.Y. Bagirei, Iro Nkamaσ, M.H. Badau & P. Y. Idakwo

IBB, University

ABSTRACT

Sorghum-Cowpea and Millet-Cowpea composite flours were produced at 70:30 cereals to legume ratios. Functional properties, proximate composition, amino acids profile and protein quality of the flours were determined. The flours were then used to produce tuwo (a stiff porridge made from flours of cereal grains, consumed in different forms across Africa and Asia), and the textural properties and acceptability of the tuwo were evaluated. Cowpea addition at 30% has significantly increased Water Absorption Capacity, Least Gelling Concentration and Gelatinisation Temperature but has no significant effect on Swelling Capacity and Bulk Density. The treatment has significantly increased the ash and protein contents but has no significant effect on fat content. Curiously, Carbohydrate content and Energy Value were significantly reduced. Methionine, tryptophan and valine contents of the samples were significantly increased by 30% cowpea addition.

Keywords: tuwo, composite flours, functional properties, tuwo texture.

Classification: DDC Code: 641.5638 LCC Code: RM237.86

Language: English

LJP Copyright ID: 392953
Print ISSN: 2631-8474
Online ISSN: 2631-8482

London Journal of Engineering Research

Volume 22 | Issue 7 | Compilation 1.0

Production of Tuwo from Sorghum-Cowpea and Millet-Cowpea Composite Flours: Assessment of Flour Quality Parameters and the Textural Properties and Acceptability of Tuwo

S.Y. Bagirei[α], Iro Nkama[σ], M.H. Badau[ρ] & P. Y. Idakwo[ꝷ]

ABSTRACT

Sorghum-Cowpea and Millet-Cowpea composite flours were produced at 70:30 cereals to legume ratios. Functional properties, proximate composition, amino acids profile and protein quality of the flours were determined. The flours were then used to produce tuwo (a stiff porridge made from flours of cereal grains, consumed in different forms across Africa and Asia), and the textural properties and acceptability of the tuwo were evaluated. Cowpea addition at 30% has significantly increased Water Absorption Capacity, Least Gelling Concentration and Gelatinisation Temperature but has no significant effect on Swelling Capacity and Bulk Density. The treatment has significantly increased the ash and protein contents but has no significant effect on fat content. Curiously, Carbohydrate content and Energy Value were significantly reduced. Methionine, tryptophan and valine contents of the samples were significantly increased by 30% cowpea addition.

Protein Efficiency Ratio (PER), Essential Amino Acids Index (EAAI), Biological Value (BV) and Nutritional Index (NI) all showed significant increases at 30% cowpea addition. The textural properties of the tuwo samples showed remarkable trends. The cooling time of tuwo and its index of hardness correlated positively ($r < 0.9$) and fit well into a linear polynomial curve.

The hardness of tuwo at any temperature can be estimated from the linear equation with good accuracy. The overall acceptability of sorghum and millet tuwo with 30% cowpea addition did not show any significant variation from control samples indicating that tuwo made from complemented cereal flours is acceptable to the consumer.

Keywords: tuwo, composite flours, functional properties, tuwo texture.

Author α: Dept. of Food Science & Technology, IBB, University, Lapai, Niger State.
ρ ꝷ: Dept. of Food Science & Technology, University of Maiduguri.
σ: Dept. of Food Science & Nutrition, University of Nigeria, Nsukka.

I. INTRODUCTION

The term complementation is used with respect to proteins when the relative deficiency of an amino acid in one is compensated by a surplus from another protein consumed at the same time. A combination of cereals and legumes where one complements the other with the deficient amino acid creates mutual balance resulting in nutritional complementation. The protein quality is greater than either protein source used alone.

This principle of nutritional complementarities of cereal and legume proteins seems to have been discovered empirically on all continents; rice with soybean in South-East Asia, sorghum or millet plus chickpea or pigeon pea in South Asia, and rice with cowpea in tropical Africa (Hulse, 1991).

Chemical analysis has shown that the amino acids deficient in the legume are generally adequately compensated by the protein of cereals and vice versa. The mutual compensation is closest to ideal when the ratio by mass of cereal to legume is roughly 70:30, in which proportion each provides about equal parts by mass of protein. Eating cereal and legumes together in this proportion has

been demonstrated to have greater complementary benefit than if the two are eaten in the similar quantitative proportions, but at different meal times (Hulse, 1991). The nutritional response of combining two proteins has been classified into four groups using rat bioassay in which *Type III* is reported to have the true complementary effect because one protein source has considerably higher concentration of the most limiting amino acid than in the other, producing a synergistic effect such as maize and soy or sorghum and soy (Bressani *et al.*, 1972).

Sorghum and millet are rated as poor cereal grains due to their high levels of anti-nutritional factors like phytic acid, polyphenols, and tannins that readily forms complexes with monovalent and multivalent cations of potassium, calcium, iron, zinc, magnesium and other cations, reducing their bioavailability and creating a deficit in their absorption (Boncompagni, *et al.*, 2018). This is in addition to the fact that they are rich in the essential sulphur-containing amino acids, methionine and cystine but deficient in lysine.

Therefore the combination of cereal grains and legumes in traditional food preparation complement each other since the latter are found to be rich in lysine but deficient in both methionine and cystine (Nkama and Sopade, 1990). Thus, the cereal-legume blends serve as major sources of calorie, proteins, minerals and vitamins. Consequently, the complementation of the grain legumes has been suggested as one way of improving the protein quality of cereal based diets (Nkama, *et al.,* 1995). Production of shelf stable maize-cowpea composite flour can increase the availability of the product for wider application in many cereal-based traditional foods like *tuwo, danwake, masa* etc. The evaluation of the functional properties, proximate composition, amino acid profile and protein quality of sorghum-cowpea and millet-cowpea composite flours can contribute to general efforts for traditional food products development and industrialisation drive for the traditional food sub-sector.

The regional ICRISAT West African trials of the International Sorghum Food Quality Trials found four important quality criteria for *tuwo* to include taste, colour, texture and overnight keeping quality (Scheuring et al., 1982). However, consumption temperature and aroma are equally regarded as quality factors. *Tuwo* is normally served immediately after preparation as hot as it were, though it may be allowed to stay in the open dish or plate for some minutes under the prevailing ambient condition for the temperature to drop enough to be comfortably cut with the bare hand. This cooling process, as insignificant as it may seem, is an important aspect of consideration in *tuwo* processing as it determines the final eating texture of the product. Upon cooling the gelatinized starch of the *tuwo* undergo retrogradation and also losses moisture which reduce the stickiness of the product and increase the *Tuwo* hardness. The desired final *tuwo* hardness determines the water: flour ratio to be mixed during production, taking into consideration the moisture loss during cooling and the subsequent texture modification.

However, research on the cooling behaviour of *tuwo* was not given enough attention probably due to fact that *tuwo* preparation is still a household process that is yet to be industrialized.

Tuwo texture preference depends to a large extend on individual choice and community practice. However, people generally tend to prefer non-sticky *tuwo* with moderate hardness. The gel should be stiff, but not dense. A person should be able to dip in his fingers, scoop out a piece and readily manipulate the piece with the forefingers and thump without the gel adhering to the fingers (Scheuring, 1982).

The colour of *tuwo* is normally the colour of the grain and the method adopted for preparing the flour. However white colour *Tuwo* is generally considered attractive and qualitative. In some practices, spent steep water is used to improve the white colour appearance by soaking the grains overnight. The taste of *tuwo*, like its colour, depends on the grain from which it is prepared and the method of flour preparation. Fermented grains tend to produce sour taste while *tuwo* prepared with added ash leachate gives characteristic tardy taste. Generally bland taste is considered most acceptable. *Tuwo* aroma is an

important consideration in the processing. In some cases the formed gel is allowed to stay on fire until it starts caking from the bottom of the pot. The resulting caramel flavor of the caramelized starch adds to the aroma of the *tuwo*.

II. MATERIALS AND METHODS

2.1 Preparation of Composite Flours

Three kilograms each of sorghum and millet grains were tempered with water using a quantity of 3% (v/w) followed by decortication of the grains in commercial dehulling machine (previously cleaned), where the germs and hulls of the grains were removed. The decorticated grains were aspirated manually to remove adhering hulls and then ground into flour using a Laboratory Hammer mill. Cowpea flour was produced by first cleaning and sorting the cowpea sample. The cleaned sample was then soaked in water at room temperature for 1hr and subjected to thermal treatment at 80°C for 20 minutes in a steam bath. The seeds were manually dehulled and dried in a solar dryer. The dried seeds were then dry-milled using a Laboratory Hammer mill.

Complementation was carried out at cereal to cowpea ratio 70:30 as recommended by Nkama, 1993. The right quantities each of the sorghum and millet flours were thoroughly mixed with the right quantities of cowpea flours using a laboratory mixer and sieved using a standard sieve with 300µm aperture and then kept in airtight polythene bags until needed.

2.2 Determination of Functional Properties

Determination of Water Absorption Capacity (WAC): Water absorption capacity was determined using the method of Sathe and Salunkhe (1981) with slight modifications. 10 ml of distilled water was added to 1.0 g of the sample in a beaker. The suspension was stirred using a glass stirrer for 5 min. The suspension obtained was thereafter centrifuged at 3555 rpm for 30 minutes and the supernatant measured in a 10 ml graduated cylinder. The density of water was taken as 1.0 g/cm3. Water absorbed was calculated as the difference between the initial volume of water added to the sample and the volume of the supernatant.

Determination of Least Gelling Concentration (LGC): The least gelation concentration was determined by the method of Sathe *et al.* (1981). Test tubes containing suspensions of 2, 4, 6, 8 up to 20% (w/v) flour in 5 ml distilled were heated for 1 h in boiling water, followed by cooling in ice and further cooling for 2 h at 4oC. The least gelation concentration was the one at which the sample did not fall down or slip when the test tube was inverted.

Determination of Gelatinization Temperature (GT): GT was determined according to the method described by Shinde (2001). 1 g of flour sample was weighed accurately in triplicate and transferred to 20 ml screw capped tubes. 10 ml of water was added to each sample. The samples were heated slowly in a water bath until they formed a solid gel. At complete gel formation, the respective temperature was measured and taken as gelatinization temperature.

Determination of Swelling Capacity (SC %): This was determined with the method described by Leach *et al.* (1959) with modification for small samples. One gram of the flour sample was mixed with 10 ml distilled water in a centrifuge tube and heated at 80°C for 30 min. This was continually shaken during the heating period. After heating, the suspension was centrifuged at 1000×g for 15 min. The supernatant was decanted and the weight of the paste taken. The swelling power was calculated as:

Swelling power = weight of the paste / weight of dry flour.

Determination of Bulk Density: This was carried out using the procedure of Narayana and Narasinga (1984). A specified quantity of the flour sample was transferred into an already weighed measuring cylinder (w_1) and gently tapped to eliminate spaces between the flour. The level was noted to be the volume of the sample and then weighed (W_2). The study was conducted in triplicate and Bulk Density obtained as follows:

Bulk density (g/cm3∓ $W_2 — W_1$/Vol. of Sample

2.3 Proximate Analyses

Moisture Content: moisture content of samples was determined by hot air oven drying method as recommended by AOAC (1990).

Crude Protein: the Kjeldahl Digestion method was used to estimate the nitrogen in the sample which was then multiplied by the nitrogen conversion factor 6.25 to obtain the percentage protein (AOAC, 1990).

Fat Content: This was carried out according to (AOAC, 1990). Diethyl ether at 50°C was used for the extraction under reflux for 5h using a Soxhlet apparatus.

Total Ash: The ash content in the sample was determined by incineration with the furnace at 5500C (method 923-03, AOAC, 1990) after a period of 31 - 32 h a white ash was removed and placed in a desiccator for 1 h and then weighed.

Ash content (%) = (Weight of Ash/ Weight of sample) x 100%

Carbohydrate: Percentage Carbohydrate was obtained by difference (AOAC, 1990). The sum of Percentage Moisture, Fat, Protein and Ash was subtracted from 100 and the balance was recorded as percentage Carbohydrate.

Energy Value (kcal.): The sample calorific value was estimated in kcal/g by multiplying the percentages of crude protein, crude fat and carbohydrate with the recommended factors (% Protein x 2.44, % Fat x 8.37 and % CHO x 3.57) as proposed by Martin and Coolidge [1978].

2.4 Amino Acids and Protein Quality

Determination of Amino Acids: Amino Acids were profiled by the Isocratic HPLC–2 methods (AOAC, 2000). Samples were solubilized, centrifuged and filtered through a 0.22 µm membrane. The filtrate was then used for the experiment. Standard solutions of the amino acids (both essential and non-essential) were prepared and serially diluted to give 25pmol of each amino acid derivative. Chromatographic separation of samples was carried on a Buck scientific BLC10/ 11–model HPLC equipped with UV 338nm detector.

Amino Acid Score: The amino acid score was calculated using the ratio of a gram of the limiting amino acid in the food to the same amount of the corresponding amino acid in the reference diet multiplied by 100. The scoring patterns suggested by the FAO/WHO/UNU6 for children of 1-2 years of age were used for this purpose.

$$Amino\ Acid\ Score\ (\%) = \frac{Value\ of\ EAA\ in\ Food\ Sample\ (\frac{g}{100g\ Protein})}{FAO\ Ref.\ Value\ for\ Essential\ Amino\ Acids}\ x\ 100$$

The Essential Amino Acid Index [EAAI]: was calculated using the method of Labuda et al. (1982) as reported by Steve, I.O., 2012, according to the following equation:

$$EAAI = \sqrt[9]{\frac{[Lys\ x\ Threo\ x\ Val\ x\ Meth\ x\ Isoleu\ x\ Leu\ Phenylal\ x\ Histi\ x\ Trypt]a}{[Lys\ x\ Threo\ x\ Val\ x\ Meth\ x\ Isoleu\ x\ Leu\ Phenylal\ x\ Histi\ x\ Trypt]b}}$$

Where: [lysine, tryptophan, isoleucine, valine, threonine, leucine, phenylalanine, histidine and methionine]a in test sample and [lysine, tryptophan, isoleucine, valine, threonine, leucine, phenylalanine, histidine and the sum of methionine and cystine]b content of the same amino acids in standard protein [%] [egg or casein] respectively.

Protein Efficiency Ratio (PER): Protein Efficiency Ratio of the samples were calculated according to the equations developed by Alsmeyer *et al.*, (1974) as used by Ogunmodimu *et al.*, (2015)

PER = 0.06320 [X10] -0.1539

Where: X10 = Thr + Val + Met + Ile + Leu + Phe + Lys + His + Arg + Tyr

Biological Value (BV): Biological Values were computed according to the methods of Mune-Mune *et al.*, 2011 as a function of EAAI.

BV = 1.09 (EAA Index) – 11.7.

Nutritional Index (NI): The nutritional index of the food samples was calculated using the formula below as described by Crisan and Sands (1978).

$$Nutritional\ Index(\%) = \frac{EAAI\ x\ \%\ Protein}{100}$$

2.5 Tuwo Preparation

Tuwo preparation method as described by Bolade *et al.* (2002) was used throughout the experiment. The overall ratio of flour to water used was 1:3.5 (w/v). Cold slurry of the flour was first prepared by mixing 20% of the desired quantity of flour (1 kg) with 25% of the desired quantity of water (3.5 l). This was followed by bringing 60% of the water into boiling and the cold slurry initially prepared was added to this boiling water coupled with vigorous stirring, using a wooden stirrer to form a consistent gruel. The remaining quantity of the flour (80% of the desired total) was then added incrementally to the boiling gruel with continuous stirring so as to avoid lumps formation and to ensure a homogenous gel is obtained. The remaining quantity of water (15% of the desired total) was finally added to the formed gel, covered properly without stirring, and allowed to cook for about 5 - 7 min, after which it was stirred vigorously to ensure smoothness of the gel. The final product so obtained is the desired *Tuwo*.

2.6 Textural Properties of Tuwo

Determination of Cooling Rate of Tuwo: 10 equal quantities (30g) of each *Tuwo* sample was taken immediately after preparation with the aid of a stainless steel die to obtain uniform sample size and surface area. The die was lined with vegetable oil to avoid sticking of the *Tuwo* sample on the inner surface of the die. The samples were kept in covered sample holders at the prevailing ambient temperature (34±1°c). Successive temperatures of the *tuwo* samples were recorded with a thermometer at intervals of 10 minutes for the first six readings and then twenty minutes subsequently until constant temperature is attained.

Determination of Index of Hardness: Index of hardness was estimated from the depth of penetration data (recorded as mm of penetration) obtained by Hand Penetrometer while maintaining constant force of penetration. Ten equal quantities of each *Tuwo* sample was taken immediately after preparation with the aid of a stainless steel die to obtain uniform sample size and surface area. The die was lined with vegetable oil to avoid sticking of the *Tuwo* sample on the inner surface of the die. The samples were kept in covered sample holders at room temperature (34±1°c). Successive temperatures and hardness were measured using a thermometer and a Hand Penetrometer respectively at 10 minutes intervals for the first one hour and 30 minutes intervals subsequently until constant temperature and hardness were recorded. The drop in temperature and increase in hardness with time were recorded as cooling behaviour.

2.7 Sensory Evaluation of Tuwo

A group of twelve people generally familiar with *tuwo* were trained for the sensory evaluation as described by Santacruz *et al.*, 2009. A seven point hedonic scale was used to rank the degree of like and dislike of the tuwo samples by the twelve semi-trained panelists. Point seven represented like extremely and point one represented dislike extremely. Samples were coded with random numbers and presented to the assessors.

2.8 Statistical Analysis

The results were analyzed by 3-way ANOVA and mean separation carried out by the Tukey-Kramer hsd using MATLAB statistical software [MATLAB7.12.0 (R2011a)]. The correlation of the *tuwo* temperature and index of hardness of *tuwo* samples were carried out by multiple regression analysis, curve fitted by linear polynomial curve fitting, and the constants evaluated from the curves were used to predict the index of hardness from 30°C to 80°C. The predicted values were used to plot the regression lines to show the impact of the treatments on the cooling behaviour of the samples.

III. RESULTS AND DISCUSSION

3.1 Quality Parameters of Composite Flours

Functional Properties: Table 1 shows the measured values of the Functional Properties of the flour samples. The influence of 30% cowpea addition on the functional properties of the samples is evident from the values recorded. The values of control samples compare favourably

with the data recorded by Chandra and Samsher, 2013, and also demonstrate the influence of cowpea addition on the functionality of cereal flours.

Table 1: Functional Properties of Flours

Property	Sorghum Flour		Millet Flour	
	Single	Composite	Single	Composite
WAC (%)	189.7 ± 2.1^{g}	192.7 ± 1.53^{h}	192.3 ± 1.8^{g}	194.2 ± 2.02^{h}
LGC (%)	8.3 ± 0.8^{g}	9.5 ± 1.0^{h}	9.7 ± 0.8^{g}	10.5 ± 0.5^{h}
GT (°C)	62 ± 1.7^{g}	63.7 ± 1.15^{h}	64.3 ± 1.2^{g}	65.3 ± 0.58^{h}
SC (%)	15.7 ± 0.6^{g}	16.1 ± 0.23^{g}	15.7 ± 0.3^{g}	16.0 ± 1.0^{g}
BD (Kg/m³)	0.53 ± 0.02^{g}	0.54 ± 0.01^{g}	0.52 ± 0.02^{g}	0.49 ± 0.02^{g}

Mean values in the same row with different superscript differ significantly ($p < 0.05$)

Water Absorption Capacity (WAC %): In cereal grain flours, WAC indicates the relative availability of starch and fibre which is important in dietary formulation (Singh, 2001). From table 1, it is observed that 30% cowpea addition caused significant increase in WAC ($p < 0.05$) in both sorghum and millet. This might have been caused by the combined WAC of the cereal and that of the legume. Each of the flour (i.e. Cereal and the Legume) has its own absorption capacity, the combination of which resulted in the observed increase in WAC of the four samples (Chandra & Shamser, 2013). The WAC of the control samples is the reflection of true nature of the grain without any treatment. *Least Gelling Concentration LGC (%)* is the lowest flour concentration at which starch gelatinization takes place which is an indication of the nature of starch and its density in a given sample which may vary from one grain to another. Both sorghum and millet exhibited similar LGC ($p > 0.05$). However, 30% cowpea addition led to significant increase ($p < 0.05$) in the value probably due to increase in non-starch components brought in by cowpea addition. millet exhibited the higher *Gelatinization Temperature (GT °C)* compared to sorghum, probably because corneous endosperms tend to exhibit higher GT than floury endosperm (Cagampang and Kirleis, 1985). The GT values recorded in this work compared favourably with that of Chandra and Samsher, 2013, but with slight disparities. Such differences may be brought about by the agronomic history of the different samples and even by the measurement precision of the various methods adopted different researchers. The extent to which a particular starch sample swells under given set of conditions is the *Swelling Capacity (SC)* of the starch which is important in process specification and material balance. 30% cowpea addition did not significantly ($p > 0.05$) affect the SC of the flours. *Bulk Density (kg/m³)* of food materials gives a measure of the amount of matter contained in the sample. Like the case of SC, cowpea addition did not significantly ($p > 0.05$) affect the BD of the flours. Values of starch density recorded in literature ranges from 1.4g/cm² to 1.6g/cm² (Rooney and Pflugfelder, 1986).

Proximate Composition and Energy Value: Table 2 shows the proximate composition of the composite flours as determined in this work.

Table 2: *Proximate Composition*

Property	Sorghum Flour		Millet Flour	
	Single	Composite	Single	Composite
Moisture (%)	11.0 ± 1.0^{g}	11.3 ± 0.6^{h}	10.6 ± 0.5^{g}	11.3 ± 0.6^{h}
Ash (%)	1.5 ± 0.5^{g}	1.7 ± 0.4^{h}	$1.1 \pm 0.2_{g}$	1.6 ± 0.4^{h}
Fat (%)	1.5 ± 0.2^{g}	1.6 ± 0.4^{g}	2.0 ± 0.2^{g}	2.1 ± 0.2^{g}
Protein (%)	12.0 ± 1.0^{g}	15.0 ± 1.0^{h}	11.3 ± 1.2^{g}	15.3 ± 1.5^{h}
Carbohydrate (%)	74.0 ± 2.3^{g}	70.4 ± 1.8^{h}	75.0 ± 1.0^{g}	69.7 ± 2.5^{h}
Energy Value (Kcal)	305.7 ± 5.1^{g}	301.5 ± 2.1^{h}	312.0 ± 2.0^{g}	303.5 ± 4.5^{h}

Mean values in the same row with different superscript differ significantly ($p < 0.05$)

Moisture Contents of the samples did not show significant variation between both sinle flours or the composite. The slight disparities recorded may be a function of the drying conditions. Moisture values of 10.82%, 10.53% for cereal flours were reported in literature (Adeoti *et al.,* 2013, Adeneke *et al.,* 2014). *Percentage Ash* contents of the samples were observed to have increased due to cowpea addition which may be attributed to the increase in total dry matter of the samples. On the other hand, cowpea addition has no significant influence on the *fat content* of the samples ($p > 0.05$). Cowpea addition has significantly increased the protein content ($p < 0.05$) of all the flours.

Percentage Carbohydrate contents and *Energy Value* of the composite flours were significantly higher than single flours. As the calorific values are obtained by multiplying the proximate values with the recommended factors, variations in the energy values of the samples follow logically from the variations in the proximate values as they are affected by the treatment.

AMINO ACIDS PROFILE: The results of amino acids profiling were presented in table 3. The result of statistical analyses showed that the amino acids were differently affected by the treatment as discussed below.

Table 3: Essential Amino Acids of Samples (g/100g Protein)

Property	Sorghum		Millet	
	Single	Composite	Single	Composite
Histidine	0.72 ± 0.014^{g}	0.63 ± 0.014^{g}	1.05 ± 0.014^{g}	1.19 ± 0.014^{g}
Isoleucine	0.96 ± 0.014^{g}	1.785 ± 0.007^{g}	2.115 ± 0.007^{g}	2.575 ± 0.007^{g}
Leucine	1.865 ± 0.021^{g}	1.725 ± 0.007^{g}	2.345 ± 0.007^{g}	2.76 ± 0.014^{g}
Lysine	2.045 ± 0.007^{g}	2.32 ± 0.014^{g}	2.035 ± 0.021^{g}	1.715 ± 0.007^{g}
Methionine	1.245 ± 0.007^{g}	1.445 ± 0.007^{h}	3.415 ± 0.007^{g}	3.64 ± 0.014^{h}
Phenylalanine	1.045 ± 0.007^{g}	0.855 ± 0.007^{g}	1.525 ± 0.007^{g}	1.74 ± 0.014^{g}
Threonine	1.055 ± 0.007^{g}	1.355 ± 0.007^{g}	1.515 ± 0.007^{g}	1.63 ± 0.014^{g}
Tryptophan	0.875 ± 0.007^{g}	1.185 ± 0.021^{h}	2.01 ± 0.014^{g}	1.76 ± 0.014^{h}
Valine	0.35 ± 0.014^{g}	0.46 ± 0.014^{h}	1.05 ± 0.014^{g}	1.35 ± 0.014^{h}
TEAA	10.16	11.76	17.06	18.36

Mean values in the same row with different superscript differ significantly ($p < 0.05$)

Leucine: it was observed that there is no significant difference at $p<0.05$ in the leucine content of the two grains, though millet (2.35) still exhibited higher leucine content compared to sorghum (1.87) but the differences are not statistically significant. *Histidine, Isoleucine, Lysine, Phenylalanine and Threonine* were observed to differ significantly between the two rains, but no significant difference was observed in their contents on the part of cowpea addition.

The histidine contents of millet (1.05g/100g protein) is higher tan tat of sorghum (0.72). This observation is consistent with reported literature where millet is generally held to be of higher nutritional value than sorghum. Significant difference was observed in the isoleucine content of the two grains with millet still having the higher value (2.12g/100g) compared to sorghum (0.96g/100g). Lysine content observed in this work for sorghum and millet do not vary significantly. Similarly, cowpea addition has slightly increased the lysine content of the samples albeit statistically insignificant at $p<0.05$. Phenylalanine content of sorghum (1.05g/100g) is significantly lower than that of millet (1.53g/100g). It was also observed that cowpea addition has significantly increased phenylalanine in the samples with millet still maintaining the lead. Threonine content of millet also showed a higher value of 1.52g/100g.

Methionine, Tryptophan, Valine: the contents of these three amino acids were significantly affected by the type of grain. The methionine content of millet was observed to be significantly the higher (3.12g/100g) than that of sorghum (1.25g/100g).

Tryptophan contents of the samples vary significantly with grain type with millet having the higher (2.01g/100g), followed by sorghum (0.88g/100g). Cowpea addition has significantly increased tryptophan in the samples. Valine

contents of the samples vary significantly with grain type; and cowpea addition significantly increased valine.

Amino Acid Score: The chemical score of each EAA expressed as the percentage of that amino acid in the sample to the same amino acid in egg which is used as the standard, is presented in table 4. The limiting amino acids observed from all the samples are tryptophan, methionine and valine. Each sample showed its unique LAA either one or any two of the three.

Table 4: Percentage Amino Acid Score (AAS %) & Limiting Amino Acids (LAA)

Property	Sorghum Flour		Millet Four	
	Single	Composite	Single	Composite
Histidine	32.73^{g}	28.64^{g}	47.73^{g}	54.1^{g}
Isoleucine	17.78^{g}	33.06^{g}	39.17^{g}	47.69^{g}
Leucine	21.69^{g}	20.06^{g}	27.27^{g}	32.1^{g}
Lysine	29.21^{g}	33.14^{g}	29.07^{g}	24.5^{g}
Methionine	13.39^{g}	15.54^{h}	36.72^{g}	39.14^{h}
Phenylalanine	22.23^{g}	18.19^{g}	32.45^{g}	37.02^{g}
Threonine	22.45^{g}	28.83^{g}	32.23^{g}	34.68^{g}
Tryptophan	18.62^{g}	25.21^{h}	42.77^{g}	37.45^{h}
Valine	5.30^{bdg}	6.97^{bdh}	15.90^{adg}	20.45^{adh}
Limiting Amino Acid	Valine, methionine	Valine	Valine	Valine

Mean values in the same row with different superscript differ significantly ($p < 0.05$)

Histidine, Isoleucine, Lysine, Phenylalanine and Threonine: the chemical score of these amino acids varies significantly between the grains and did not show any significant variation with cowpea addition. The chemical score of lysine in sorghum and millet did not show any significant difference. The score of phenylalanine in sorghum is significantly lower than the chemical score of the amino acid in millet. Similar observations can be deduced for the chemical score of histidine, isoleucine and threonine from table 4.

Leucine: the chemical score of leucine in the samples did not show any significant variation with neither the rain nor the treatment. the chemical scores of *Methionine, Tryptophan, Valine* vary significantly with grain type and with cowpea addition.

Calculated Protein Quality: Calculated Protein quality of the samples are shown in table

Table 5: Calculated Protein Quality of Samples

Property	Sorghum Flour		Millet Four	
	Single	Composite	Single	Composite
PER (g/100g)	0.53^{g}	0.64^{h}	0.91^{g}	1.05^{h}
EAAI (%)	18.41^{g}	21.3^{h}	32.34^{g}	34.96^{h}
BV (%)	8.37^{g}	11.52^{h}	23.55^{g}	26.41^{h}
Nutritional Index	2.21^{g}	3.2^{h}	3.65^{g}	5.4^{h}

Mean values in the same row with different superscript differ significantly ($p < 0.05$)

Protein Efficiency Ratio (PER): varies significantly among grain types and with cowpea supplementation, but neither pregelatinization nor fermentation has affected PER significantly. Like most of the amino acids quality parameters, millet recorded highest PER value of 0.91g/100g, followed by sorghum (0.53) then maize (0.29). Cowpea supplementation has increased by 75.9%, sorghum by 20.8%, and millet by 15.4%.

Essential Amino Acids Index (EAAI): the EAA index was observed to vary significantly with grain type and with cowpea supplementation. Supplementation increased the EAAI of maize by 57.1%, sorghum by 15.7% and millet by 8.1%.

Biological Value (BV): BV of the samples varies significantly with grain type with millet still maintain the lead. Pregelatinization and

fermentation did not significantly affect the BV, but cowpea supplementation has significantly increased the BV of all the samples. The value for maize was increased by 2,530%, (from 0.27 to 7.1), sorghum by 37.7%, and millet by 12.1%.

Nutritional Index (NI): NI of the samples varies significantly with all the three factors but not with any of their interactions. Pregelatinization has increased the NI of maize tuwo by 15.6%, but decreased that of sorghum and millet by 9% and 14.8% respectively. Fermentation, on the other hand, has increased the NI of maize tuwo by 130%, sorghum by 21.7% and millet by 15.9%. Cowpea supplementation has equally increased the NI of maize by 212%, sorghum by 44.8% and millet by 47.9% which are all significantly higher than those of non-supplemented samples.

3.2 Textural Properties and Acceptability of Tuwo

Cooling Behaviour: One of the most important changes that take place immediately after *tuwo* preparation is the hardening of the texture as the temperature drops with time.

Temperature Drop: Cooling rates of the different *tuwo* samples were estimated as the record of temperature fall with time under the prevailing ambient conditions. Table 6 shows the rate of temperature drop of the food samples with time.

Table 6: Temperature Readings (°C) with Time for Various tuwo Samples

Grain	Flour	Cooling Time in Minutes									
		0	10	20	30	40	50	70	90	110	130
Sorghum	Single	82.5	73	64.5	61.5	54.5	51.5	41.5	34	33.5	33
	Composite	82	73.5	65	59.5	55.5	50.5	45	36	33.5	34
Millet	Single	80	72.5	66.5	61	56.5	50.5	44.5	36	34.5	33.5
	Composite	80.5	71	65	59	54	49	44	36	33	34.5

Values are means of two readings

Index of Hardness: As *tuwo* is subjected to natural cooling process, moisture is being lost to the environment as starch retrogradation also takes place causing increase in the forces of attraction between the molecules leading to increase in hardness with time. Tables 7 give the penetrometer readings of the *tuwo* samples with time. The penetrometer readings recorded was observed to vary in inverse proportion to the cooling time until a constant value was attained.

Table 7: Penetrometer Readings in mm as Index of Hardness of *tuwo* Samples

Grain	Flour	Cooling Time in Minutes									
		0	10	20	30	40	50	70	90	110	130
Sorghum	Single	15.1	14.8	12.1	10.1	9.8	8.5	7	5.5	5	4.9
	Composite	13.8	13.7	12	9.3	9.6	9	6.7	4.9	4.1	4
Millet	Single	18.5	17.1	15.3	13.5	11.5	10.1	8.1	6.6	6.2	6.2
	Composite	18.5	17.1	15.3	13.5	11.5	10.1	8.1	6.6	6.2	6.2

Values are means of two readings

Hardness of cereal flour meals is attributable to the inherent associative forces within the starch molecules such as amylose/amylopectin ratio, and the level of chemical transformation during *tuwo* preparation (Bolade, 2010)). Mua and Jackson 1997 observed that higher amylose content and longer amylopectin chains could contribute to the hardness of a food gel from maize. Mua and Jackson further observed that flour preparation methods could affect the inherent associative forces within the starch molecules and by extension that of the food prepared from such flour. This is seen in the differences in penetrometer readings between supplemented and non-supplemented samples

Correlation of Temperature and Hardness with Time: The temperature and index of hardness of non-supplemented samples recorded with time all show positive correlation (Table 8). That means as

penetrometer readings between supplemented and non-supplemented samples

Correlation of Temperature and Hardness with Time: The temperature and index of hardness of non-supplemented samples recorded with time all show positive correlation (Table 8). That means as the temperature of the samples decreases with time so does the index of hardness. But the index of hardness is the extent of the penetration of the spindle into the *tuwo* sample meaning that the harder the sample the less the penetration.

Therefore the positive correlation observed between decreasing temperature and decreasing index of hardness means a negative correlation between the temperature drop and actual hardness of the sample: meaning as temperature of the sample decreases, the actual hardness increases. This is attributable to several factors (Mua & Jackson, 1997); at lower temperatures, the forces of attraction between the molecules are higher than at elevated temperatures leading to harder texture. Starch retrogredation as an inherent property of plant starches also lead to harder textures at lower temperatures.

Table 8: Correlation Coefficients (r) of Temperature & Index of Hardness for Non-supplemented Samples

	1	2	3	4	5	6
SCN (P)	0.97910	0.97682	1			
SCN (T)	0.99572	0.99079	0.99221	1		
MiCN (P)	0.99767	0.98801	0.97381	0.99443	1	
MiCN (T)	0.99007	0.99732	0.97719	0.99340	0.99377	1

Table 9: Correlation Coefficients (r) of Temperature and Index of Hardness for Supplemented Samples

FLOUR	1	2	3	4	5	6
SCS (P)	0.97285	0.97559	1			
SCS (T)	0.99381	0.98821	0.95716	1		
MiCS (P)	0.98704	0.98586	0.98998	0.98386	1	
MiCS (T)	0.99430	0.99321	0.97939	0.99445	0.99624	1

Curve Fitting [Index of Hardness (mm) Against Temperature (°C)]: As strong correlation was established between index of hardness and temperature, a linear polynomial curve was fitted to enable the prediction of hardness at any given temperature. The slope of the curve β and the intercept ε were evaluated, while r-square indicated the goodness of fit of the data to the curve. These constants were presented in table 4.10. The values of rsquare for all the samples approached zero indicating that curves were all well fitted to the data. This means that the values of hardness predicted from these constants will approximate closely to experimental data.

Table 10: Table of Constants for the Linear Regression Curves

Grain	Flour	β Slope of the Curve	E Intercept of the curve	r^2 Goodness of Fit	Adjusted r^2
Sorghum	Single	0.2197	-2.5650	0.9845	0.9806
	Composite	0.1798	-1.2970	0.9161	0.8952
Millet	Single	0.1933	-1.1510	0.9575	0.9469
	Composite	0.2101	-2.7480	0.9925	0.9906

The constants evaluated from the curves were used to predict the index of hardness between 30 to 80°C to observe the effects of grain type, processing methods and cowpea supplementation on the hardening pattern of *tuwo*.

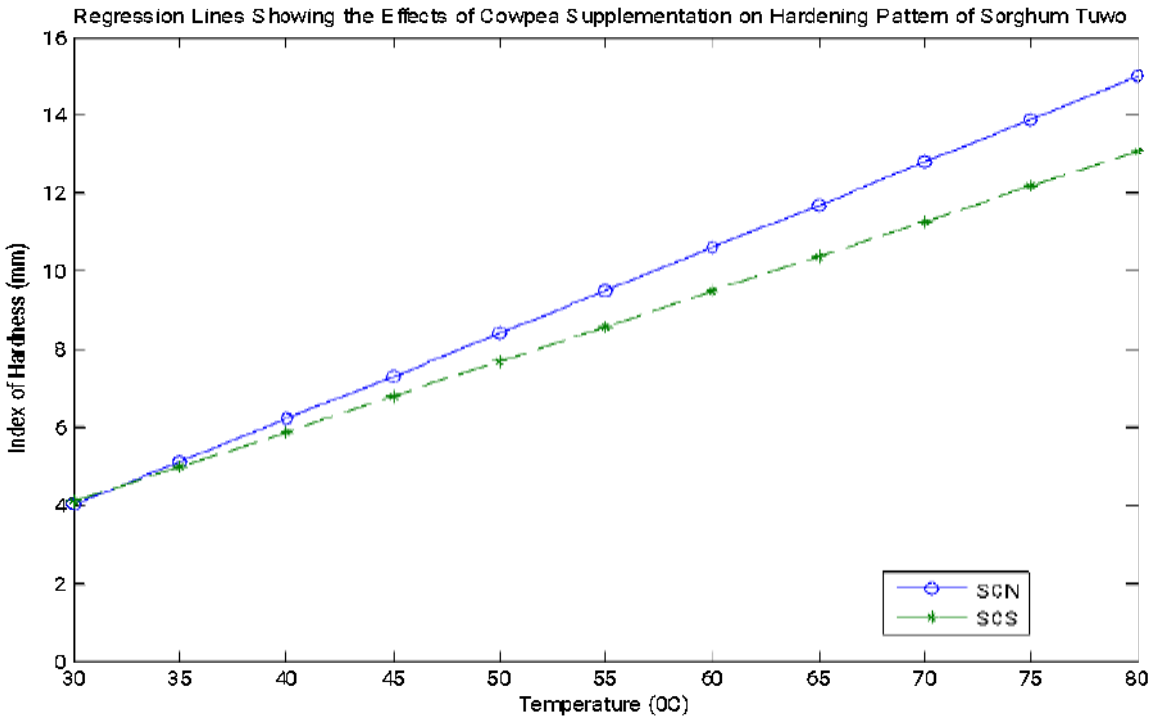

Figure 1: Regression Lines Showing the Effects of Supplementation on the Hardening pattern of Sorghum *Tuwo*

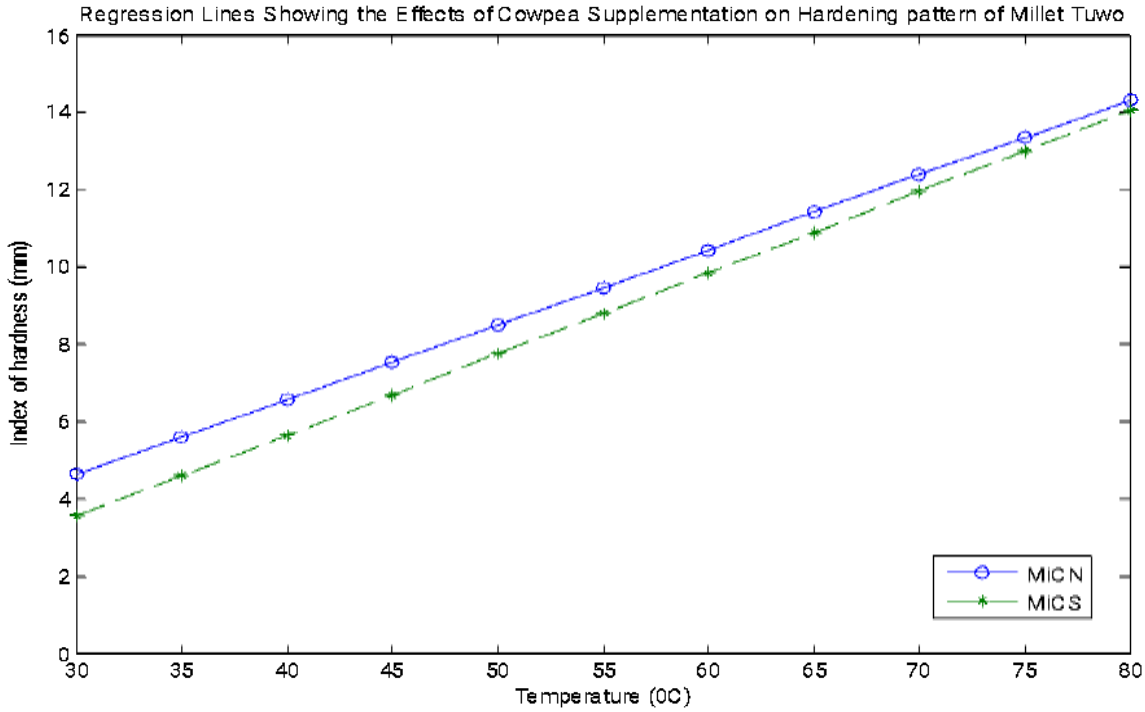

Figure 2: Regression Lines Showing the Effects of Supplementation on the Hardening pattern of Millet *Tuwo*

3.3 Tuwo Acceptability

Table 10: Sensory Evaluation scores of Tuwo Samples

Attribute	Sorghum		Millet	
	Single	Composite	Single	Composite
Colour	4.83 ± 1.64^{bdg}	3.58 ± 1.08^{bdg}	4.17 ± 2.12^{bdg}	3.58 ± 1.17^{bdg}
Aroma	4.75 ± 1.22^{adg}	3.33 ± 1.50^{adg}	4.92 ± 1.88^{adg}	3.17 ± 0.84^{adg}
Taste	4.75 ± 0.75^{bdg}	3.67 ± 1.16^{bdg}	4.08 ± 2.23^{bdg}	3.25 ± 0.87^{bdg}
Texture	4.67 ± 1.44^{bdg}	3.92 ± 1.44^{bdg}	4.58 ± 2.02^{cdg}	4.17 ± 1.47^{cdg}
Overall Acceptability	5.0 ± 0.74^{bdg}	4.00 ± 1.13^{bdg}	4.67 ± 1.72^{bdg}	3.50 ± 1.17^{bdg}

Mean values in the same row with different superscript differ significantly ($p < 0.05$)

Colour: the colour ratings of the samples vary significantly only in grain type. Pregelatinization, fermentation and cowpea supplementation did not significantly affect the colour ratings. Among the grain types, the ratings of sorghum (4.83) and millet (4.17) do not differ significantly from each other but the ratings of the two are significantly lower than that of from maize (5.75). This may be a reflection of the survey data which indicated that maize is the most preferred grain for tuwo.

Aroma: the aroma ratings of the samples did not show any significant variation with any of the three factors studied in this work. This may be due the fact that tuwo aroma does not matter much to consumers since tuwo is normally eaten with soup.

Taste: the taste ratings of the samples vary significantly with grain type and processing method, and also in the interaction of processing method and supplementation. The taste ratings of sorghum (4.75) and millet (4.08) are not significantly different from each other but both ratings are significantly lower than that of maize (5.67). This may also be a reflection of the most proffered grain for tuwo. Pregelatinization has significantly reduced the taste ratings of all the grains probably due to the loss of soluble substances without generating any taste inducing substances. Fermentation, on the other hand, has significantly reduced the taste ratings of maize and sorghum but significantly increased that of millet, probably due to flavor modification induced by the fermentation process. The increased taste rating due to fermentation observed in millet but not in sorghum and maize may be due to the higher amino acid quality recorded in millet; the interaction of which resulted in improved taste for the fermented millet tuwo.

Texture: the texture ratings of the samples differ significantly with grain type and processing methods, and with their interactions. Both pregelatinization and fermentation have significantly reduced the texture ratings of the samples, while cowpea supplementation did not have any significant effect on the texture ratings.

Overall Acceptability: on the overall, the acceptability of the tuwo samples varies significantly only with grain type and with the interaction of grain and processing method.

Pregelatinization, fermentation and cowpea supplementation all did not significantly affect the acceptability of the tuwo samples. This is an indication that improved cereal flours can be well accepted to the consumer.

IV. CONCLUSION

Cowpea supplementation significantly increased WAC, LGC, GT. Has no significant effect on SC and BD. Cowpea addition has significantly increased the ash and protein contents but has not significantly affected the fat content. CHO content and E.V were significantly reduced while Inv.D was significantly increased. Methionine, tryptophan and valine contents of the samples were significantly increased by cowpea addition.

Protein Efficiency Ratio (PER), Essential Amino Acids Index (EAAI) and Biological Value (BV) all showed significant difference among the grains and in cowpea supplementation. Nutritional Index (NI) showed significant variation with cowpea addition.

The cooling rate of *tuwo* and Index of hardness are positively correlated and fit well into a linear polynomial curve. The hardness of tuwo at any temperature can be estimated from the linear equation with good accuracy.

Cowpea addition did not significantly affect the colour ratings. Aroma and texture ratings of the samples did not show any significant variation with 30% cowpea addition. The overall acceptability of sorghum and millet *tuwo* with 30% cowpea supplementation did not show any significant variation from control samples indicating that *tuwo* made from improved cereal flours can be well accepted to the consumer.

REFERENCES

1. Adebowale, Y.A, Adeyemi, I.A. Oshodi, A.A., (2005). Functional and Physicochemical Properties of Flours of Six Mucuna Species. Afr. J. Biotech. 4(12), pp 1461 – 1468.
2. Adenekan, M.K, Oguntoyinbo, S.I, Odunmbaku, L.A and Nupo S.S. (2014). Effect of Sprouted Pigeon pea (cajanus cajan) on Proximate Composition and Sensory Value of Tuwo. Journal of Sciences & Multidisciplinary Research. Vol.6 (2).
3. Adeoti, O.A., Elutilo, O.O., Babalola, J.O., Jimoh, K.O, Azeez, L.A and Rafiu, K.A, (2013). Proximate, Mineral, Amino Acid and Fatty Acid Compositions of Maize Tuwo-Cirina Forda Flour Blends. Greener Journal of Biological Sciences. Vol. 3 (4), pp. 165-171. Available online at www.gjournals.org.
4. Alsmeyer RH, Cunigham AE, Hapich ML (1974). Equations predicted (PER) from amino acid analysis. Food Technol., 28, 34 – 38. In: Ogunmodimu et al., 2015.
5. AOAC (2000). Association of Official Analytical Chemists. 18th ed.Official Methods of Analyses. Washington D.C.
6. AOAC (1990). Association of Official Analytical Chemists. 18th ed.Official Methods of Analyses. Washington D.C.
7. Bolade, M.K., Usman, M.A., Rasheed, A.A., Benson, E.L., Salifou, I., (2002). Influence of Hydro-thermal treatment of maize grains on the quality and acceptability of tuwon masara (traditional maize gel). Food Chem., 79: 479-483.
8. Bolade, M.K., (2010). Evaluation of suitability of commercially available maize grains for tuwo production in Nigeria. Afr.. J. food. Sci.vol. 4(6)pp 371 - 381.
9. Cagampang, G.B., and Kirleis A.W., 1985. Properties of Starches Isolated from Floury and Corneous endosperm. Starch/Staerke 37:253-257. In: Dendy, D.A.V., 1995. Sorghum and Millets: Chemistry and Technology. American Association of Cereal Chemists. Minnesota.
10. Chandra, S., and Samsher, 2013. Assessment of Functional Properties of Different Flours. Afric. J. Agric. Res. Vol. 8 (38), pp 4849-4852. Available online at www.academicjournals.org.
11. Crisan E.V, Sands A (1978). Biology and Cultivation of Edible Mushrooms. Hangeri Academic Press, New York, 137-142. In: Ogunmodimu et al., 2015.
12. Cianciaruso B, Jones M.R, Kopple J.D., 1981. Histidine, an essential amino acid foradult dogs. Journal of Nutrition, 111:1074–1084.
13. Cox, R. E., and R. H. Higby. 1944. A better way to determine the jelling power of pectins. Food Ind. 16, 441.
14. Da, S, Akingbala, J.0, Rooney, L.W and Miller, F.R, (1982). Evaluation of to quality in sorghum breeding program. Pp 11-23 In: Proceedings of the International Symposium on sorghum grain quality. Rooney L.W and Murty, D.S eds. ICRISAT. India.
15. FAO/WHO/UNU, 2002: Joint FAO/WHO/UNU Expert Consultation on Protein and Amino Acid Requirements in Human Nutrition, Geneva, Switzerland. WHO Technical FAO Food and Nutrition Paper No.92, 2013: Dietary Protein Quality Evaluation in Human Nutrition. Report of an FAO Expert Consultation 31 March–2 April, 2011, Auckland, New Zealand.
16. Hamaker, B.R., Kirleise A.W., Butler, L.G., Axtell J.D., and Mertz E.T., 1987. Improving the in vitro protein digestibility of sorghum with reducing agents. Proc. Nat. Acad. Sci. USA 84:626-628. In: Dendy, D.A.V., 1995. Sorghum and Millets: Chemistry and

Technology. American Association of Cereal Chemists. Minnesota.
17. Hulse, J.H, (1991). Nature, Composition and Utilization of Grain Legumes pp 11-27. In: ICRISAT, 1991.
18. Kirleis, a.W., 1990. The prolamins of sorghum: their role in protein digestibility. In: Dendy, D.A.V., 1995. Sorghum and Millets: Chemistry and Technology. American Association of Cereal Chemists. Minnesota.
19. Labuda J, Kacerovský O, Kováè M, Štìrba A (1982). Výživa a krmenie hospodárskych zvierat. Príroda, Bratislava. p. 164s. In: Steve, I.O., 2012.
20. Leach, H.W., McCowen LD, Schoch TJ (1959). Structure of the starch granules. In: Swelling and Solubility patterns of various starches. Cereal Chem. 36:534-544.
21. Martin, E.A., Coolidge, A.A., (1978). Nutrition in Action, 4th ed. Holt, R and Wilson Co. New York, USA.
22. Mune-Mune, M.A., Minka, S.R., Mbome I.L., Etoa F.X. (2011). Nutritional Potential of Bambara Bean Protein Concentrate. In: Steve, I.O., 2012.
23. Narayana, K., and Narsinga, R.S.M., (1982). Functional Properties of Raw and Heat Processed Winged Bean (Psophocarpus tetragonolobus) Flour. J. Food Sci. 42: 534-538.
24. Nkama, I., (1993). Traditional Methods of Production of High Protein Energy Foods from Grain Legumes in the North-Eastern States of Nigeria. Annals of Borno 10: 138-148.
25. Nkama, L, Ogbo, E.N., and Igene, J.O., (1994). Proximate Composition, Shelf Stability and Consumer Acceptance of Groundnut Butter. J Arid agric. 3:7, 66-75.
26. Ogunmodimu, O. O, Ijarotimi, O. S and Fagbemi, T. N, 2015. Evaluation of nutritional properties of high protein-fiber based snacks formulated from wheat, soybean concentrate and cassava fiber. Sky Journal of Food Science Vol. 4(3), pp. 030–041. Available online http://www.skyjournals.org/SJFS .
27. Rooney, L.W., and pflugfelder, R.L., 1986. Factors affecting starch digestibility with special emphasis on sorghum and corn. J. Anim. Sci. 63:1607-1623. In: Dendy, D.A.V., 1995. Sorghum and Millets: Chemistry and Technology. American Association of Cereal Chemists. Minnesota.
28. Shinde, B.G., (2001). Isolation and characterization of starch horse grain. Unpublished M.Sc. Thesis. Mahatma Phule Krishi Vidyapeeth, Rahuri (India). pp. 16-17. In: Chandra and Shamsher, (2013).
29. Steve O.I and Olufunmilayo O.K, (2011). Determination of Amino Acid, Fatty Acid, Mineral, Functional and Choking Properties of Germinated and Fermented Popcorn (Zea mays everta) Flour. European Journal of Food Research & Review 1(2): 102-122. Available at www.sciencedomain.org.
30. Steve, I.O., 2012. Influence of germination and fermentation on chemical composition, protein quality and physical properties of wheat flour (Triticum aestivum). Journal of Cereals and Oil seeds Vol. 3(3), pp. 35-47, November 2012. Available online at http://www.academicjournals.org/JCO.
31. WHO/FAO/UNU (2007) Protein and Amino Acid Requirements in Human Nutrition; Report of a joint WHO/FAO/UNU Expert Consultation, WHO Tech. Rep. Ser. No.935. Geneva: WHO.

Improving Drainage Systems in Urbanised Areas under Projections of Land-Use Changes: Case Study of Kakia and Esamburmbur Channels of Narok Town, Kenya

Etienne Umukiza, James M. Raude, Andrea Petroselli, Simon M. Wandera, Ciro Apollonio & John. M. Gathenya

Pan African University

ABSTRACT

The changes in land use/land cover (LULC) during the process of urbanization have a profound influence on runoff increases and flooding incidents. Narok town, in Kenya, experienced numerous disasters associated with cyclic flash floods that produced human losses and economic damages. Design hydrograph and its peak flow are the key elements to determine hydraulic geometrical properties in designing an adequate drainage system. Due to the continuous occurrence in LULC changes resulting in variability of design hydrograph, this study was carried out to evaluate existing channels geometric properties (conveyance capacity), with field measurements through a ground survey using Real-Time Kinematic equipment at Kakia and Esamburmbur channels of Narok town.

Keywords: esamburmbur, kakia, hydraulic design structures, lulc changes, peak flow.

Classification: DDC Code: 363.349360973 LCC Code: TC530

Language: English

London Journals Press

LJP Copyright ID: 392954
Print ISSN: 2631-8474
Online ISSN: 2631-8482

London Journal of Engineering Research

Volume 22 | Issue 7 | Compilation 1.0

Improving Drainage Systems in Urbanised Areas under Projections of Land-Use Changes: Case Study of Kakia and Esamburmbur Channels of Narok Town, Kenya

Etienne Umukiza[α], James M. Raude[σ], Andrea Petroselli[ↀ], Simon M. Wandera[¥], Ciro Apollonio[§] & John. M. Gathenya [χ]

ABSTRACT

The changes in land use/land cover (LULC) during the process of urbanization have a profound influence on runoff increases and flooding incidents. Narok town, in Kenya, experienced numerous disasters associated with cyclic flash floods that produced human losses and economic damages. Design hydrograph and its peak flow are the key elements to determine hydraulic geometrical properties in designing an adequate drainage system. Due to the continuous occurrence in LULC changes resulting in variability of design hydrograph, this study was carried out to evaluate existing channels geometric properties (conveyance capacity), with field measurements through a ground survey using Real-Time Kinematic equipment at Kakia and Esamburmbur channels of Narok town. To further improve the drainage system in the main channels, the evaluated peak flows under assumed future LULC scenarios were used to design hydraulic geometrical properties (width, depth) for a sustainable urban drainage system.

Three geomorphic-based hydrological and hydraulic models (EBA4SUB, Manning's equation, and Civil 3D) were used under different LULC scenarios for computing channel geometry and correspondent water level. Results show that infrastructures such as highway bridges and commercial buildings contributed to narrow the channel downstream. The change in channel geometries was found to obstruct free flow for different scenarios of peak discharge and flow volume. The design conveyance capacity for the two channels considering the evaluated peak discharge from the assumed LULC scenarios can be used in improving the drainage system by local Municipal bodies to mitigate flood hazards.

Keywords: esamburmbur, kakia, hydraulic design structures, lulc changes, peak flow.

Author α: Civil Engineering and Environmental, Pan African University, Institute of Science, Technology and Innovation/Jomo Kenyatta University of Agriculture and Technology, Kenya.
σ χ: Soil, water, and Environmental Engineering Department, Jomo Kenyatta University of Agriculture and Technology, Kenya.
ↀ: Department of Economics, Engineering, Society and Business (DEIM), Tuscia University, 01100, Viterbo, (VT), Italy.
¥: Department of Civil, Construction and Environmental Engineering, Jomo Kenyatta University of Agriculture and Technology (JKUAT), Kenya.
§: Department of Agriculture and Forest Sciences (DAFNE), Tuscia University, 01100, Viterbo, (VT), Italy.

I. INTRODUCTION

Land use/land cover (LULC) can be defined as how the land is used by humans regarding the functional role of land for economic activities (Vojtek & Vojteková, 2019). Urbanization is probably the most important driver in LULC changes due to developments of facilities such as roads, houses, schools (Habete & Ferreira, 2016; Han et al., 2009), and has been the most intense form of LULC changes in many developed areas (Ohana-Levi et al., 2018; Vojtek et al., 2019).

Rapid socio-economic and urbanization are drivers of significant changes in land use and can cause, as consequence, high potential runoff (Han et al., 2009). Moreover, various human activities

have profoundly influenced the hydrological cycle and water resources management due to the growth of society and the economy (Umukiza et al., 2021). Uncontrolled land use is among the main cause of changes in hydrologic and hydraulic processes (Zope et al., 2016). Furthermore, urbanization processes as part of LULC tend to increase runoff rates and peak discharges due to the increased imperviousness and reduced along the built-up area (Ohana et al., 2013). As a matter of the fact, the process of urbanization is accompanied by vegetation removal as consequence, leading to increased runoff.

For instance, Shaina Beegam & Prince Arulraj (2018) reported urbanization as a direct effect on the environment which in turn affects the variations in runoff, which ultimately turn to flood. Recanatesi and Petroselli (2020) concentrated on the relationship between LULC change and flood risk, selecting a strategic case study in the peri-urban environment of the metropolitan area of Rome, Italy, and determined that the increase in the flood risk is more pronounced in the part of the selected area that has been more extensively interested by the soil loss. LULC changes are indeed an important factor in causing variability of rainfall-runoff properties. In recent decades, urbanization has become an environmental concern in many developing countries (Guo et al., 2011). Moreover, urban development planning should be considered as an integrated tool, taking into account drainage systems as the peri-urban area can potentially be converted into a built-up area.

Globally, floods are among the most devastating natural hazards and their frequency is increasing. There are several causes of floods, such as natural factors (e.g. climate change, heavy rainfall, high tides), and anthropogenic activities such as blocking of drainage channels, uncontrolled land use, and deforestation in headwater regions (Tingsanchali, 2012; Młyński et al., 2018). Each year, floods cause major disruption throughout the world, leading to loss of both human and animal life and damage to properties (Sharif et al., 2016). However, some land-use measures if correctly planned and implemented can help in reducing the flooding problems through the developed mitigation measures. For instance, urbanization in floodplain areas increases the risk of flooding due to the increase of peak discharge (Suriya & Mudgal, 2012).

Locally, there has been an increase in floods in Narok town, Kenya, in recent years, resulting from the fact that Narok county is urbanizing at a rapid rate like many towns in developing countries (Mwangi et al., 2019). Furthermore, population growth commonly leads to urbanization and expansion of agricultural land, hence this circumstance adversely affects hydrological processes (Coomes et al., 2001).

Also, the lack of an adequate urban drainage network can increase the risk of flooding (Alfarajat, 2014).

To further improve the drainage conveyance capacity due to the effects of LULC changes such as continuous urban expansion and intensification of agricultural activities towards the upstream area, the drainage system should take into account the transitions in land-use changes to appropriately design hydraulic structures such as channel, culverts, bridges, etc.

The design hydraulic structures for water control are sized to resist a design event, characterized by a hydrograph associated with a fixed probability of occurrence (Erpicum et al., 2021). Moreover, engineers and hydrologists deal with periodic peak flows when designing water management and drainage systems (Oluwatobi & Oluwole, 2017). Generally, hydraulic structures are designed based on design hydrograph and its peak discharge to ensure efficiency and safety during service life. In many parts of the world, hydraulic structures are mostly considered safety-focused, risk-averse, and display hesitancy to use unproven innovation over legacy tools. Indeed, hydraulic structures engineering should involve and respond to the increasing sustainability to reverse the challenges of today and the future (Erpicum et al., 2021).

Although obtaining runoff estimation in ungauged catchments is very important when designing hydraulic structures, it is indeed a challenging problem to predict runoff for these basins because

of the difficulty in obtaining adequate historical flow observations (Petroselli et al., 2020a). Thus, accurate estimation of flood discharge remains one of the major challenges to many engineers and planners who are involved in drainage project design (Heritage & Entwistle, 2020).

A recent study (Umukiza et al., 2021) evaluated future projections on the Narok town watershed in terms of LULC scenarios and related design flows for the best mitigation of floods and effective land planning. The study investigated the effects of projected LULC changes on peak flow and total runoff for the two catchments (Kakia and Esamburmbur) of Narok town, Kenya using the Event-Based Approach for Small and Ungauged Basins (EBA4SUB) rainfall-runoff model (Piscopia et al., 2015; Petroselli & Grimaldi, 2018; Petroselli et al., 2020b) to determine the design hydrographs and peak discharge in the investigated catchments.

As consequence of the aforementioned study, the present work aims to 1) carry out the hydraulic and geometric properties design of Kakia and Esamburmbur channels based on the peak flow determined under forecasted LULC change scenarios on watersheds, and 2) propose adequate conveyance capacity of the channels based on predicted effects of LULC changes as future likely scenarios to occur on rainfall-runoff regime within the watershed. After the quantification of peak discharges under different scenarios, the management structures are designed to convey the stream flow. Such knowledge will help in managing structure measures necessary for controlling the potential overflow hazard risks. In brief, this study attempts to propose channel geometries considering the expected peak flow estimated under different LULC change scenarios, for improving the urban drainage system to achieve sustainable development with good control of flood risk.

II. DATA USED, MATERIALS AND METHODS

2.1 General Overview of the Study Area

The County Government of Narok lies between latitudes 0°50′ and 1°50′ South and latitude 35°28′ and 36°25′ East. It borders the Republic of Tanzania to the South, Kisii, Migori, Nyamira, and Bomet counties to the West, Nakuru County to the North, and Kajiado County to the East. It covers a total area of 17,933 km². The study area, shown in Figure 1, is a small portion of Narok county territory, being characterized by a total extension of 46.2 km² (Umukiza et al., 2021) and it pertains to the hydrographic catchments of two seasonal streams, Kakia and Esamburmbur.

The precipitations of the area are characterized by an average rainfall of 750 mm per year, with the majority of the rainfall occurring in March and May. The temperature ranges from a minimum of 8°C to a maximum of 28°C.

The elevation of the investigated area lies between 1,844 m to 2,138 m above sea level and the water flow length is estimated to cover a maximum distance of 10,000 m to the outlet, for Kakia stream. The main economic activities are commercial farming (wheat, maize, and potatoes), livestock farming, and tourism in the famous Maasai Mara area.

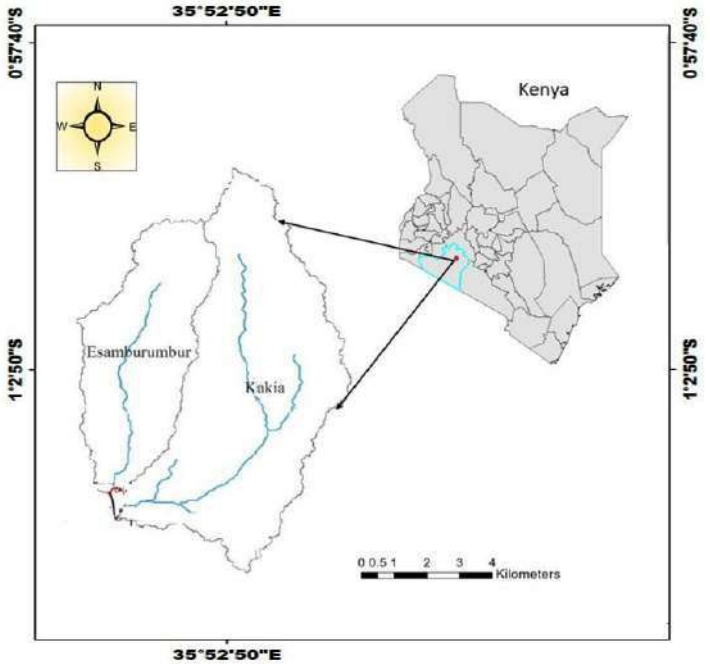

Figure 1: Kakia and Esamburmbur sub-catchments. Source: Umukiza et al. (2021)

2.2. LULC Changes in Narok Town Sub-catchment

The study by Marie Mireille et al. (2019) reported that LULC change that occurred in the investigated area in the period 1985-2019 showed a decrease in forest and pasturelands which were replaced by agriculture and built-up areas. Therefore, the major observed LULC changes were processed using supervised classification methods to assign different future scenarios starting from the Landsat image of November 2019, using Erdas Imagine 2015 (Umukiza et al., 2021).

To further understand the future likely impacts of various activities in the catchment, we hypothesized in Umukiza et al. (2021) four projected future scenarios, based on major types of LULC identified in 2019 (scenario "0").

Therefore, due to LULC changes previously mentioned, we considered in Scenario one (1) that the built-up area is 20% of the total area, the agricultural area is 75%, and the pastureland is assumed to be in poor condition with a rate of 5% of the total area. In this scenario, we assumed an intense increase in urbanization and agricultural activities leading to a drastic decrease in forest areas and rangelands.

Scenario (2) consisted of 15% of the entire catchment for the built-up area, 40% for the agricultural area, 30% for pastureland, and 15% for the forest. In this scenario, we assumed a small increase in built-up area and reforestation, while agriculture is assumed to reduce and give an increase of rangeland.

Scenario 3 assumes 50%, 40%, and 10% for the built-up area, agricultural area, and rangelands, respectively, of the entire catchment. In this scenario, we assume a considerable increase in a built-up area, we maintain the same extent of the agricultural area as Scenario 2, and we reduce the forest with a small part of rangeland.

Scenario 4 assumed 20%, 5%, 30%, 40% and 5% for pastureland, forest, built-up area, agriculture and open space, respectively. In this scenario, we assumed a regular step of 10% of the proportion from pastureland, built-up area, an agricultural area, and a small rate for forest and open space. A summary describing the current and the assumed future scenarios is presented in Table 1.

Table 1: Details of Projected Scenarios Based on Major Types of LULC Transition Found for LULC in 2019. Source: Umukiza et al. (2021)

Different Rates LULC (In Percentage) of the Entire Catchment					
LULC	2019	Scenario 1	Scenario 2	Scenario 3	Scenario 4
Forest	06.30	00.00	15.00	00.00	05.00
Pastureland	25.90	05.00	30.00	10.00	20.00
Agricultural	55.40	75.00	40.00	40.00	40.00
Open Space	00.00	00.00	00.00	00.00	05.00
Built-up area	12.50	20.00	15.00	50.00	30.00

In the present work, we focus on design channel geometry based on the peak discharges evaluated in Umukiza et al. (2021) under different scenarios of LULC. The effect of LULC changes have been expressed using the Natural Resources Conservation Services (NRCS) – Curve Number (CN), an important parameter related to the generation of runoff as presented in the study by Umukiza et al. (2021). CN value ranges between 0 (no runoff, all rainfall becomes infiltration) and 100 (no infiltration, all rainfall becomes runoff) and was calculated with the combination of spatial LULC data, soil type, and assuming an Antecedent Moisture Condition (AMC) equal to II (average soil humidity) following what was done in Umukiza et al. (2021). The average CN value for the two investigated catchments from the projected LULC scenarios was determined according to Equation 1 (Gajbhiye et al., 2014):

$$CN = \frac{\sum CN_i A_i}{A} \quad (1)$$

Where CN_i, and A_i are CN value (-) and area value (Km^2), respectively, of the generic LULC parcel, CN_i (-) is the weighted CN considering the specific areas as weights and A (km^2) is the total area of the investigated catchment.

2.3 Evaluation of Design Peak Discharge

Engineering designs of hydraulic structures such as bridges, culverts, spillways, urban drainage systems, etc., require estimated design peak flow and flow volume for flood management (Heritage & Entwistle, 2020). For small and ungauged catchments, as is the case in our study area, usually enough observed flow data are not available (Heritage & Entwistle, 2020), so calibration of the advanced hydrological and hydraulic model is difficult. Therefore, the Event-Based Approach for the Small and Ungauged Basins (EBA4SUB) rainfall-runoff model was used in Umukiza et al. (2021), since it is particularly suited to estimate design hydrograph, peak discharge, and flow volume in ungauged basins (Młyński et al. 2020). In detail, the inputs data needed by the model are the Digital Elevation Model (DEM) of the investigated catchments, the LULC data, and the rainfall data while the main parameters of the model are CN and concentration-time T_c (Petroselli & Grimaldi, 2018; Petroselli et al., 2020; Piscopia et al., 2015).

For the complete application and detailed inputs used for the EBA4SUB model to estimate flood hydrograph, flow rate, and flow volume with regards to the investigated catchments, refer can be made to the aforementioned work. Based on this, the evaluated values related to peak discharges for 50 and 100 years return periods for the different projected scenarios are summarized in Table 2.

Table 2: Peak discharge for different return periods under various LULC Scenarios (Kakia and sub-catchment). Source: Umukiza et al. (2021)

		Kakia		Ensamburmbur	
LULC	Discharge /Tr	Tr50	Tr100	Tr50	Tr100
2019	Peak Discharge (m^3/s)	130.3	164.1	75.1	94.2
Scenario 1	Peak Discharge (m^3/s)	154.2	191.1	88.9	110.1
Scenario 2	Peak Discharge (m^3/s)	121.4	154	70.8	89
Scenario 3	Peak Discharge (m^3/s)	172.2	210.4	100.6	121.8
Scenario 4	Peak Discharge (m^3/s)	145.3	181	83.4	104.2

2.4. Engineering Works and Flood Channel Dynamics

2.4.1. Evaluating Engineering Works

In the present work, a detailed engineering survey using the RTK instrument was carried out to obtain channel dimensions at each cross-section and the items that may affect channel efficiency were noted. The key dimensions like depth, width, and bottom slope for both streams for their complete length were determined. Parameters such as the flow channel length and width at each level of bifurcation as well as the curvature of the turning area of flow channels were particularly investigated. The real dimensions of the channels and identification of materials with which the banks and bottoms of the channels are constructed were noted to estimate Manning's roughness coefficients. The measurements of dimensions in terms of width, depth, and slope along the existing channels were carried out at an interval of 10 m to 20 m focusing on the position of constructions across the lined channel like footbridges and bridges (see Figure 2).

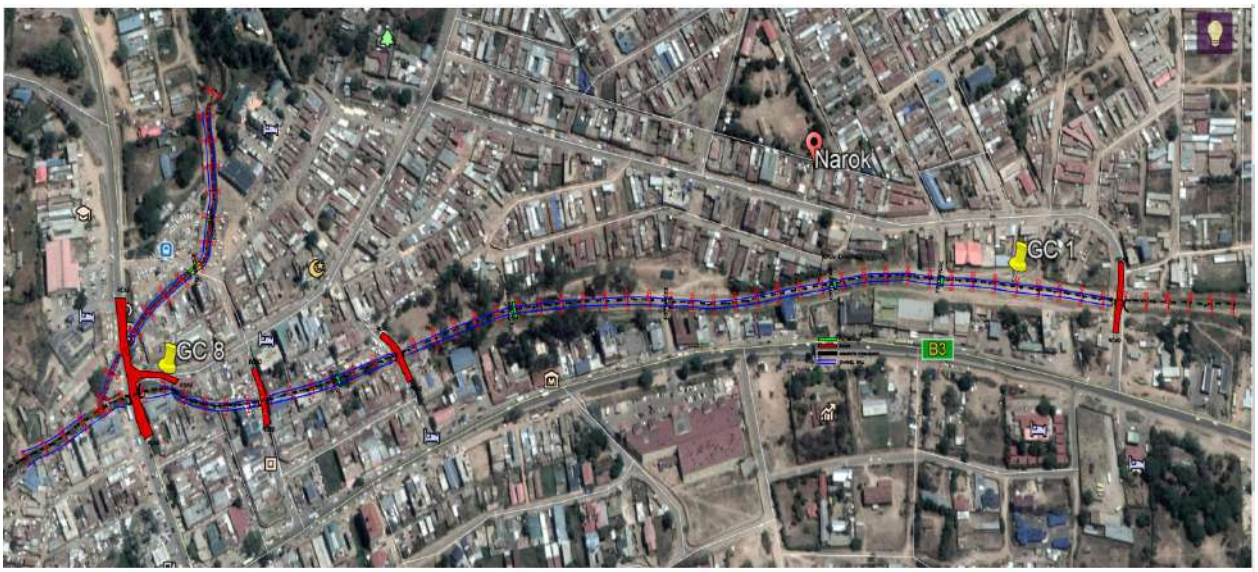

Figure 2: Surveyed Channels and Identified Cross-Sections and Infrastructures

2.4.2. Computation of Channel Geometric Properties

The highest peak discharge estimated from each of the different forecasted LULC scenarios was the fundamental feature to convey into the channel. Also, the determination of flow rates in the stream channels is a central task of surface water drainage. Hence, the present work considered the determined flow corresponding to the important water that can be overflowing the channel embankment from different scenarios. The peak discharge estimated in Umukiza et al. (2021) under different LULC scenarios and assuming

return periods equal to 50 and 100 years was used as a design discharge. A hydraulic structure may be defined as any structure that is designed to handle water in any way, such as the retention, conveyance, control regulation, and dissipation of the energy of the water (Gitleman, 2014).

However, the hydraulic design consists of the calculation and application of the most suitable geometry like width, shape, elevation, and orientation of the structure. The design procedure took into consideration the following considerations:

1. The flow is one-dimensional; depth and velocity vary only in the longitudinal direction of the channel. This implies that the velocity is constant and the water surface is horizontal across any section perpendicular to the longitudinal axis.
2. Flow is assumed to vary gradually along the channel so that hydrostatic pressure prevails and vertical accelerations can be neglected (Chow, 1959).
3. The longitudinal axis of the channel is approximated as a straight line.
4. The bottom slope of the channel is small and the channel bed is fixed; that is, the effects of scouring and deposition are negligible.
5. Resistance coefficients for steady uniform turbulent flow are applicable so that relationships such as Manning's equation can be used to describe resistance effects·

Therefore, the estimated peak discharges were conveyed into the channel by using Manning's and continuity equations. The parameters of the canal geometry (width and depth) were computed and the freeboard was reserved. For improving the existing lined channel (rectangular cross-section), the morphology of the channel is considered to be a rectangular cross-section for the first step, and trapezoidal in the second step for determining the suitable case to convey a given flow at the corresponding scenario of predicted runoff due to LULC.

Under such hypothesis, Manning's Equation is expressed as follows.

$$Q = \frac{A^{*}R^{\frac{2}{3}}\ S^{1/2}_{f}}{n} \quad (2)$$

Where: n is Manning's roughness value, R is Hydraulic radius (m), Q is peak flow (m^3/s), A is the wetted area (m^2); S is the bottom slope (m/m). The minimum velocity was checked to ensure that there is no scouring of the channel bed and no siltation as the water flows.

III. RESULTS AND DISCUSSION

3.1. Engineering Constructions across the Channels

Concerning Kakia channel, from the upstream to the downstream direction, the channel was found to be no uniform with regard to height and width due to features constructed across the channel.

For the Esamburmbur channel, it was observed that the channel narrowed downstream and that the banks decreased in height due to the bridge positioning. This situation can obstruct the flow leading to overflowing. Hence, the changes in channel geometry affect the free flow and may cause overflow in the narrower section of the channel. Table 3 presents the characteristics of the cross-sections engineering constructions.

Table 3: Geometrical Parameters and Constructions on cross-sections of Kakia and Esamburmbur Channels

Distance from upstream to downstream (m)	Height of the banks (m)	Width (m)	Construction
Kankia Chanel			
460	2.30	7.65	footbridge
650	3.45	7.27	footbridge
820	3.02	8.80	footbridge
1120	2.67	5.85	Bridge
1300	2.50	8.70	Bridge

Esamburmbur Channel			
120	2.55	7.10	footbridge
170	2.00	6.95	footbridge
295	2.50	4.00	Bridge at highway

The narrowed channel section of the active channel on the lowest 295 m of Esamburmbur channel may contribute to the overflow. The channel widths near the bridges were relatively narrow which can influence more overtopping discharge. The upstream and downstream of aligned channel with regard to the height and width were found to decrease due to features constructed across the channel. Moreover, Kiss & Blanka (2012) argued that stream flow derived from surface runoff is responsible for the determination of channel cross-section capacity. Hence, poor design of the channel especially narrowing of the channel towards the bridge is likely contributing to flooding. Therefore, the morphology of the channels and their conveyance capacity should be adjusted to prevent flow conditions. For better flood control, the construction of embankments should consider straightening the channel and maintain a uniform and efficient width. Figure 3 represents the surveyed profiles of Kakia and Esamburmbur channels.

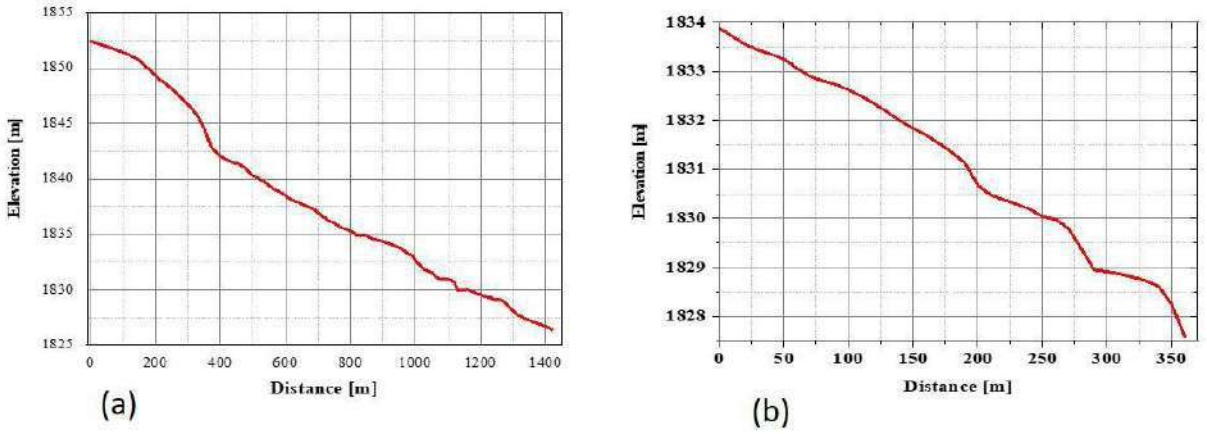

Figure 3: (a) Bottom Profile of Kakia Channel, (b) Profile of Esamburmbur Channel

From the survey data analysis, the real dimensions in terms of length, width, slope, and banks height of the channels were identified. The total lengths were found to be 1420 m and 360 m for Kakia and Esamburmbur respectively. While the elevation of the channel varies from 1827.59 m and 1833.87 m for the Esamburmbur channel and from 1826.42 m to 1852.43 m for Kakia. The slopes were found to be 1.8% and 1.7% for Kakia and Esamburmbur channels respectively.

3.2. Channel Dynamic and Geometric Properties

The calculation of geometric properties of the channel was performed with Civil 3D hydro flow extension, based on the Manning and continuity equations to obtain an accurate geometry of the channel, to convey designed peak discharge for all scenarios in different return periods. As the walls of the channel are formed with unfished concrete, the Manning's "n" coefficient for the concrete channel. It was hence selected here as equal to 0.017. Therefore, Figure 4 represents the water level and the variation of discharge for rectangular and trapezoidal shapes respectively.

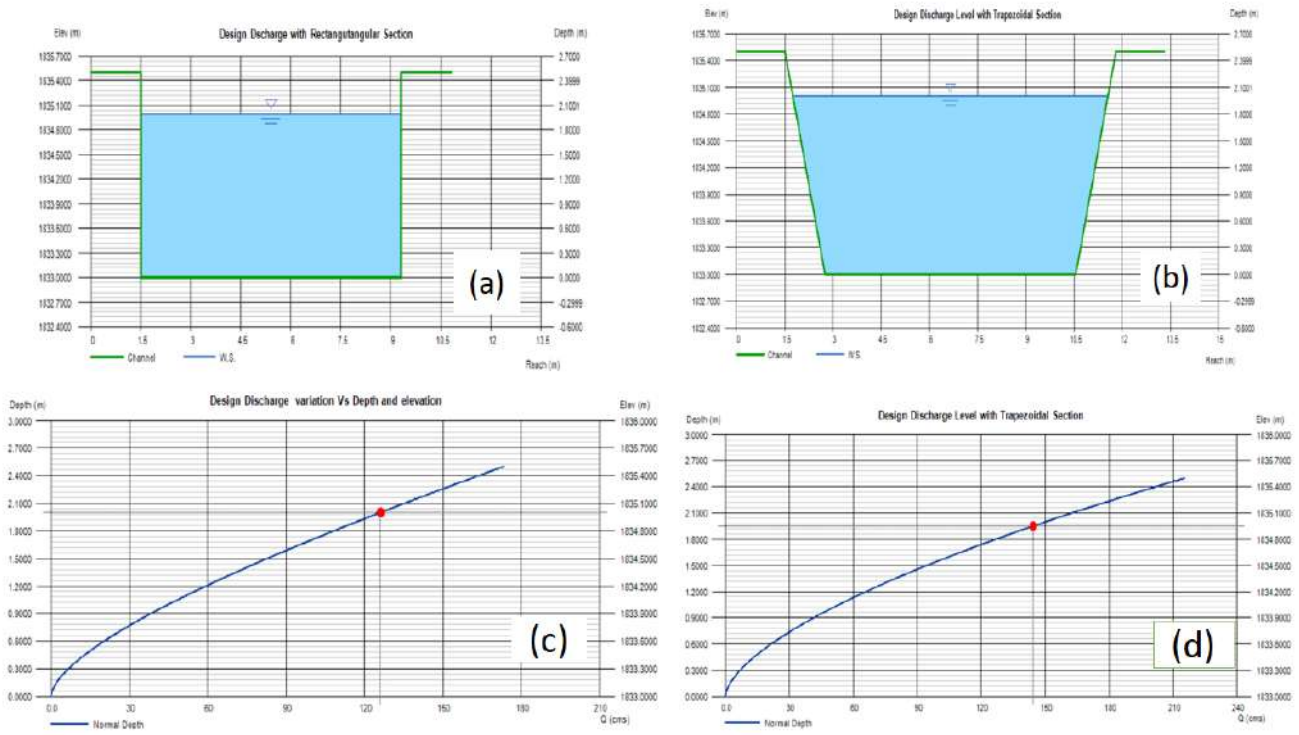

Figure 4: (a) Design Discharge Level with Rectangular Section (b) Design Level of Discharge with Trapezoidal Channel with 0.5 m (c) Maximum Depth vs Peak Discharge Variation for Trapezoidal (d) Maximum Design Depth vs Peak Discharge for Rectangular Section

The cross-section was taken at the level of bridges constructed across the channel. Channel crossings were found to require adequate and careful design. They must functionally allow for the passage of the maximum amount of water that can reasonably be expected to occur within the lifetime of the structure. For the case of Kakia and Ensamburmbur channels, many constructions across the channel were found downstream and the channel width changes from one point to the other in these locations. Also, the area is potentially an affected zone in the situation of the flood occurring according to the inhabitants that were interviewed during the surveys. It should be pointed out that inadequate water passage structures to accommodate peak flow can result in flood and construction failures.

Regardless of the channel cross-sectional shapes (rectangular and trapezoidal), they should be all confirm to proper design standards with regards to alignment with the channel conveyance capacity. Therefore, the conveyance capacity was evaluated to cause no direct or indirect property damage and designed to accommodate increased runoff which could be occasioned by upstream and development. For rectangular cross-sections, the depth is the same considering a given section across an entire channel, while in a trapezoidal cross-section, the depth decreases with a bankside slope. The channel is gradually varied from cross-section to cross-section, hence the depth changes also. However, with the same bottom width, rectangular section was opted compared to a trapezoidal section due to its necessity to increase the top width where space is critical, to efficiently allow the estimated peak flow. Changes in a conveyance from cross-section to cross- section are important to determine the adequacy of stream drainage. For instance, within a cross-section, the conveyance was used to compare overbank flow and channel carrying capacity. Hence, the designed peak discharge and corresponding channel properties, in consideration of their conveyance capacity for Kakia and Ensamburmbur channel, are presented in Table 5.

Table 5: Design discharges and channel geometry characteristics for Kakia and Esamburmbur channel

					Kakiachannel			
Total Depth (m)	Depth of water	Area (m^2)	Velocity (m/s)	Wetted Perimeter (m)	Width (m)		Discharge (m^3/s)	Comments (Tr = return period)
					Botto m	Top		
2.50	2	17.11	8.4283	12.1603	7.8	9.75	144.2	The design channel geometry presented here can convey peak flow estimated in scenarios 2 and 2019 at 50 years return periods.
2.50	2	20	8.5138	14	10	10	170.3	Can apply for 2019 and scenario 2 with Tr100
2.6	2.16	21.64	8.8258	14.32	10	10	191	Fit for peak flows estimated in all scenarios except scenario 3 with Tr 100
2.78	2.28	17.15	8.4746	12.0721	7.5	7.5	145.5	Designed for peak flow estimated in scenarios 4 with 50 years return periods.
3	2.39	20.34	8.8995	13.2854	8.5	8.5	181	Designed channel geometry with peak flow estimated in Scenario 4 at 100 years returns period and can be adequate in case of scenario 3 with a design return period of 50 years
2.50	2	8.010	6.5221	8	4	4	52.18	The current geometric properties represented at the position at the main bridge can be adequate to convey, the peak discharge estimated in scenario 4 with 10 years return period.
2.80	2.35	9.425	6.8650	8.7123	4	4	64.7	The designed channel properties can fit to convey peak discharges regarding 2019 at 25 years return period
2.75	2.21	9.985	7.0102	8.9379	4.5	4.5	70.08	The designed geometric properties can fit for the peak discharge estimated in scenario 2 with 50 years return periods
2.85	2.27	11.38	7.3258	9.5538	5	5	83.40	Channel geometric properties are designed for scenario 4 with 50 years return period
2.85	2.34	14.06	7.8287	10.6879	6	6	110.1	Can be designed for peak flow in specific scenario 1 with Tr 50 over design for the rest except scenario 3

Esamburmbur channel

From the channel dynamics, the design peak discharge was evaluated under different cases depending on the assumed LULC transition. The results show a big difference between the current channel geometric properties of the two channels when compared to the required dimensions for both channels to convey the estimated peak flow in the different scenarios and return periods.

Thus the dimensions as per the current peak flow can be addressed either by adjusting the channel height or width to accommodate the extra flow water. For an appropriate design to convey the assumed peak discharge, the design should be based on a 50 years return period (Storm Water Drainage System Design Manual, 2007). Also, it was noticed that for the same depth and peak flow, the shape of the rectangular sections is preferable since it presents the same dimensions at the bottom and top while for a trapezoidal section, the top width needs to be wider which could be difficult to realize. Moreover, the larger the channel width, the maximum discharge, the maximum flow velocity, and the maximum water level will be (Natasha et al., 2019). Therefore, knowing the peak flow that is more likely to happen, can give the idea of corresponding channel geometries that are adequate to carry the designed peak discharge (Flow et al., 2019). The study by Jaeger et al. (2019) investigated different approaches to optimize flows in misaligned

structures and concluded that aligned construction according to flow direction tailored reinforcement and redesigned stream embankment can contribute to containing overflowing. The option of increasing the height of the embankments is determined by design peak flow (determined with a return period of flood) and the freeboard above the flood level (Ankum, 2002).

From the findings, we can suggest that the rate of urbanization assumed in Scenario 3 is not recommended as it can increase the flood risk. However, the application and implementation of some regulations related to LULC practices as in Scenario 2 show little increase in runoff response. From this, we conclude that an increase in urbanization and agricultural activities is preferred with respect to the increase of pastureland, open space, and allowing space for vegetation as demonstrated that deep-rooted plants impact runoff generation (Apollonio et al., 2021a). For instance, nonstructural measures can be encouraged such as open space preservation can be encouraged in the context of ecological, recreational, and aesthetic values, and regulation of agricultural areas not in sense of declining economy but practice land-use policies for sustainable and protective environment measures.

IV. CONCLUSIONS

The study investigated the channel dynamics due to different scenarios of LULC for Kakia and Ensamburmbur sub-cathments. As between the years 1985 and 2019 some changes in land-cover occurred in Narok town's watershed, the same process is expected to continue occurring in future. This trend was a result of an alternation between agricultural and urbanized landscapes growth against forest, range land and open space, hence the necessity to evaluate the channel's capacity in function of the peak flow resulted from the future likely LULC transition.

The engineering constructions (highway bridges and other infrastructures) were found to contribute to channel narrowing down that may obstruct channel dynamics at different scenarios of peak discharge and flow volume. The current channel design was found also to require improvement to accommodate the estimated peak flow for both channels (Kakia and Esamburmbur) by increasing their cross-sections. Moreover, the results from this study indicate that peak discharge is a key-based element to design channel geometry for improving the existing drainage system for the two investigated channels.

Earlier studies highlighted that impervious area's growth due to uncontrolled LULC has a considerable effect on the increase of runoff volume (Apollonio et al., 2016; Dionizio & Costa, 2019; Vojtek & Vojteková, 2019). The land-cover trend is toward residential cover and urbanization, mostly occurring along the rural-urban fringe. This might be due to processes including immigration, natural growth, economic processes, planning policies, etc. (Ohana et al., 2013). With regard to channel geometric properties under different scenarios, the engineering constructions (highway bridges and other infrastructures) contributed to channel narrowing down that may obstruct channel dynamics at different scenarios of peak discharge and flow volume. The channel geometric properties were designed as an improvement to convey the estimated peak flow for both the investigated channels by increasing their cross-sections. Structural mitigation was here used to improve the geometric properties of the channel by increasing the height of embankments and enlarging the cross-sectional area. Future research will concentrate on: 1) expanding the surveys in other parts of the river network in the investigated case studied, using also UAV devices that proved to be effective in flood risk management (Annis et al., 2020); 2) using bidimensional hydraulic models to map eventual flood prone areas; and 3) employ Biosystems engineering techniques, like natural lamination basins, in the upslope area of the investigated catchments (e.g. Apollonio et al., 2021b) in order to mitigate the urban flood risk.

Author Contributions: E.U., J.M.R., A.P., S.M.W. and J.M.G. conceptualized the idea and designed the research; E.U. investigated and carried out the research; A.P. conceived the software; E.U. and J.M.G. prepared data; Supervision J.M.R. and

S.M.W.; writing draft manuscript E.U.; review and editing A.P.; C.A and J.M.R. All authors have read and agreed to the published version of the manuscript.

REFERENCES

1. Alfarajat, et al. (2014). Mitigation Environmental Risk Of Floods In Jorthhwestern Parts Of Jordan. 300.
2. Ankum, P. (TU D. (2002). Design of Open-Channels and Hydraulic Structures. Lecture Notes for CT3410.
3. Apollonio, C., Balacco, G., Novelli, A., Tarantino, E., & Piccinni, A. F. (2016). Land use change impact on flooding areas: The case study of Cervaro Basin (Italy). Sustainability (Switzerland), 8(10). https://doi.org/10.3390/su8100996.
4. Apollonio, C., Petroselli, A., Tauro, F., Cecconi, M., Biscarini, C., Zarotti, C., & Grimaldi, S. (2021). Hillslope Erosion Mitigation : An Experimental Proof of a Nature-Based Solution.
5. Coomes, O. T., Lambin, E. F., Turner, B. L., Geist, H. J., Agbola, S. B., Angelsen, A., Folke, C., Bruce, J. W., Coomes, O. T., Dirzo, R., George, P. S., Homewood, K., Imbernon, J., Leemans, R., Li, X., Moran, E. F., Mortimore, M., Ramakrishnan, P. S., Richards, J. F., … Xu, J. (2001). The causes of land-use and land-cover change : Moving beyond the myths The causes of land-use and land-cover change : moving beyond the myths Helle Sk a. May 2014.
6. Dionizio, E. A., & Costa, M. H. (2019). Influence of land use and land cover on hydraulic and physical soil properties at the cerrado agricultural frontier. Agriculture (Switzerland), 9(1), 1–14. https://doi.org/10.3390/agriculture9010024.
7. Erpicum, S., Crookston, B. M., Bombardelli, F., Bung, D. B., Felder, S., Mulligan, S., Oertel, M., & Palermo, M. (2021). Hydraulic structures engineering: An evolving science in a changing world. Wiley Interdisciplinary Reviews: Water, 8(2), 1–11. https://doi.org/10.1002/wat2.1505.
8. Flow, O. C., Equation, M., Energy, S., Flow, G. V., & Transitions, C. (n.d.). Course Number : CE 365K Topic 8 : Open Channel Flow. 1–45.
9. Gajbhiye, S., Mishra, S. K., & Pandey, A. (2014). Relationship between SCS-CN and Sediment Yield. Applied Water Science, 4(4), 363–370. https://doi.org/10.1007/s13201-013-0152-8
10. Gitleman, L. (2014). Guo, H., Li, X., Huang, Q., & Zhang, D. (2011). Effect of lulc change on surface runoff inurbanization area Zhongchang SUN.
11. Habete, D., & Ferreira, C. M. (2016). Impact of Forecasted Land Use Change on Design Peak Discharge at Watershed and Catchment Scales: Simple Equation to Predict Changes. Journal of Hydrologic Engineering, 21(7), 04016019. https://doi.org/10.1061/(asce)he.1943-5584.0001384.
12. Han, J., Hayashi, Y., Cao, X., & Imura, H. (2009). Evaluating Land-Use Change in Rapidly Urbanizing China: Case Study of Shanghai. Journal of Urban Planning and Development, 135(4), 166–171. https://doi.org/10.1061/(asce)0733-9488(2009)135:4(166).
13. Heritage, G., & Entwistle, N. (2020). Impacts of river engineering on river channel behaviour: Implications for managing downstream flood risk. Water (Switzerland), 12(5). https://doi.org/10.3390/W12051355.
14. Jaeger, R., Jacobs, C., Tondera, K., & Tindale, N. (2019). Improving flows in misaligned culverts. Water (Switzerland), 11(9), 1–15. https://doi.org/10.3390/w11091932.
15. Kiss, T., & Blanka, V. (2012). River channel response to climate- and human-induced hydrological changes: Case study on the meandering Hernád River, Hungary. Geomorphology, 175–176, 115–125. https://doi.org/10.1016/j.geomorph.2012.07.003.
16. Marie Mireille, N., M. Mwangi, H., K. Mwangi, J., & Mwangi Gathenya, J. (2019). Analysis of Land Use Change and Its Impact on the Hydrology of Kakia and Esamburmbur Sub-Watersheds of Narok County, Kenya. Hydrology, 6(4), 86. https://doi.org/10.3390/hydrology6040086.

17. Mwangi et al. (2019). Understanding urban environment problems in the newly urbanizing areas of kenya, a case of narok town. International Journal of Scientific and Technology Research, 8(6), 236–241.
18. Natasha, G., Suharjito, & Noviantri, V. (2019). Saint-venant model analysis of trapezoidal open channel water flow using finite difference method. Procedia Computer Science, 157, 6–15. https://doi.org/10.1016/j.procs.2019.08.135.
19. Ohana-Levi, N., Givati, A., Alfasi, N., Peeters, A., & Karnieli, A. (2018). Predicting the effects of urbanization on runoff after frequent rainfall events. Journal of Land Use Science, 13(1–2), 81–101. https://doi.org/10.1080/1747423X.2017.1385653.
20. Ohana, N., Karnieli, A., Egozi, R., & Peeters, A. (2013). Effects of land-cover change on rainfall-runoff relationships: a case study of the Yarkon-Ayalon watershed, Israel. First International Conference on Remote Sensing and Geoinformation of the Environment (RSCy2013), 8795, 87951G. https://doi.org/10.1117/12.2027190.
21. Petroselli, A., & Grimaldi, S. (2018). Design hydrograph estimation in small and fully ungauged basins: a preliminary assessment of the EBA4SUB framework. Journal of Flood Risk Management, 11, S197–S210. https://doi.org/10.1111/jfr3.12193.
22. Petroselli, Andrea, Asgharinia, S., Sabzevari, T., & Saghafian, B. (2020). Comparison of design peak flow estimation methods for ungauged basins in Iran. Hydrological Sciences Journal, 65(1), 127–137. https://doi.org/10.1080/02626667.2019.1686506.
23. Piscopia, R., Petroselli, A., & Grimaldi, S. (2015). A software package for predicting design-flood hydrographs in small and ungauged basins. Journal of Agricultural Engineering, 46(2), 74–84. https://doi.org/10.4081/jae.2015.432.
24. Shaina Beegam, N., & Prince Arulraj, G. (2018). A review article on impact of urbanization on hydrological parameters. International Journal of Civil Engineering and Technology, 9(199–208), 199–208.
25. Sharif, H. O., Al-Juaidi, F. H., Al-Othman, A., Al-Dousary, I., Fadda, E., Jamal-Uddeen, S., & Elhassan, A. (2016). Flood hazards in an urbanizing watershed in Riyadh, Saudi Arabia. Geomatics, Natural Hazards and Risk, 7(2), 702–720. https://doi.org/10.1080/19475705.2014.945101. Storm Water Drainage System Design Manual. (2007). August.
26. Suriya, S., & Mudgal, B. V. (2012). Impact of urbanization on flooding: The Thirusoolam sub watershed - A case study. Journal of Hydrology, 412–413, 210–219. https://doi.org/10.1016/j.jhydrol.2011.05.008.
27. Tingsanchali, T. e. al. (2012). Urban flood disaster management. Procedia Engineering, 32, 25–37. https://doi.org/10.1016/j.proeng.2012. 01.1233.
28. Umukiza, E., Raude, J. M., Wandera, S. M., Petroselli, A., & Gathenya, J. M. (2021). Impacts of Land Use and Land Cover Changes on PeakDischarge and Flow Volume in Kakia and Esamburmbur Sub-Catchments of Narok Town, Kenya. Hydrology, 8(2), 82. https://doi.org/10.3390/hydrology8020082.
29. Vojtek, M., & Vojteková, J. (2019). Land use change and its impact on surface runoff from small basins: A case of Radiša basin. Folia Geographica, 61(2), 104–125.
30. Zope, P. E., Eldho, T. I., & Jothiprakash, V. (2016). Impacts of land use-land cover change and urbanization on flooding: A case study of Oshiwara River Basin in Mumbai, India. Catena, 145, 142–154. https://doi.org/10.1016/j. catena.2016.06.009.

This page is intentionally left blank

Pseudo S-Geodetic Number of a Fuzzy Graph

Sameeha Rehmani

ABSTRACT

In this paper, the concept of Pseudo s-geodetic number of fuzzy graphs is introduced and it is shown that the Pseudo s-geodetic set is not in general a complementary s-geodetic set of a fuzzy graph. An upper and lower bound for the Pseudo s-geodetic number is exhib- ited. The Pseudo s-geodetic number of paths, fuzzy trees and of com- plete bipartite fuzzy graphs are obtained. An application of Pseudo s-geodetic sets in Location Theory has also been illustrated.

Keywords: s-geodetic cover, s-geodetic basis, s-geodetic number, pseudo s-geodetic set, pseudo s-geodetic number.

Classification: DDC Code: E LCC Code: PZ7.M267

Language: English

London Journals Press

LJP Copyright ID: 392955
Print ISSN: 2631-8474
Online ISSN: 2631-8482

London Journal of Engineering Research

Volume 22 | Issue 7 | Compilation 1.0

Pseudo S-Geodetic Number of a Fuzzy Graph

Sameeha Rehmani

ABSTRACT

In this paper, the concept of Pseudo s-geodetic number of fuzzy graphs is introduced and it is shown that the Pseudo s-geodetic set is not in general a complementary s-geodetic set of a fuzzy graph. An upper and lower bound for the Pseudo s-geodetic number is exhib- ited. The Pseudo s-geodetic number of paths, fuzzy trees and of com- plete bipartite fuzzy graphs are obtained. An application of Pseudo s-geodetic sets in Location Theory has also been illustrated.

Keywords: s-geodetic cover, s-geodetic basis, s-geodetic number, pseudo s-geodetic set, pseudo s-geodetic number.

Author: Department of Mathematics Sullamussalam Science College, Areacode-673639 Kerala, India.

I. INTRODUCTION

Zadeh in 1965 [27] brought the concept of fuzzy sets into existence which gave a platform for describing the uncertainties prevailing in day-today life situations. Later on, the theory of fuzzy graphs was developed by Rosenfeld in the year 1975 [21] along with Yeh and Bang [26]. Rosenfeld also obtained the fuzzy analogue of several graph theoretic concepts like paths, cycles, trees and connectedness along with some of their properties [21] and the concept of fuzzy trees [17], automorphism of fuzzy graphs [2], fuzzy interval graphs [14], cycles and co-cycles of fuzzy graphs [15] etc has been established by several authors during the course of time. Fuzzy groups and the notion of a metric in fuzzy graphs was introduced by Bhattacharya [1]. The concept of strong arcs [5] and geodesic distance in fuzzy graphs [4] were introduced by Bhutani and Rosenfeld in the year 2003. The definition of fuzzy end nodes and some of their properties were established by the same authors in [3]. Several other important works on fuzzy graphs can be found in [18, 12, 24]. Studies in fuzzy graphs using μ-distance was carried out by Rosenfeld [22] in 1975 and was further studied by Sunitha and Vijayakumar in [24]. In crisp graph, the concept of geodetic iteration number was first introduced by Harary and Nieminen in 1981 [10]. This concept along with that of geodetic numbers in graphs was again discussed by several authors in [6], [8] and [7]. Later on, these concepts were extended to fuzzy graphs using geodesic distance by Suvarna and Sunitha in [25] and the same based on μ-distance was introduced by Linda and Sunitha in [11].The concept of sum distance and some of its metric aspects was introduced by Mini Tom and Sunitha in [13]. s-Geodetic iteration number and s-geodetic number of a fuzzy graph based on sum distance was introduced by Sameeha and Sunitha in [19].

In this paper, the concept of Pseudo s-geodetic number of fuzzy graphs is introduced. The Pseudo s-geodetic number of paths, fuzzy trees and of complete bipartite fuzzy graphs are obtained. The limiting values of Pseudo s-geodetic numbers are established.

II. PRELIMINARIES

A fuzzy graph [16] is a triplet $G : (V, \sigma, \mu)$ where V is vertex set, σ a fuzzy subset of V and μ a fuzzy relation on σ such that $\mu(u, v) \leq \sigma(u) \wedge \sigma(v), \forall u, v \in V$.

We assume that V is finite and non-empty, μ is reflexive (*i.e.*, $\mu(x, x) = \sigma(x), \forall x$) and symmetric (*i.e.*, $\mu(x, y) = \mu(y, x), \forall (x, y)$). Also we denote the underlying crisp graph [9] by $G^* : (\sigma^*, \mu)$ where $\sigma^* = \{u \in V / \sigma(u) > 0\}$ and $\mu^* = \{(u, v) \in V \times V / \mu(u, v) > 0\}$. Here we assume $\sigma^* = V$.

A fuzzy graph $G : (V, \sigma, \mu)$ is called trivial if $\sigma^* = 1$. Otherwise it is called non-trivial.

London Journal of Engineering Research

A fuzzy graph $G : (V, \sigma, \mu)$ is a complete fuzzy graph [16] if $\mu(u, v) = \sigma(u) \wedge \sigma(v)\ \forall u, v \in \sigma^*$.

A weakest arc of $G : (V, \sigma, \mu)$ is an arc with least non zero membership value. A path P of length n is a sequence of distinct nodes $u_0, u_1, ..., u_n$ such that $\mu(u_{i-1}, u_i) > 0$, $i = 1, 2, 3, ..., n$ and the degree of membership of a weakest arc in the path is defined as its strength. The strength of connectedness between two nodes u and v is defined as the maximum of the strengths of all paths between u and v, and is denoted by $CONN_G(u, v)$. A $u - v$ path P is called a strongest $u - v$ path if its strength equals $CONN_G(u, v)$. A fuzzy graph $G : (V, \sigma, \mu)$ is connected if for every u, v in σ^*, $CONN_G(u, v) > 0$.

An arc (u, v) of a fuzzy graph is called strong if its weight is at least as great as the strength of connectedness of its end nodes u, v when the arc (u, v) is deleted and a $u - v$ path P is called a strong path if P contains only strong arcs [5].

Two nodes u and v in a fuzzy graph $G : (V, \sigma, \mu)$ are neighbors if $\mu(u, v) > 0$ and v is called a strong neighbor of u if the arc (u, v) is strong. Also $N(u)$ denotes the set of neighbors of u other than u and degree of u is $deg(u) = N(u)$. A node u with $deg(u) = 1$ is an end node and a node u with $deg(u) > 1$ is an internal node. A node v is called a fuzzy end node of G if it has exactly one strong neighbor in G [3].

A connected fuzzy graph $G : (V, \sigma, \mu)$ is called a fuzzy tree [21] if it has a spanning fuzzy subgraph $F : (V, \sigma, \nu)$ which is a tree such that for all arcs (u, v) not in F, $CONN_F(u, v) > \mu(u, v)$.

A fuzzy graph G is said to be bipartite [23] if the vertex set V can be partitioned into two non-empty sets V_1 and V_2 such that $\mu(v_1, v_2) = 0$ if $v_1, v_2 \in V_1$ or $v_1, v_2 \in V_2$. Further if $\mu(u, v) = \sigma(u) \quad \sigma(v)\ \forall u \in V_1$ and $v \in V_2$, then G is called a complete bipartite fuzzy graph and is denoted by $K_o 1,\sigma 2$, where σ_1 and σ_2 are respectively the restrictions of σ to V_1 and V_2.

For any path $P : u_0 - u_1 - u_2 - ... - u_n$, length of P, $L(P)$, is defined as the sum of the weights of the arcs in P. That is, $L(P) = \Sigma^n \mu(u_{i-1}, u_i)$.

If $n = 0$, define $L(P) = 0$ and for $n \geq 1$, $L(P) > 0$. For any two nodes u, v in $G : (V, \sigma, \mu)$, if $P = \{P_i : P_i$ is a u-v path, $i = 1, 2, 3, ...\}$, then the sum distance between u and v is defined as $d_s(u, v) = Min\{L(P_i) : P_i \in P, i = 1, 2, 3, ...\}$[13].

Any path P from x to y whose length is $d_s(x, y)$ is called s-geodesic from x to y [19].

Let $S \subseteq V$ be a set of nodes of a connected fuzzy graph $G : (V, \sigma, \mu)$. Then the s-geodetic closure of S, with respect to sum distance, is the set of all nodes of S as well as all nodes that lie on s-geodesics between nodes of S and is denoted by (S) [19].

A set $S \subseteq V(G)$ such that every node of G is contained in an s-geodesic joining some pair of nodes in S is called an s-geodetic cover(s-geodetic set) of G. In other words if $(S) = V(G)$, then S is an s-geodetic cover of G [19].

The s-geodetic number of G, denoted by $s\text{-}gn(G)$, is the minimum order of its s-geodetic covers and any cover of order $s\text{-}gn(G)$ is an s-geodetic basis [19].

A node v in a fuzzy graph G is called an extreme node if the fuzzy sub- graph induced by its neighbors is a complete fuzzy graph [19].

Throughout this paper we consider only connected fuzzy graphs.

III. PSEUDO S-GEODETIC NUMBER OF A FUZZY GRAPH

In fuzzy graph theory, the concept of Pseudo geodesic number, using geodesic distance, was introduced by Sameeha and Sunitha in [20]. In this section, using sum distance, we introduce the concept of Pseudo s-geodetic number of fuzzy graphs. We also show that a Pseudo s-geodetic set is not in general a complementary s-geodetic set of a fuzzy graph.

Definition 3.1: Let $G : (V, \sigma, \mu)$ be a connected fuzzy graph and S be an s-geodetic basis of G. Then the set of nodes which do not belong to any s-geodetic basis of G is the Pseudo s-geodetic set S' of G.

The cardinality of Pseudo s-geodetic set S' is called Pseudo s-geodetic num- ber and is denoted by $s\text{-}gn'(G)$.

Example 3.2: Consider the fuzzy graph G given in Fig.1.

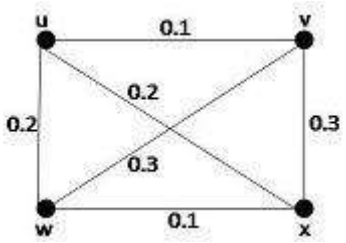

Fig. 1

Here, if $S = \{v, x, w\}$ then $(S) = \{u, v, x, w\} = V(G)$. Therefore S is an s-geodetic cover of G. Also S is the unique s-geodetic basis of G and so $s\text{-}gn(G) = 3$. Hence $S' = \{u\}$ and so $s\text{-}gn'(G) = 1$.

Remark 3.3: For the fuzzy graph G given in Fig.1, $S' = S^c$ and hence
$s\text{-}gn'(G) = |V - S|$.
But in general S' is not the complement of the set S.

Example 3.4: Consider the fuzzy graph G given in Fig.2.

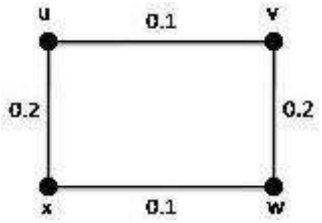

Fig. 2

Here $S_1 = \{u, w\}$ and $S_2 = \{v, x\}$ are both s-geodetic bases of G and so
$S' = \varphi$. Hence $s\text{-}gn'(G) = 0$.

Proposition 3.5. [19] For any non-trivial connected fuzzy graph G on n nodes, $2 \leq s\text{-}gn(G) \leq n$.

Proposition 3.6. For a connected fuzzy graph G on n nodes, $0 \leq gn'(G) \leq n - 2$.
Proof. The proof follows directly from Proposition 3.5 that $2 \leq s\text{-}gn(G) \leq n$.

Since $s\text{-}gn(G) \geq 2$, we get $s\text{-}gn'(G) \leq n - 2$. Also since $s\text{-}gn(G) \leq n$, we get $s\text{-}gn'(G) \geq 0$*Proposition 3.7.* If $S_1, S_2, \ldots, S_n$ are the s-geodetic bases of a fuzzy graph
$G : (V, \sigma, \mu)$, then the pseudo s-geodetic number $s\text{-}gn'(G) = |\cap_{i=1}^{n} S_i^c|$.

Proof. Let S' be the pseudo s-geodetic set of G. To show that $s\text{-}gn'(G) = |\cap_{i=1}^{n} S_i^c|$ it is enough to show that $S' = |\cap_{i=1}^{n} S_i^c|$

Let v be a node of G such that $v \in S'$.

Then by definition 3.1, v does not belong to any s-geodetic basis of G.

i.e, $v \notin S_i \ \forall i = 1, 2, \ldots, n$.
$\Rightarrow v \in S_i^c \ \forall i = 1, 2, \ldots, n$.
$\Rightarrow v \in \cap_{i=1}^{n} S_i^c$.
$\Rightarrow S' \subseteq \cap_{i=1}^{n} S_i^c$ .....(1)

Conversely, let u be a node of G such that $u \in \cap_{i=1}^{n} S_i^c$.
Then $u \in S_i^c \ \forall i = 1, 2, \ldots, n$.
$\Rightarrow u \notin S_i \ \forall i = 1, 2, \ldots, n$.
Hence by definition 3.1, $u \in S'$ and so $\cap_{i=1}^{n} S_i^c \subseteq S'$.....(2)
From (1) and (2), $S' = \cap_{i=1}^{n} S_i^c$ and so $s\text{-}gn'(G) = |\cap_{i=1}^{n} S_i^c|$.

Remark 3.8. The set of internal nodes (non end-nodes) of a path P_n $(n \geq 2)$ is its Pseudo *s*-geodetic set so that $s - gn'(P_n) = n - 2$. Thus the path P_n has the largest possible Pseudo *s*-geodetic number $n - 2$.

Proposition 3.9. No extreme node of a fuzzy graph $G : (V, \sigma, \mu)$ belongs to its Pseudo *s*-geodetic set.

Proof. Let S be an *s*-geodetic cover of G and v be an extreme node of G. Let $\{v_1, v_2, ..., v_n\}$ be the neighbors of v and (v, v_i), $1 \leq i \leq n$ be the edges incident on v. Since v is an extreme node, v_i and v_j are adjacent for $i \neq j$ $(1 \leq i, j \leq n)$. Hence any *s*-geodetic which contains v, is either (v_i, v), $(1 \leq i \leq n)$ or $u_1, u_2, ..., u_m, v_i, v$ where each $'u_i, (1 \leq i \leq m)$ is different from vi. Hence it follows that $v \in S$ and so $v \in /S$.

Proposition 3.10. [19] Let $G : (V, \sigma, \mu)$ be a fuzzy tree such that G^* is a tree. Then the set of all fuzzy end nodes of G form an *s*-geodetic basis for G and $s\text{-}gn(G)$ is the number of fuzzy end nodes of G.

Proposition 3.11. The Pseudo *s*-geodetic number of a fuzzy tree $G : (V, \sigma, \mu)$ such that G^* is a tree equals the number of non fuzzy end-nodes in G.

Proof. By Proposition 3.10 a fuzzy tree, whose underlying crisp gaph G^* is a tree, has a unique *s*-geodetic basis consisting of its fuzzy end nodes. Thus for such a fuzzy tree $G : (V, \sigma, \mu)$, the set of all non fuzzy end-nodes of G is the Pseudo *s*-geodetic set of G. Hence, the Pseudo *s*-geodetic number $s\ gn'(G)$ equals the number of non fuzzy end-nodes in G.

Remark 3.12. However, the above result is not true in general for every fuzzy tree.

Example 3.13. Consider the fuzzy tree G given in Fig.3.

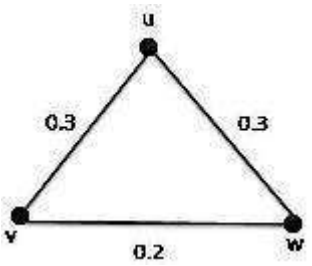

Fig: 3

Here v and w are the fuzzy end nodes of G but $\{v, w\}$ is not an *s*-geodetic cover since $(\{v, w\}) = \{v, w\} = V(G)$ and the *s*-geodetic basis is $\{u, v, w\}$.

Thus the Pseudo s-geodetic set $S' = \emptyset$. Hence, $s\text{-}gn'(G) = 0$. But the number of non fuzzy end nodes in G is 1.

Proposition 3.14. For a complete bipartite fuzzy graph $K_{\sigma_1,\sigma_2} = (V_1 \cup V_2, \sigma, \mu)$, the Pseudo *s*-geodetic number

1. $s\text{-}gn'(K_{\sigma_1,\sigma_2}) = 0$ if $|V_1| = |V_2| = 1$.
2. $s\text{-}gn'(K_{\sigma_1,\sigma_2}) = |V_1|$ if $|V_1| = 1$ and $|V_2| \geq 2$.
3. $s\text{-}gn'(K_{\sigma_1,\sigma_2}) = max\{r, s\}$ if $|V_1| = r$ and $|V_2| = s$ where $r, s \geq 2$, $r \neq s$.
4. $s\text{-}gn'(K_{\sigma_1,\sigma_2}) = 0$ if $r = s$.

Proof:

1. This follows directly from Remark 3.8.
2. This follows from Proposition 3.11.
3. Let $r, s \geq 2$. First assume that $r < s$.

Let $V_1 = \{u_1, u_2, ..., u_r\}$ and $V_2 = \{w_1, w_2, ..., w_s\}$ be a bipartition of K_{σ_1,σ_2}. Let $S = V_1$. We prove that S is an *s*-geodetic basis of K_{σ_1,σ_2}. That is, we prove that S is an *s*-geodetic cover of K_{σ_1,σ_2} having minimum cardinality.

Any node w_j, $(1 \leq j \leq s)$ lies on the *s*-geodesic $u_i w_j u_k$ for any i, so that S is an *s*-geodetic cover of K_{σ_1,σ_2}. Let T be any set of nodes such that $|T| < |S|$. If $T \subset V_1$ then there exists a vertex $u_i \in V_1$ such that $u_i \in /T$. Then the only *s*-geodesics containing u_i are $u_i w_j u_k$, $(k = /i)$, $(1 \leq j \leq s)$ and $w_j u_i w_l$, $(l \neq j)$ and so u_i cannot lie on an *s*-geodetic joining 2 nodes of T.

Thus T is not an *s*-geodetic cover of K_{σ_1,σ_2}.
If $T \subset V_2$, then by a similar argument, T is not an *s*-geodetic cover of $K\sigma_1,\sigma_2$.

Now if $T \subset S \cup V_2$ such that T contains at least one node from each of S and V_2, then since $|T| < |S|$, there exists nodes $u_i \in V_1$ and $w_j \in V_2$ such that $u_i \notin T$ and $w_j \notin T$. Then clearly at least one of the end nodes of the edge (u_i, w_j) does not lie on an s-geodesic connecting 2 nodes of T so that T is not an s-geodetic cover.

Thus in any case, T is not an s-geodetic cover of $K_{\sigma 1,\sigma_2}$. Hence S is the unique s-geodetic basis of $K_{\sigma 1,\sigma_2}$. so that $s\text{-}gn(K_{\sigma_1,\sigma_2}) = |S| = r = min\{r, s\}$.

Thus S' $= V_2$ and so $gn'(K_{\sigma_1,\sigma_2}) = |V_2| = s = max\{r, s\}$.

4. Now if $r = s$, then as in (3), V_1 and V_2 are both s-geodetic basis of $K_{\sigma 1,\sigma_2}$. Hence by defintion, $s\text{-}gn'(K_{\sigma_1,\sigma_2}) = 0$.

IV. AN APPLICATION OF PSEUDO S-GEODETIC SETS IN LOCATION THEORY

Location theory addresses questions of what economic activities are located where and why. It is generally assumed that agents act in their own self- interest. Firms thus choose locations that maximize their profits and indi- viduals choose locations that maximize their utility.

The topic of location theory generally observes patterns across geographic space typically associated with human settlement, industry siting, service competition, and, more generally, consumer behavior. Ultimately, location theory aims at gaining a sound grasp on the factors associated with loca-tional decision making and the question of what makes a good location.

In this section, the concept of pseudo s-geodetic sets is utilized in locating areas least suitable for placing Gas stations in a locality, the main agenda being to choose locations that maximize utility and minimize the number of Gas stations. For example, being the head of the city, we know that the Mayor of a city officially speaks for both the government and the community as a whole.

Suppose the Mayor issues an oder that the Gas stations in the city should be placed in such a way that they are minimum in number and of maximum utility to the consumers. The s-geodetic number of a fuzzy graph representation of a city, with each node representing important places in the city and each edge representing the roads connecting them, gives an idea about the minimum number of Gas stations to be placed so as to get maximum utility among consumers. Hence the s-geodetic bases give appro- priate locations for placing these Gas stations. A node that does not belong to any of the s-geodetic bases will eventually represent a location that is least suitable for placing a Gas station. In other words, the pseudo s-geodetic sets represent locations that are least suitable for placement of Gas stations in a certain city so as to satisfy the norms put forward by the Mayor of the city.

An illustrative example

Consider the fuzzy graph $G : (V, \sigma, \mu)$ given in Figure 4.

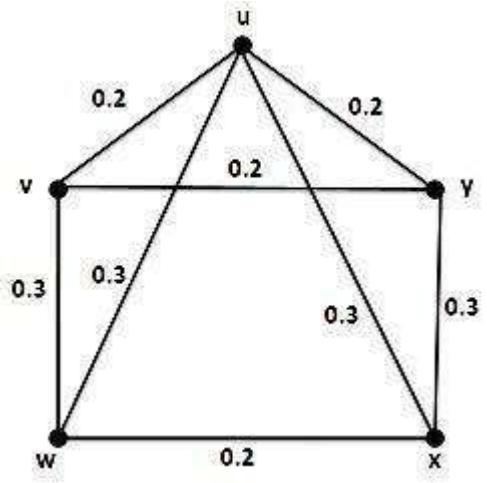

Fig. 4

Suppose that G is a fuzzy graph model of a city with nodes representing important places in the city and edges representing the roads connecting them. $S_1 = \{w, y\}$ and $S_2 = \{v, x\}$ are the s-geodetic bases of G. Therefore, $s\text{-}gn(G) = 2$. Thus the minimum number of Gas stations to be placed in such a way that utility is maximum among consumers is 2 and they can be placed either at the nodes w and y or at v and x as all other nodes lie on the s-geodetic paths joining w to y or on the s-geodetic path joining v to x. Here, the pseudo s-geodesic set $S' = u$. Thus the node u is least suitable for placing a Gas station.

V. CONCLUSION

In this paper, we introduced the idea of Pseudo *s*-geodetic number of fuzzy graphs and showed that a Pseudo *s*-geodetic set need not be the comple- ment of its geodesic basis always. An upper and a lower bound for Pseudo *s*-geodetic number of fuzzy graphs is exhibited. The Pseudo *s*-geodetic num- ber of paths, fuzzy trees and of complete bipartite fuzzy graphs are obtained. The concept of pseudo *s*-geodetic numbers have numerous applications in various real-life situations. One such application has been demonstrated in Location theory where the concept of pseudo *s*-geodetic sets is utilized in locating areas least suitable for placing Gas stations in a locality, the main agenda being to choose locations that maximize utility and minimize the number of Gas stations.

ACKNOWLEDGEMENT

The first author is grateful to the University Grants Commission (UGC), New Delhi, India, for providing the financial assistance.

REFERENCES

1. Bhattacharya. P.: Some Remarks on fuzzy graphs, Pattern Recognition Lett., 6 (1987), 297-302.
2. Bhutani. K. R.: On automorphisms of fuzzy graphs, Pattern Recognition Lett., 9 (1989), 159-162.
3. Bhutani. K. R., Rosenfeld. A.: Fuzzy end nodes in fuzzy graphs, In- form.Sci. 152(2003), 323-326.
4. Bhutani. K. R., Rosenfeld. A.: Geodesics in fuzzy graphs, Electronic Notes in Discrete Mathematics, 15(2003), 51-54.
5. Bhutani. K. R., Rosenfeld. A.: Strong arcs in fuzzy graphs, Information Sciences, 152(2003), 319-322.
6. Chartrand. G., Harary. F., Zhang. P.: On the Geodetic Number of a Graph, Networks, 39 (2001).
7. Chartrand. G., Zhang. P.: The Geodetic Number of an Oriented Graph, Europ. J. Combinatorics, 21 (2000), 181-189.
8. Goudar. V. M., Ashalatha. K. S., Venkatesha, Muddebihal. M. H.: On the Geodetic Number of Line Graph, Int.J.Contemp.Math.Sciences, 7 (2012), 2289-2295.
9. Harary. F.: Graph Theory, Addison-Wesley (1969).
10. Harary. F., Nieminen. J.: Convexity in Graphs, J.Differential Geometry, 16 (1981), 185-190.
11. Linda. J. P., Sunitha. M. S.:Geodesic and Detour distances in Graphs and Fuzzy Graphs, Scholars' Press, (2015).
12. Mathew. S., Sunitha. M. S.: Types of arcs in a fuzzy graph, Information Sciences, 179(2009), 1760-1768.
13. Mini Tom, Sunitha. M. S.: Sum Distance and Strong Sum Distance in Fuzzy Graphs, LAP Lambert Academic Publishing, 2016, ISBN 10: 3659821969ISBN 13: 9783659821967.
14. Mordeson. J. N.: Fuzzy line graphs, Pattern recognition Lett., 14(1993), 381-384.
15. Mordeson. J. N., Nair. P. S.: Cycles and Cocycles of fuzzy graphs, In- formation Sciences, 90(1996), 39-49.
16. Moderson. J. N., Nair. P. S.: Fuzzy Graphs and Fuzzy Hypergraphs, Physica-Verlag, Heidelberg, 2000.
17. Mordeson. J. N, Yao. Y. Y.: Fuzzy cycles and fuzzy trees, The Journal of Fuzzy Mathematics, 10 (1) (2002), 189-202.
18. Narayan. K. R. S., Sunitha. M. S.: Connectivity in a fuzzy graph and its complement, General Mathematics Notes, 9(1) (2012), 38-43.
19. Rehmani. S., Sunitha. M. S.: On the geodetic iteration number and geodetic number of a fuzzy graph based on sum distance, International Journal of Advanced Research in Science, Engineering and Technology, Vol. 7, Issue 8, (2020).
20. Rehmani. S., Sunitha. M. S.: On Different Types of Geodesic Numbers in Fuzzy Graphs, Scholar's Press, (2019) ISBN 10: 6138831977 ISBN 13: 9786138831976.
21. Rosenfeld. A.: Fuzzy graphs, In: L.A.Zadeh, K.S.Fu and M.Shimura(Eds), Fuzzy Sets and their Applications, Academic Press, New York, (1975) 77- 95.

22. Rosenfeld. A.: Fuzzy graphs, In:Fuzzy Sets and their Application to Cognitive and Decision Processes, Academic Press, (1975).
23. Somasundaram. A., Somasundaram. S.: Domination in fuzzy graphs-I, Pattern Recognition Letters 19 (1998), 787-791.
24. Sunitha. M. S., Vijayakumar. A.: Some metric aspects of fuzzy graphs, Proceedings of the Conference on Graph Connections, CUSAT, Allied Publishers, (1999), 111-114.
25. Suvarna. N. T., Sunitha. M. S.: Convexity and Types of Arcs & Nodes in Fuzzy Graphs, Scholar's Press, (2015).
26. Yeh. R. T., Bang. S. Y.: Fuzzy relations, fuzzy graphs and their applica- tion to clustering analysis, In Fuzzy sets and their Application to Cog- nitive and Decision Processes, Zadeh. L. A., Fu. K. S. Shimura M.Eds, Academic Press, New York, (1975), 125-149.
27. Zadeh. L. A.: Fuzzy sets, Information and Control, 8(1965), 338-353.

This page is intentionally left blank

Education in the Handling of the Solid Residues of Construction in the Work of the High School Industrial Hermilio Valdizan

Guillermo Gomer Cotrina Cabello, Yoel Bustillos Bonilla & Dr. Pedro David Córdova Trujillo

Universidad Nacional Daniel

SUMMARY

The objective matched, evaluating the effect of the education in the handling of the solid residues of the construction in the work of the high school industrial Hermilio valdizan – Huánuco, Metodología The study was experimental because signs of comparisons in two groups where you took the proof of process were evaluated and the posprueba, the utilized instruments were blackboards, bulletins, questionnaires. Proven to be obtained to the one (70 % - 26 %) belonging to formulated opinion polls they responded very frequent and frequent, (2 % - 2 %); Occasionally (52 % - 44 %) very frequently.() Cárcamo (2010), music suggests organic and inorganic waste matter of urbane type remains of constructions and works and works of demolition. The obtained data (52 %) very frequent (44 %) frequent and (2 %) never.() Galarza (2011), you indicate the materials waste under construction of civil construction reaches a minimum the percentages of use of materials, low accumulation of generated leveled grounds under construction obtained data the 46 % and (32 %) they responded very frequent and (34 %) (24 %) and rarely (6 %) and never (4 %)() Chamoli (2015) indicates edifications the 92 % enters music proven to be of misuse of step of solid residues of civil works, and the final disposition.

Keywords: inorganic residues, final disposition, reutilización, environmental education, unsafe materials.

Classification: DDC Code: 628.03 LCC Code: TD9

Language: English

London Journals Press

LJP Copyright ID: 392956
Print ISSN: 2631-8474
Online ISSN: 2631-8482

London Journal of Engineering Research

Volume 22 | Issue 7 | Compilation 1.0

Education in the Handling of the Solid Residues of Construction in the Work of the High School Industrial Hermilio Valdizan

Educación en El Manejo De Los Residuos Solidos De Construcción en La Obra Del Colegio Industrial Hermilio Valdizan

Guillermo Gomer Cotrina Cabello[α], Yoel Bustillos Bonilla[σ] & Dr. Pedro David Córdova Trujillo[ρ]

RESUMEN

El objetivo fue, evaluar el efecto de la educación en el manejo de los residuos sólidos de construcción en la obra del colegio industrial Hermilio valdizan – Huánuco, Metodología El estudio fue experimental porque se evaluó muestras de comparaciones en dos grupos donde se tomó la prueba de proceso y la posprueba, los instrumentos utilizados fueron las pizarras, boletines, cuestionarios. Resultados obtenidos al (70% - 26%) de encuestas formuladas respondieron muy frecuente y frecuente, (2% -2%); ocasionalmente (52% - 44%) muy frecuentemente.() Cárcamo (2010), indica desechos orgánicos e inorgánicos de tipo urbano son restos de construcciones y obras y trabajos de demolición. Los datos obtenidos (52%) muy frecuente (44%) frecuente y (2%) nunca.

()Galarza (2011), indica el desperdicio de materiales en obras de construcción civil se minimiza los porcentajes de uso de materiales, baja acumulación de desmontes generados en obras. datos obtenidos el 46 % y (32%) respondieron muy frecuente y (34%) (24%) y raramente (6%) y nunca (4%) ()Chamoli (2015) indica las edificaciones entra el 92% son resultados de mal manejo de gestión de residuos sólidos de obras civiles, y la disposición final.

Conclusiones La calidad de vida depende significativamente de buena gestión y disposición de los residuos sólidos de construcción. el (70% - 26%) y, (58% - 32%) respondieron muy frecuentey frecuente distingue, el (4% - 4%), y el (44% - 42%) frecuente saben diferenciar restos de plástico dejados en obra son residuos sólidos.

Palabras clave: residuos inorgánicos, disposición final, reutilización, educación ambiental, materiales peligrosos.

Author α: Docente en la Universidad Nacional Daniel Alcides Carrión de Cerro de Pasco. Orcid 0000-0003-2367-2240.
σ: Docente de la Universidad Nacional Daniel Alcides Carrión de Cerro de Pasco,
ρ: Docente de la universidad nacional Hermilio Valdizan de Huánuco, Orcid:0000-0002-1305-5401.

SUMMARY

The objective matched, evaluating the effect of the education in the handling of the solid residues of the construction in the work of the high school industrial Hermilio valdizan – Huánuco, Metodología The study was experimental because signs of comparisons in two groups where you took the proof of process were evaluated and the posprueba, the utilized instruments were blackboards, bulletins, questionnaires. Proven to be obtained to the one (70 % - 26 %) belonging to formulated opinion polls they responded very frequent and frequent, (2 % - 2 %); Occasionally (52 % - 44 %) very frequently.() Cárcamo (2010), music suggests organic and inorganic waste matter of urbane type remains of constructions and works and works of demolition. The obtained data (52 %) very frequent (44 %) frequent and (2 %) never.() Galarza (2011), you indicate the materials waste

under construction of civil construction reaches a minimum the percentages of use of materials, low accumulation of generated leveled grounds under construction obtained data the 46 % and (32 %) they responded very frequent and (34 %) (24 %) and rarely (6 %) and never (4 %)() Chamoli (2015) indicates edifications the 92 % enters music proven to be of misuse of step of solid residues of civil works, and the final disposition. Findings The quality of life depends significantly on good step and disposition of the solid residues of the construction the (70 % - 26 %) and, (58 % - 32 %) they answered very frequent and frequent distinguish, the (4 % - 4 %), and the (44 % - 42 %) frequent know how to tell apart remains of plastic left in work they are solid residues.

Keywords: inorganic residues, final disposition, Reutilización, environmental education, unsafe materials.

I. INTRODUCCIÓN

El Perú con economía relevante de crecimiento económico su principal actividad es de construcción de las infraestructuras lo que genera el mayor número de mano de obra calificada, impulsado por los gobiernos centrales, regionales, municipales, en la construcción de los colegios, puentes, pistas, veredas, la construcción de la infraestructura de la educación educativa del colegio industrial Hermilio Valdizan – Huánuco.

En las provincias de la región Huánuco, el crecimiento de las infraestructuras se ha incrementado en obras de infraestructura, como actividad primaria de la reactivación económica y beneficiando a las familias que de la zona urbana (Galarza 2011). Indica para solucionar los problemas de deposición y disposición de los desechos de escombros, residuos de materiales de tierra, residuos de fierro, alambres, trapos, vidrios, esta situación provoca la reducción de poblaciones de animales silvestres lo que ocasiona una serie de problemas en la salud de la población por las sustancias tóxicas de polvos, ruidos, y sustancias dañinas emitidas por escombros al medio ambiente, la reducción de la calidad del agua, suelo, por presencia y acumulación de residuos. Esto permite el riesgo para la salud humana, por intoxicación aguda, mediante inhalación, ingesta o absorción dérmica, o por la exposición crónica, por la presencia de residuos inorgánicos según (Cconislla 2014). menciona desarrollar los seminarios, cursos, charlas para la población quienes se encuentran al entorno de la ejecución de la obra, ello permite el aporte de conocimiento a la población sobre la ejecución de las obras de infraestructuras. Para efectuar cambios necesitamos información científica y acciones prácticas en diferentes niveles. García (2013), indica la Herramienta para la reducción de residuos sólidos en los proyectos de construcción. En su investigación tuvo como herramienta para la reducción de residuos sólidos los estudios de los impactos ambientales de construcción con el fin mitigar el impacto negativo que tiene su producción en el medio ambiente.

II. METODOLOGÍA

El trabajo de investigación se desarrolló en la ciudad de Huánuco, en la Construcción en la Obra del Colegio Industrial Hermilio Valdizan, la población estuvo Investigación exploratoria – descriptivo. La ecuación utilizada fue

2.1 Tipo y Nivel De Investigación

El tipo de investigación es Experimental y el nivel Aplicada por que busca aplicar un conocimiento teórico en una determinada situación problemática, Población Estuvo integrado por 50 trabajadores en la obra "Construcción Del Colegio Industrial Hermilio Valdizan, Muestra_N=n del total de 50 trabajadores todos se incluirán en la investigación. Será población muestra porque estará conformado por 25 trabajadores del módulo 1,2 y 25 trabajadores del módulo 3,4 de la Obra.

2.2 Diseño De Investigación

Es experimental, porque está orientado a describir esa variable como los efectos que ha probado sobre la variable dependiente, que es el otro fenómeno.

III. RESULTADOS

Con lo que se indica a la educación en el manejo de los residuos sólidos de construcción en la obra del colegio industrial Hermilio Valdizan de Huánuco, respecto si colocan los residuos de construcción en los depósitos indicados en obra; el (70% - 26%) en el manejo de los residuos de construcción en los depósitos indicados; respondieron muy frecuente y frecuente, el (2% -2%); respondieron ocasionalmente y raramente; sobre el tema si distingue los residuos inorgánicos dejados en obra el (52% - 44%) responde muy frecuentemente y de manera frecuente, se corroboran los resultados de la investigación realizada por Cárcamo (2010), indica en su trabajo de investigación los desechos orgánicos e inorgánicos de tipo urbano son desechos y restos de las construcciones y obras en construcción, el resultado son datos y fuentes obtenidas de los trabajos de construcción y demolición mediante la utilización de un sistema de información geográfica que permite obtener datos específicos y exactos. En cuanto a la pregunta que se realizó si distingue los residuos inorgánicos dejados en obra (52%) muy frecuente (44%) frecuente y (2%) nunca lo realiza. Con respecto a los residuos inorgánicos dejados en obra indica en su trabajo de tesis ejecutado según Galarza (2011), menciona en su tesis sobre el tema desperdicio de materiales en obras de construcción civil que se minimiza los porcentajes de uso de materiales y la baja acumulación de desmontes generados por las obras, los trabajos consistieron en controlar los materiales en desecho como ejemplo de: acero y concretos rotos y dejados en obra que generan montículos de albañilería. Con 46 % de desmonte; con respecto a la pregunta 6 de la encuesta si deposita los residuos orgánicos en el tacho correspondiente de las personas encuestadas respondieron el (32%) respondieron muy frecuente y (34%) respondieron frecuente ocasionalmente respondieron (24%) y raramente (6%) y nunca (4%) frente a los datos de estas investigación también corroboran en los resultados de investigación Chamoli (2015) menciona que la los trabajos que se desarrolla durante las edificaciones entra en dos procesos de construcción y demolición en la región Huánuco y la ciudad de Huánuco el total de 92% En su investigación planteada los resultados sobre el mal manejo de gestión del residuos sólidos de las obras civiles, son los problemas de la disposición final en su mayoría son arrojados en la canteras de los ríos y en canteras de la carreteras causando dificultades que afecta la libre transitabilidad de los peatones y la contaminación ambiental del ecosistema. la reutilización los desperdicios de fierro dejados en obra a las personas encuestados muy frecuentemente nadie respondió a la pregunta (0%) muy frecuente mente el (2%) respondieron a la pregunta, ocasionalmente (6%) raramente (52%) de personas respondieron y nunca lo hicieron el (40%) de personas encuestados, manifestaron y corroboran en su trabajo de investigación. Formoso (2002) menciona en su trabajo de investigación los escombros, desmontes generados de la construcción son los restos de metales los que causan problemas al medio ambiente encontrándose entre ellos el acero, el concreto pre mezclado, los ladrillos y bloques, las cerámicas, la arena, y cables. Con el 56%. los Desechos encontrados en los residuos de fierro y otros relacionadas al trabajo de investigación, seguido a ello se le pregunto si reutiliza los restos de alambre utilizados en obra respondieron a la preguntas muy frecuente el 0% frecuente respondieron el (2%) ocasionalmente respondieron (16%) y la que respondieron raramente fueron (36%) y el (46 %) respondieron nunca, en su trabajo de investigación corrobora Burgos (2010) define los residuos sólidos de construcción y demolición los escombros y desmontes generados por la edificaciones de la obra son el 15% reutilizan los residuos de obras como alambre y otros desechos en controlados que son considerado su reutilización para trabajos extras en construcción civil y obras civiles.

IV. DISCUSIONES

Los resultados obtenidos en el presente trabajo de tesis de investigación es la identificación de los residuos sólidos de construcción de la infraestructura y su disposición final recae en la responsabilidad de la municipalidad provincial de Huánuco, el (70% - 26%) respondieron muy frecuente, Ocasional y raramente, el (58% - 32%)

respondieron muy frecuente y frecuente distingue los residuos orgánicos dejados en obra, el (4% - 4%), y el (44% - 42%) respondieron muy frecuente y frecuente conocen diferenciar si los restos de plástico dejados en obra son residuos sólidos. Se ha identificado los residuos inorgánicos el (78 % a 18%) respondieron muy frecuente y frecuente, y el (52% a 40%), reciclan los sobrantes de fierro utilizados en Obra lo trabajan raramente o nunca (54% a 40%). Las encuestada era la población habitante que radica en el entorno de la construcción del Colegio Industrial Hermilio Valdizan – Huánuco. Se logró controlar los sensibilizar a la población en el manejo restos de construcción de la obra del Colegio Industrial Hermilio Valdizan de Huánuco. Y se minimizo los efectos que reutilizan los residuos inflamables en obra, el (44 %. 46%) y el (6% - 2%), respondieron que depositan los residuos inflamables en el lugar adecuado de manera muy frecuente y frecuente, otros lo realizan de manera ocasionalmente y raramente.

V. CONCLUSIONES

Los residuos orgánicos e inorgánicos utilizados en la ejecución de las obras de construcción lo primero es conocer las normas básicas de su manejo seguro, dirigido a todos los trabajadores, en el uso de adecuado, conocer sobre normas y recomendaciones relacionadas con el uso y manipulación de los herramientas, uso de los residuos y manejo de desechos inorgánicos, en el transporte, el almacenaje, la eliminación de residuos, para reducir los riesgos de daños al trabajador al visitante y esto permite cuidar el ambiente. Fomentar las capacitaciones, charlas, seminarios, a la población en temas de uso y manejo de los residuos orgánicos e inorgánicos de los desechos de manejo de los residuos sólidos; mediante las recomendaciones adecuadas que pueden transmitir a la población; sobre los peligros de los fierros, vidrios de uso pertinentes y los mecanismos de gestión de los restos desechos de la construcción del colegio industrial Hermilio Valdizan - Huánuco. disposición final y usos y reciclajes de los residuos orgánicos e inorgánicos de los desechos de los trabajos en construcción y edificaciones, de las disposiciones finales de los fierros alambre, vidrios y otros. dirigidas a los personales, obreros, funcionarios responsables de las obras civiles, incluir programas de educación ambiental a fin de lograr una buena disposición de los residuos indicados, ya que estos son arrojados en las riberas de los ríos y contaminando el medio acuático.

AGRADECIMIENTO

Agradecerle con amor y cariño al ser más querido quienes se encuentran a mi lado y a todos ellos que dieron su apoyo anímico en los momentos de dificultad del desarrollo del trabajo de investigación. a mis seres queridos que siempre estuvieron presente en el desarrollo del trabajo de investigación.

REFERENCIAS BIBLIOGRÁFICAS

1. Abarca, K., & Freire, C. (2009). Aprendizaje interactivo con CD para el desarrollo de. Ecuador: universidad Estatal de Milagro. Recuperado el 7 de febrero de 2016.
2. Acosta, D. (2002). Reducción y gestión de los residuos de construcción y demolición. Venezuela.
3. Agencia medio ambiental de los Estados Unidos. (2003). EPA. Recuperado el 17 de Setiembre de 2015.
4. Aguirre (2004), Mercader (2010) y Ocampo (2013) Ministerio de Medio Ambiente de Colombia. Reglamento de Protección y Control de la Calidad del Aire. Decreto 948 del 5 de junio de 1995. Artículo 2.
5. Aldana, J., & Serpell, A. (2012). Temas y tendencias sobre residuos de construcción y demolición.
6. Aquino, E. (2015). Reciclaje de residuos de la construcción para la fabricación de ladrillos sustentable. Distrito federal de México, México: UNAM. Recuperado el 24 de Enero de 2016.
7. Bergsdal, H. (2007). Projection of construction and demolition waste in Norway. Recuperado el 4 de Marzo de 2016.
8. Bermúdez, O. (2003) Reutilización de residuos de construcción y demolición: Departamento de Urbanismo, Vivienda y Medio Ambiente, nº 12, 1994, 1-61.

London Journal Press Membership

For Authors, subscribers, Boards and organizations

London Journals Press membership is an elite community of scholars, researchers, scientists, professionals and institutions associated with all the major disciplines. London Journals Press memberships are for individuals, research institutions, and universities. Authors, subscribers, Editorial Board members, Advisory Board members, and organizations are all part of member network.

Read more and apply for membership here:
https://journalspress.com/journals/membership

For Authors

Author Membership provide access to scientific innovation, next generation tools, access to conferences/seminars /symposiums/webinars, networking opportunities, and privileged benefits.
Authors may submit research manuscript or paper without being an existing member of LJP. Once a non-member author submits a research paper he/she becomes a part of "Provisional Author Membership".

For Institutions

Society flourish when two institutions come together." Organizations, research institutes, and universities can join LJP Subscription membership or privileged "Fellow Membership" membership facilitating researchers to publish their work with us, become peer reviewers and join us on Advisory Board.

For Subscribers

Subscribe to distinguished STM (scientific, technical, and medical) publisher. Subscription membership is available for individuals universities and institutions (print & online). Subscribers can access journals from our libraries, published in different formats like Printed Hardcopy, Interactive PDFs, EPUBs, eBooks, indexable documents and the author managed dynamic live web page articles, LaTeX, PDFs etc.

GO GREEN AND HELP
SAVE THE ENVIRONMENT

JOURNAL AVAILABLE IN

PRINTED VERSION, INTERACTIVE PDFS, EPUBS, EBOOKS, INDEXABLE DOCUMENTS AND THE AUTHOR MANAGED DYNAMIC LIVE WEB PAGE ARTICLES, LATEX, PDFS, RESTRUCTURED TEXT, TEXTILE, HTML, DOCBOOK, MEDIAWIKI MARKUP, TWIKI MARKUP, OPML, EMACS ORG-MODE & OTHER

SCAN TO KNOW MORE

support@journalspress.com
www.journalspress.com

*THIS JOURNAL SUPPORT AUGMENTED REALITY APPS AND SOFTWARES